



HAL
open science

Identification des perturbations CEM conduites dans les convertisseurs statiques par la méthode du filtre de Wiener

Piotr Musznicki

► **To cite this version:**

Piotr Musznicki. Identification des perturbations CEM conduites dans les convertisseurs statiques par la méthode du filtre de Wiener. Sciences de l'ingénieur [physics]. Institut National Polytechnique de Grenoble - INPG, 2007. Français. NNT: . tel-00400074

HAL Id: tel-00400074

<https://theses.hal.science/tel-00400074>

Submitted on 29 Jun 2009

HAL is a multi-disciplinary open access archive for the deposit and dissemination of scientific research documents, whether they are published or not. The documents may come from teaching and research institutions in France or abroad, or from public or private research centers.

L'archive ouverte pluridisciplinaire **HAL**, est destinée au dépôt et à la diffusion de documents scientifiques de niveau recherche, publiés ou non, émanant des établissements d'enseignement et de recherche français ou étrangers, des laboratoires publics ou privés.

POLITECHNIKA GDAŃSKA
WYDZIAŁ ELEKTROTECHNIKI I AUTOMATYKI

mgr inż. Piotr Musznicki

**Conducted EMI identification in power
electronic converters using the Wiener filtering
method**

Rozprawa doktorska

zrealizowana w ramach współpracy między Politechniką Gdańską (Polska) i
Institut National Polytechnique de Grenoble (Francja)

Promotorzy:

dr hab. inż. Piotr Jerzy Chrzan
prof. PG

prof. Jean Luc Schanen

Konsultant naukowy:

dr Pierre Granjon
maître de conférences - INPG - ENSIEG

Praca naukowa finansowana ze środków na naukę w latach 2005 - 2006 jako
projekt badawczy.

Gdańsk 2006

Contents

Acknowledgements	V
List of symbols	VI
List of figures	IX
1 Introduction	1
1.1 Background	1
1.2 Accurate simulation	4
1.3 Wiener filtering	5
1.4 Objectives and dissertation outline	7
2 Models of circuit components	9
2.1 Introduction	9
2.2 Semiconductor parameters determination	10
2.3 Passive component models	12
2.4 Parasitic layout modeling	15
3 DC-DC boost converter	21
3.1 Introduction	21
3.2 Accurate simulation	22
3.3 Sensors influence	24
3.4 Sensitivity study	27
3.4.1 Semiconductors influence.	27
3.4.2 Layout influence	28
3.5 Simplification of boost model for forecasting EMI	30
3.6 Experimental results	32
3.7 Wiener filter	35
3.7.1 The converter state independent method	35
3.7.2 Wiener filter with state detection	36
3.8 Conclusion	40

4	Hard switching inverter	43
4.1	Introduction	43
4.2	Simulation	44
4.3	Wiener filter	47
4.3.1	Specifying inverter states	48
4.3.2	Validation of Wiener filter method	50
4.4	Conclusion	58
5	Soft switching inverter	59
5.1	Introduction	59
5.2	Simulation	60
5.3	Experimental results	65
5.4	Wiener filter	66
5.5	Conclusion	69
6	Conclusion and future work	73
6.1	Summary and overview	73
6.2	Future work	74
	Bibliography	75
A	Appendix A	83

Acknowledgments

It is a pleasure to thank the many people who made this thesis possible. First of all, I would like to thank to my supervisor, Prof. Piotr Chrzan, for his careful guidance during my study years. He gave me the opportunity to enroll as a Ph.D. student. He provided encouragement, smart advice, good teaching, good company, and lots of great ideas.

I would like to thank Prof. Jean Luc Schanen for giving me the opportunity to work in Laboratoire d'Electrotechnique - ENSIEG at the INP Grenoble. He helped to supervise me, provided resources and subjects, offered direction and wise criticism and helped me in difficult life situations in „the strange land”.

I must also acknowledge Dr Pierre Granjon from Laboratoire des Images et des Signaux - ENSIEG for sharing with me his knowlage about digital signal processing, answering all my questions, sense of humor that always makes me feel good.

I would also like to thank all people from Katedra Energoelektroniki i Maszyn Elektrycznych EiA PG where I was surrounded by knowledgeable and friendly people who helped me every day, especially to Sławomir Mandrek for providing vital information about soft switching technique.

I have found the friendly and supportive atmosphere in équipe d'Électronique de Puissance in LEG INPG where I have benefited from many discussions with many people which I would like to thank, particuraly Christian Martin and Franck Barruel.

I cannot end without thanking my family, on whose constant encouragement and love I have relied throughout my studies.

Piotr Musznicki
Gdańsk
December 18, 2006

List of symbols

SYMBOL DESCRIPTION

Acronyms

<i>EMI</i>	: Electromagnetic Interference
<i>EMC</i>	: Electromagnetic Compatibility
<i>LISN</i>	: Line Impedance Stabilization Network
<i>IMS</i>	: Insulated Metal Substrate
<i>PCB</i>	: Printed Circuit Board
<i>PEEC</i>	: Partial Element Equivalent Circuit
<i>PWM</i>	: Pulse Width Modulation
<i>PDM</i>	: Pulse Density Modulation
<i>DM</i>	: Differential Mode noise
<i>CM</i>	: Common Mode noise
<i>IGBT</i>	: Insulated Gate Bipolar Transistor
<i>MOSFET</i>	: Metal-Oxide Semiconductor Field-Effect Transistor
<i>PQRDCLI</i>	: Parallel Quasi Resonant DC link Voltage Inverter

Physics

V_{ds}	: MOSFET Dren - Source Voltage
I_d	: MOSFET Dren Current
V_{gs}	: MOSFET Gate - Source voltage

SYMBOL	DESCRIPTION
V_{switch}	: voltage across the semiconductor device
V_{LISN}	: voltage across LISN 50 Ω resistor
V_f	: inverter DC link voltage
ϵ	: the dielectric constants
$dv/dt.$: voltages velocity changes
$di/dt.$: current velocity changes

Mathematic

J	: the cost function
$E[\cdot]$: the expectation operator
S_{vv}	: the power spectrum of v ,
S_{vp}	: the cross spectrum between v and p .
FFT	: Fast Fourier Transform
abs	: the absolute value and complex magnitude

List of Figures

1.1	The differential-mode and and common-mode noise paths	2
1.2	Standardized line impedance stabilizing network	3
1.3	Wiener filtering applied to EMI estimation	5
2.1	The method principle to determine semiconductor parameters . . .	11
2.2	View of the MOSFET Motorola 65V HD3 lot 27601 wafer7	12
2.3	Saber - Model Architect	13
2.4	The inductor model	13
2.5	The inductor impedance measured and modeled	14
2.6	The capacitor model	14
2.7	The comparaive results of the capacitor impedance measurement and simulation	15
2.8	The geometrical description for inductance calculation	16
2.9	The reduction of PEEC inductive model for one interconnection . .	17
2.10	The reduction of PEEC capacitive model for one interconnection . .	19
2.11	The boost converter: view and INCA model.	20
3.1	The fundamental schematic diagram of boost converter	21
3.2	The simple driver schema	22
3.3	The common mode filter between driver and boost	23
3.4	The Saber circuitof the boost converter	23
3.5	The LISN voltage spectrum obtained with Saber	24
3.6	The layouts of DC-DC boost without sensors and with sensors . . .	24
3.7	The comparison of voltage V_{DS} for boost with and without sensors .	25
3.8	The comparison of current (I_D) for boost with and without sensors .	25
3.9	The comparison of diode voltage for boost with and without sensors	26
3.10	The comparison of diode current for boost with and without sensors	26
3.11	The comparison of generated perturbation from boost with and without sensors	27
3.12	Influence of MOSFET parameters on LISN spectrum	28
3.13	Influence of power diode parameters on LISN spectrum	28

3.14	The influence of inductive connections on LISN spectrum	29
3.15	The influence of parasitic capacitances on LISN spectrum	29
3.16	The spectrum of LISN voltages for PCB and IMS (real)	30
3.17	Schema of simplified boost converter model for EMI forecasting . .	31
3.18	Spectrum of LISN voltages obtained with simplified Mathcad model	31
3.19	The transfer function between semiconductor switch voltage from DC-DC boost converter and perturbation	32
3.20	View of DC-DC boost converter, driver and LISN	32
3.21	The differential mode cancellation and common mode current path	33
3.22	LISN voltage spectrum obtained with spectrum analyzer	34
3.23	Temporary MOSFET voltage comparison measured and simulated	34
3.24	The temporary LISN voltage comparison measured and simulated	34
3.25	The perturbation reconstruction for MOSFET signal	36
3.26	Zoom of V_{LISN} for „slow” driver real and reconstructed	37
3.27	The perturbation waveforms for „fast” driver real and reconstructed	37
3.28	Two different systems for each state of the MOSFET	38
3.29	The signals dividing using one threshold or two thresholds	39
3.30	The voltage waveforms simulated and reconstructed by Wiener filter.	40
3.31	The voltage waveforms measured and reconstructed with the Wiener filter	41
3.32	The separating and reconstruction of driver contribution	42
3.33	The perturbation divided for driver, open and close state	42
4.1	The DC/AC motor fed system	43
4.2	Inverter schema from SaberSketch	45
4.3	The switches and LISN voltages waveform obtained by simulation	45
4.4	The switches and LISN voltages spectra obtained by simulation . .	46
4.5	Differential-mode and common-mode separation	47
4.6	The voltages used to inverter state definition.	48
4.7	Wiener filters and the inverter	51
4.8	The semiconductors and LISN voltage waveforms obtained from simulation and Wiener filter	51
4.9	The LISN voltage spectra from simulation and estimation	52
4.10	The perturbations source identification using data from simulation	53
4.11	The transfer functions for different states of inverter	53
4.12	The impulse response for different states of inverter	54
4.13	The measured voltage of semiconductors and LISN waveforms for PWM modulation	55
4.14	The measured voltage of semiconductors and LISN waveforms for PWM modulation	56
4.15	The LISN voltage spectra for PWM modulation from measured and Wiener filter estimation	56
4.16	The measured voltage of semiconductors and LISN voltage wave- forms for PDM modulation	57

4.17	The LISN voltage spectra for PDM modulation from measured and Wiener filter estimation	58
5.1	PQRDCLI circuit topology	59
5.2	The PQRDCLI schema from SaberSketch	61
5.3	The PQRDCLI inverter simulation waveforms	62
5.4	The spectra of DC link voltage and perturbation obtained from simulation	63
5.5	The comparison of the generated perturbation for two different times	64
5.6	The differential-mode and common-mode noise comparison	64
5.7	The comparison of the perturbation spectra for soft and hard switching inverter	65
5.8	View of the quasi resonant DC link voltage inverter and LISN . . .	65
5.9	The measured waveforms of DC link voltage and perturbation . . .	66
5.10	The DC link and LISN voltages from simulation and Wiener filter .	67
5.11	The Wiener filter transfer functions for two states of inverter . . .	68
5.12	The DC link and LISN voltage waveforms from measurement . . .	68
5.13	The influence of external DC/DC converter and T_2 commutation . .	69
5.14	The separation of perturbation from external DC/DC converter . .	70
5.15	The LISN voltage spectra - separation of perturbation from DC/DC converter	71

Il n'y a pas de problèmes résolus, il y a seulement des problèmes plus ou moins résolus.

Henri Poincaré

1.1 Background

Nowadays, there is a trend for increasing switching frequencies of switch-mode power supplies. It is strongly connected with increasing of electromagnetic interference (EMI) emissions. EMI is any electromagnetic disturbance that interrupts, otherwise obstructs, or otherwise modifies an equipment performances, which leads to a general electromagnetic compatibility (EMC) degradation for devices, especially in field of power electronics. Many EMC standards and regulations such as the Federal Communications Commission (FCC), the International Electrotechnical Commission (IEC) and the International Special Committee on Radio Interference (CISPR) standards have been organized for controlling the quantity of EMI emission. As a consequence, better understanding of EMI generation phenomena is needed in order to forecast, minimize and reduce it. Moreover, it is important to pay attention of EMI performance before converter is built, EMI forecast or estimation should be made during design process.

Understanding electromagnetic capability is very important for power electronics design, where traditional viewpoints and the approximations of electrical circuit theory start to break down. The new approaches and tools are needed to understand the law of this challenging art .

The EM disturbance can be described in three steps:

- the source: this is the device or equipment where the noise or disturbance is generated. The reason for this could be e.g. fast signals, fast rise and fall time, resonance, antenna structures, wrong termination, reflections and electric potential differences.
- the victim: the electrical circuit which becomes influenced by the perturbations coming from the source and possessing major impact on the functionality of inside signals or work of the whole application.
- the coupling path: the paths or medium where the disturbance is propagated from the source to the victim.

Electromagnetic interference can be categorized in four groups:

- conducted emissions
- radiated emissions
- conducted susceptibility
- radiated susceptibility

The first two groups deal with the undesirable signals generated in a particular piece of equipment, and the second two groups are connected with an equipment's ability to reject disturbances from external sources. Contractually, the frequency range of conducted emissions extends from 50 kHz to 30 MHz and for radiated emissions over 30 MHz. In this thesis the first type of EMI - conducted emissions - has been taken into consideration.

Switch-mode power applications generate high frequency perturbations because of fast semiconductor devices commutation [32]. The magnitude of emitted noise relies on the electrical performance which depends on geometrical structures of the system, devices packaging, layout of the circuit, parasitic components, current (di/dt) and voltage (dv/dt) slew rates. The generated noise can have influences on control circuitry and surrounding equipment.

Conventionally, the total conducted EMI noise can be divided in two basic mechanisms, the differential-mode (DM) and the common-mode (CM) noise. Generally, the DM noise (symmetrical disturbance) is related to switching produced by current flowing along either the live or neutral conductor and returning by the other one (fig.1.1a). The CM noise (asymmetrical disturbance) is mainly related to parasitic self and to ground capacitances of components of the circuit produced by current flowing along conductors and returns via the safety earth (fig.1.1b).

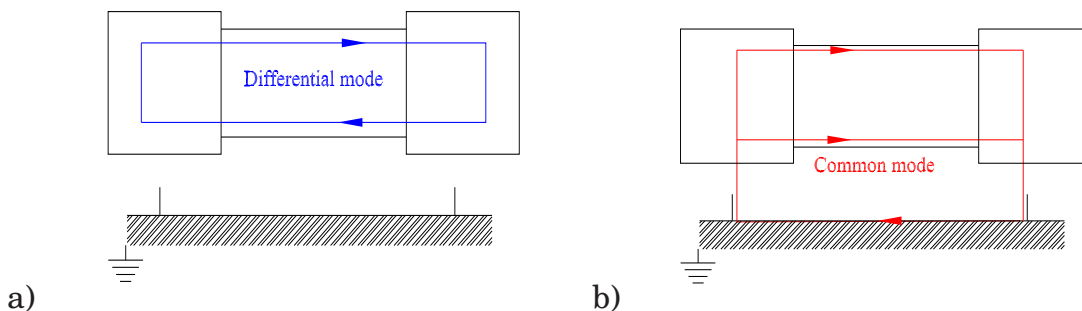


Figure 1.1: The differential-mode (a) and common-mode (b) noise path

1.1. BACKGROUND

The conducted EMI measurement in both time and frequency domain is usually realized with the standardized line impedance stabilizing network (LISN). The LISN is also used for blocking all noise from the power supply network and providing a line impedance with a known high frequency characteristic. There are several LISN topologies, in all investigations in this thesis structure presented in figure (1.2) has been used.

The results of measurement give total noise, but comparing LISN voltages V_{L1} and V_{L2} , it is possible to separate CM and DM as it is presented in this following formulas:

$$V_{CM} = \frac{V_{L1} + V_{L2}}{2} \quad (1.1)$$

$$V_{DM} = V_{L1} - V_{L2} \quad (1.2)$$

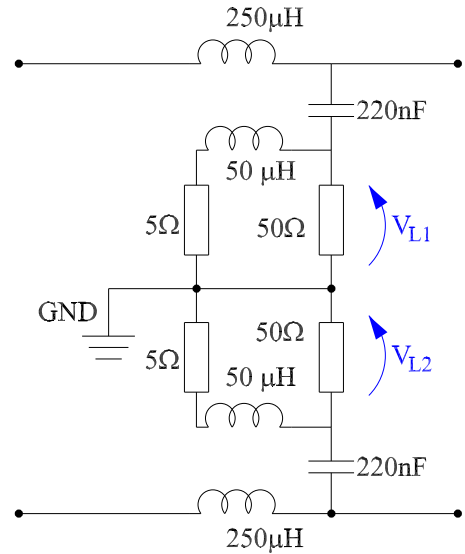


Figure 1.2: Standardized line impedance stabilizing network

The EMI behavior of power electronics converters can be investigated using various approaches:

- expert knowledge and experience
- simply model calculation in time or frequency domain
- computer simulation
 - estimation based on simply circuit model
 - accurate simulation in the time domain
 - estimation based on transfer functions
 - digital signal processing methods

In this thesis two kinds of EMI estimation technique have been presented: accurate computer simulation and method based on digital signal processing - Wiener filtering. The simulation has been done using powerfull simulator *Saber*®.

1.2 Accurate simulation

Since full measurements of EMC behavior of converters can only be made with assembled and ready to work application, EMC problems are often emerged in a last phase of the product development process, bringing expensive and time-consuming design correction. To avoid project changes, EMC forecast should be done in a design phase, which allows to avoid additional expense. The EMC properties of electronic devices can be checked by computer simulation which is more fast and cost-effective. Enormous research effort has concentrated on EMI modeling and simulation. Variety of EMI models for power electronic converters have been presented in many publications [53],[54],[38]. These studies have tried to analyze the complex EMI production mechanism and shed a light on a better understanding of perturbation generation process. The simulation circuits can be developed depending on assumptions, simplifications and properties of physical phenomena. The simplifications make possibility of easy way of object description, but have an impact on solution inaccuracy. If a model is too simple, some important features could be omitted, if it is too complex, calculations could be problematical and numerical errors can appear. Because of complexity of models, authors have made some simplifications [16], [37], [58],[66] or they have focused on empirical models [9], [33],[35],[93], [92] or on impact to the load [58],[60].

The aim of simulation is to obtain total EMI noise generated in converter which agree with true values from real application. Because of very high time constants in typical power electronic application with LISN and load, long simulations have been carried out to obtain steady state of working system. Powerful simulator is needed, which allows to make simulations with a sufficient small time step, according to EMC frequency range required. Simulations of complex model of the converters can be carried out using the circuit simulators like *Saber*® , *Spice*® or *TCad* [28]. The most important difficulties arise from parasitic elements which require very small calculation step in comparison with time constants of the whole system. The calculation step has to be defined according to the smallest dynamic of the system in the steady state. Moreover, the serious problem in this simulator is that different calculation time step can generate different results what could occur especially in the high frequencies range. According to the Nyquist - Shannon theorem, sampling frequency should be greater than twice highest frequency of considered signal or bandwidth. In order to obtain sufficient information about the simulated the waveform, adequately small step should be chosen (for frequencies of emitted EMI above 30 MHz it must be smaller than $0.016 \mu\text{s}$). The calculation with such a little step takes a lot of computer power, memory and of course time.

The numerical solution is strongly dependent on chosen method and step calculation. Cause of large number of non linear elements and differential equation, solution is stable in a narrow range. All presented solutions have been made with Newton-Raphson algorithm with variable step size. The exploitation

of simulation in term of EMI, is simply achieved with fast Fourier transformation (FFT) of LISN voltage in frequencies range between 50[kHz] and 30[MHz]. It needs to be said that, even if the global shape the EMI spectrum is similar, a 10 dB difference is still noticeable between simulation and measurement, cause of normalization coefficients used in FFT algorithms applied in used software and measurement equipment. In this thesis, simulations have been done with *SaberSketch*® or *Matlab*®, with models presented in chapter 2.

1.3 Wiener filtering

Wiener theory [79], [43] formulated by Norbert Wiener during the 1940s and published in 1949 [84], allows to find the numerical description of data-dependent linear least square error filters. The Wiener filtering is used in order to minimize the average squared error between the filter output and a desired signal. Formally, the Wiener theory assumes that the signals should be stationary. However, for periodically filter coefficients recalculation for every block of N signal samples, self-adaption is done to the average characteristics of the signals. This kind of adaptation allows to remove noise from signals waveforms and to make their smoother. Thus, an optimal filter can be calculated from a solution on the basis of scalar methods. It can be said that, this technique allows to find how many "information" in output signal come from the input signal.

It can be used to investigate phenomena connected with EMC noise generation, to obtain the level of disturbances for circuit working with another condition and to develop simply model for EMI forecasting. In this method of sources identification, EMI behavior of power electronic converter and LISN are represented by the system which contains transfer function between source of disturbances and noises measured on LISN.

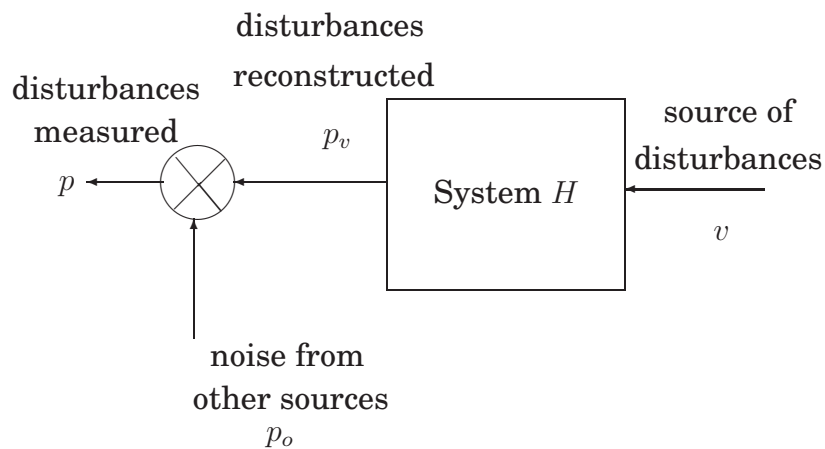


Figure 1.3: Wiener filtering applied to EMI estimation

The main assumptions of Wiener filtering theory are as follows:

- the unknown system H is linear and time-invariant, which means that it can be completely described by its frequency response or its impulse response,
- the noise due to other sources of disturbance p_o is additive and not correlated with measured input signal v .

Thanks to the previous model and assumptions, all signals can be easily expressed in the frequency domain. Indeed, the Fourier transform of the disturbance p_v , noted $P_v(j\omega)$, is expressed as:

$$P_v(j\omega) = H(j\omega)V(j\omega), \quad (1.3)$$

where:

$V(j\omega)$ is the Fourier transform of v ,

$H(j\omega)$ is the frequency response of H .

The estimation error $E_r(j\omega)$ is defined as the difference between the measured disturbance $P(j\omega)$ and the reconstructed one $P_v(j\omega)$:

$$E_r(j\omega) = P(j\omega) - P_v(j\omega) = P(j\omega) - H(j\omega)V(j\omega) \quad (1.4)$$

The mean square error between measured and reconstructed disturbances can now be defined in the frequency domain as:

$$\mathbf{E} [|E_r(j\omega)|^2] = \mathbf{E} [(P(j\omega) - H(j\omega)V(j\omega))^* (P(j\omega) - H(j\omega)V(j\omega))], \quad (1.5)$$

where $\mathbf{E}[\cdot]$ denotes the expectation operator and $*$ the complex conjugate.

The aim is to find the optimal value of the frequency response which minimizes this error. Therefore, the derivative of complex quadratic form. (1.5), which has unique minimum, is calculated with respect to $H(j\omega)$ to zero by using complex derivative rules [79], which leads to :

$$\frac{\partial \mathbf{E} [|E_r(j\omega)|^2]}{\partial H(j\omega)} = 2H(j\omega)S_{vv}(j\omega) - 2S_{vp}(j\omega) = 0, \quad (1.6)$$

where:

$S_{vv}(j\omega) = \mathbf{E}[|V(j\omega)|^2]$ is the power spectrum of v ,

$S_{vp}(j\omega) = \mathbf{E}[P(j\omega)V^*(j\omega)]$ is the cross spectrum between v and p .

The optimal value $H_o(j\omega)$, for which this derivative is zero, is the frequency response of the optimal or Wiener filter. Its expression in the frequency domain is given by:

$$H_o(j\omega) = \frac{S_{vp}(j\omega)}{S_{vv}(j\omega)} \quad (1.7)$$

The same study can also be carried out in the time domain [79]. In this case, the impulse response of the Wiener filter is obtained as a function of the autocorrelation function of v and the crosscorrelation function between v and p .

These results show that the optimal filter only depends on quantities that can be estimated from measured signals v and p : their auto- and cross- spectra or correlation functions. Once this filter is estimated, it can easily be applied to v in order to best estimate the unknown signal p_v . In this application, p_v represents the EMI only generated by the source v , i.e. denoised from the EMI p_o which is generated by the other components of the converter.

In this way, EMI behavior of power electronic converters in the range of conducted perturbation frequency (defined from 10kHz to 30MHz) is represented by the system, which contains transfer functions between the different sources of noise and perturbations. It will be considered in this work that the sources of noise will be the switching devices in the converter.

1.4 Objectives and dissertation outline

The conducted EMI reconstruction in three kind of power electronics converters, is investigated: the DC/DC boost converter with only one transistor, the DC/AC hard switching bridge inverter and next the DC/AC soft switching inverter on the example a new PQRDCLI topology [42]. The simulations of complex circuit, including the most accurate models of all system components, are presented. Moreover, the approach of perturbation reconstruction based on digital signal processing method - the Wiener filtering - is proposed. The source identification method is used by determining the transfer function between the source and generated perturbations. This methodology allows to:

- I. quantify the electromagnetic disturbance of each independent switch (eg. MOSFET, IGBT, diode),
- II. estimate the propagation path of these disturbances at each time instant,
- III. find the contribution of the disturbance source on the global EMI generation and propagation.

The dissertation primary is to prove that, EMI level and shape, depend on converter state. In the chapter 2, the basis of the power electronic circuit components modeling for EMI analysis is presented. Accurate models of semiconductor devices, passive component and conductor is investigated. It is proved in chapter 3, that perturbation generation and propagation in DC/DC boost converter depend unambiguously on the only one transistor switch operation. For three phase bridge inverter, where EMI noise depends on current direction in diode-transistor switches, the 24 states were defined (detail in chapter 4). Finally, perturbation generation in ZVS parallel quasi resonant dc link voltage inverter is studied in chapter 5

Chapter 2

Models of circuit components

I am never content until I have constructed a [...] model of the subject I am studying. If I succeed in making one, I understand; otherwise I do not.

Lord Kelvin

2.1 Introduction

The main aim of simulations is obtaining precise waveforms from working circuit including parasitic currents and voltages. Their magnitudes are determined by the (dv/dt) and (di/dt) particularly in the moments of commutation and depend on geometrical properties of a circuit. Simulation schema - besides essential components - implicate also cabling and parasitic models. Accurate modeling is extremely difficult due to a great number of parameters and factors, which must be considered. Moreover, models of all components should have the same characteristic (static and dynamic) as real ones in the considered frequencies range. Furthermore, in order to obtain correct waveforms with this equivalent circuit, powerful simulator is needed, which allows to make simulations with suitable for EMC calculation time step. Since, power electronic circuits are complicated and number of components is high, simulations can bring serious numerical problems even in such powerful simulators as PSpice or Saber.

Simulation schemes, presented in this thesis, have been built using three kind of models:

- active semiconductor elements such as transistors and diodes can be identified as disturbance sources, thus waveforms obtained from simulation during the switching should be possibly the same like ones from real application, especially dynamic parameters should be get with high accuracy.
- passive components should be taken into account, an electrical equivalent circuit of resistors, capacitors and inductors should give the same characteristic like real components in whole emitted perturbation frequency range.
- cabling, bonding and all conductors cannot be neglected. Although interconnection parasitic (inductance, capacitance) cannot be easily measured, it can be calculated with high precision using different modeling methods.

Thus, complete electrical equivalent circuit can be obtained, including the converter itself with all complex models of components and parasitic elements, but also the measurement equipment like the Line Impedance Stabilization Network (LISN) and the cabling

2.2 Semiconductor parameters determination

Accurate semiconductor models are needed in order to forecast EMI phenomena, since they are linked to switching waveforms. The number of publications in the semiconductor modeling area have introduced a variety of models [5], [46]. The semiconductors have unipolar and non linear components and therefore are the most difficult power components to be modeled: bipolar effects are the most tricky (PIN diode, IGBT). Inexact values of parameters and improper model could lead to incorrect results of simulations.

Several effects - like resistivity modulation, charge storage, junction capacitance, etc - should be considered with high accuracy since they have a great impact on the high frequency characteristics. In typical electronic simulators conventional, physics based models can easily be used for EMI prediction. However, the model parameters must be determined with sufficient accuracy including most important static and dynamic parameters. These models can be constructed using parameters from producer data sheet, but usually they aren't sufficient for wide band modeling, since manufacturer data are not always stay with an agreement to true values. Furthermore, models attached to simulation software can be applied, but it can be noticed, that models provided with Saber or Spice libraries are not very accurate for EMI modeling, especially dependencies in time domain don't stay with agreement to real ones. In practice, the libraries don't contain all commercial components, so characteristic values should be extracted from real semiconductor devices.

One of the highest accuracy was obtained using specific parameter extraction method based on bibliography research [45]. The method is based on an optimization algorithm, which minimizes the error between measured static characteristic and simulated one. It can be implemented for direct shaping of electrical characteristics and identification of chosen parameters. The algorithm of parameters extraction, presented in fig.2.1, can be divided into 5 stages:

1. experimental data acquisition
2. selection of a model and simulator
3. quality standard choice (the function cost J)
4. selection of optimization method
5. verification

2.2. SEMICONDUCTOR PARAMETERS DETERMINATION

The optimization method exploits all information available and uses them to minimize the function cost:

$$J = \|r\|_k = \left(\sum_{i=1}^n |\delta_i|^k \right)^{\frac{1}{k}} \quad (2.1)$$

where δ is error norm between k values experimental y_m and simulated y_s :

$$\delta = \left[\frac{y_m - y_s}{y_m} \right] \quad (2.2)$$

In general, the optimization methods are the numerical procedures which allows to find solution of minimization problems [46].

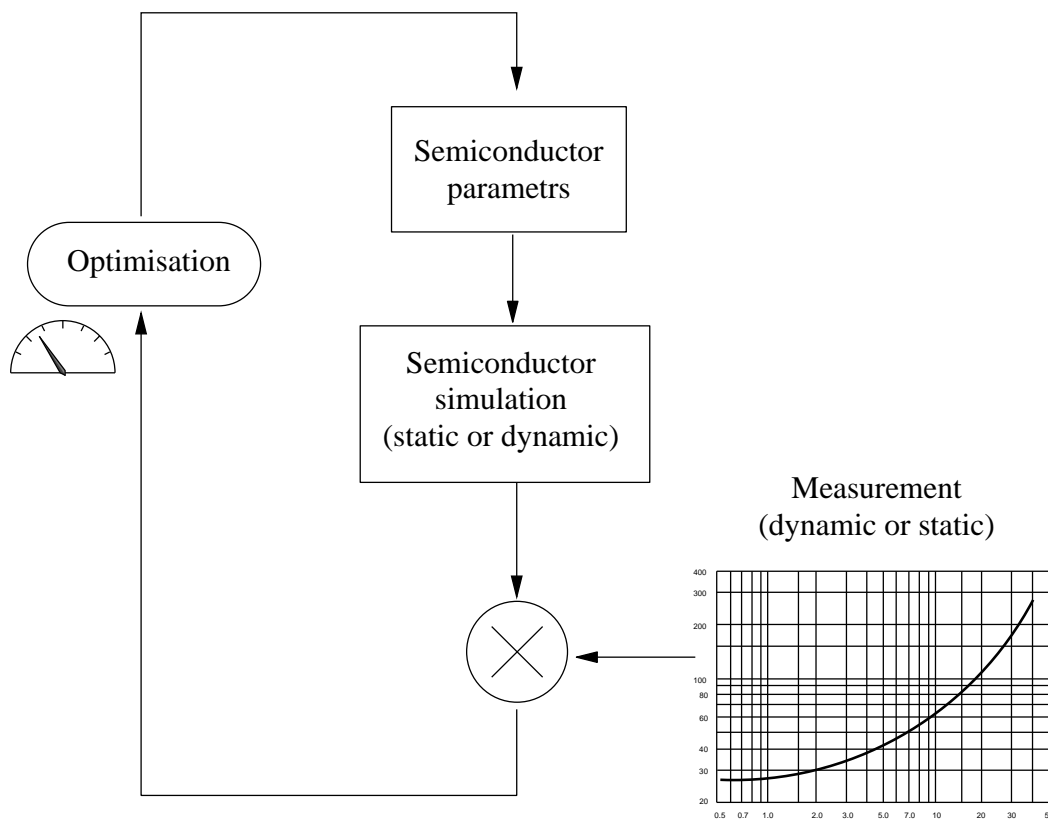


Figure 2.1: The principle of optimization method to determine semiconductor parameters. 1st step: static measurement, 2nd step, dynamic measurement

All types of transistor models needs minimum ten parameters, and diode four for accurate forecasting of their EMI behavior. Among these parameters, some have an influence on static behavior, and can be deduced from a curve tracer [57], [21]. The dynamic (transient) model operation depends on characteristics of non linear capacitance. Care must be taken in order to avoid self heating of the component, what usually happen during this static measurement: the current pulse must be short. Conventional tracers are often not adapted, and specific experimental setup has to be build.

For example "static" parameters have been determined and a dynamic test (in a chopper cell) is used with the optimization approach, in order to find the parameters of MOSFET Motorola 65V HD3 lot 27601 wafer7 and Schottky diode used in boost converter (chapter 3). Parameters are listed below from [45]:

1. for MOSFET

- V_{TO} - Zero-bias threshold voltage 3.76[V],
- I_S - Bulk p-n saturation current 1[pA],
- K_P - Transconductance 83.2,
- R_D - Drain ohmic resistance 1[m Ω],
- R_S - Source ohmic resistance 1[m Ω],
- R_G - Gate ohmic resistance 10[Ω],
- $THETA$ - Mobility modulation 2.025[V⁻¹],
- $C_{rss} = 1.14$ [nF], $C_{oss} = [0.1n]$, $C_{iss} = 14.8$ [nF], $C_{gs} = 14.8$ [nF] and $C_{ds} = 2.09$ [nF] - the interelectrode capacitances.

2. for diode

- I_s - saturation current injection 1[nA],
- r_s - series resistance 7.4[m Ω],
- V_j - voltage injection 0.3[V],
- C_j - junction capacitance 1.47[nF],

Nowdays, simulation software like Saber contains an additional utility *Model Architect* (presented in figure 2.3) for creation and characterization of new models. This tool allows for interactive tuning of semiconductor parameters from producer data sheet or extracted values. All types of the semiconductors are strong non linear objects, there is a danger of numerical noise generation, if the model parameters and numerical method are taken improperly [30]. All presented in this chapter semiconductor modeling approaches have been used in simulations in this thesis.

2.3 Passive component models

In order to forecast EMI behavior of converters, wide band models of inductors and capacitors are needed. It can be said that there are no ideal components. All components also contain inductive, capacitive and resistive elements.

The inductor model should describe the behavior of a real one. Beside the main parameter - inductance, model includes additional components. Since an

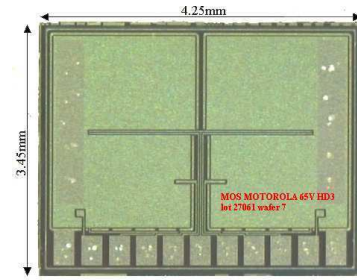


Figure 2.2: View of the MOSFET Motorola 65V HD3 lot 27601 wafer7

2.3. PASSIVE COMPONENT MODELS

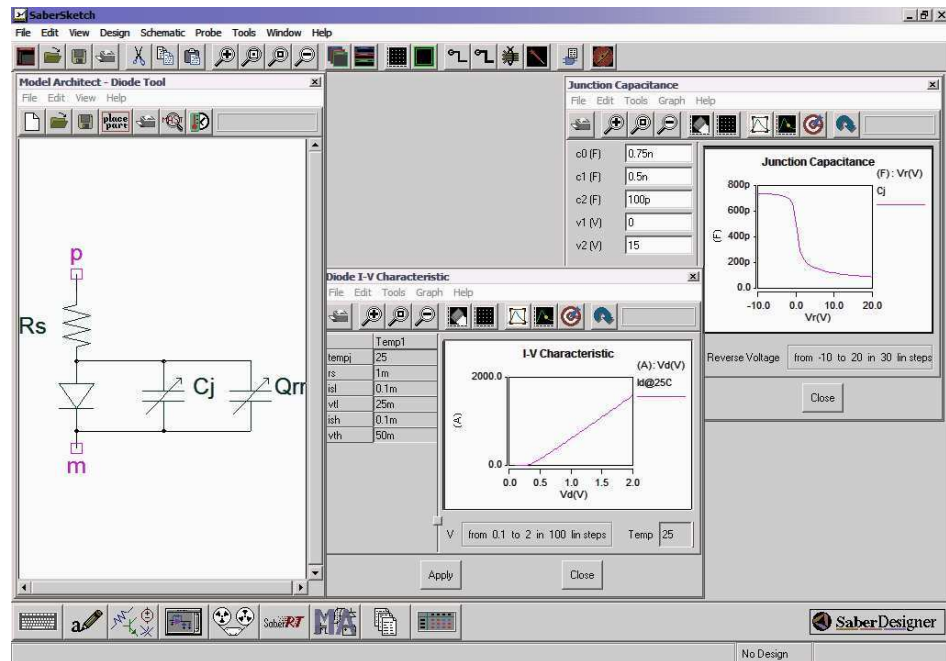


Figure 2.3: Saber - Model Architect

inductor has windings, the model contains DC resistance - R , which will dissipate power as current flows through the inductor. Stray capacitive coupling between the windings and the physical packaging of the inductor should be taken into consideration. The reactance of this parasitic capacitance C determines the high frequency performance of the inductor. Of course, inductor model can be more complex (accounting for the variation of parameters with the frequency, core losses) [13], but it was not estimated to be necessary in this work, where the level of modelling of each component must be consistent.

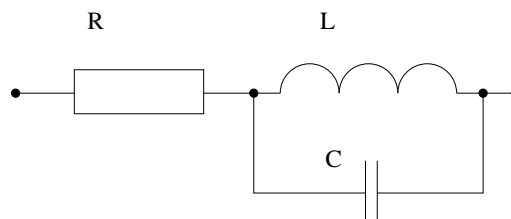


Figure 2.4: The inductor model

These parameters could be obtained from producer data sheet, but similarly as for semiconductors (section 2.2), they usually don't agree with real values. For example, verification for SESI 18K 1WR [72] inductor has been made with impedance bridge (in this case HP 4194A was used). Magnitude curve (fig 2.5) have been obtained using the suitable test fixture, which allows a DC current polarization. The data sheet of inductor presented by manufacturer are different from DC measurement (table 2.1)

As far as conducted EMI are considered, a typical ESL (Equivalent Series Inductance) and ESR (Equivalent Series Resistance) representation is sufficient for capacitors (fig 2.6). The high quality ceramic decoupling capacitors have

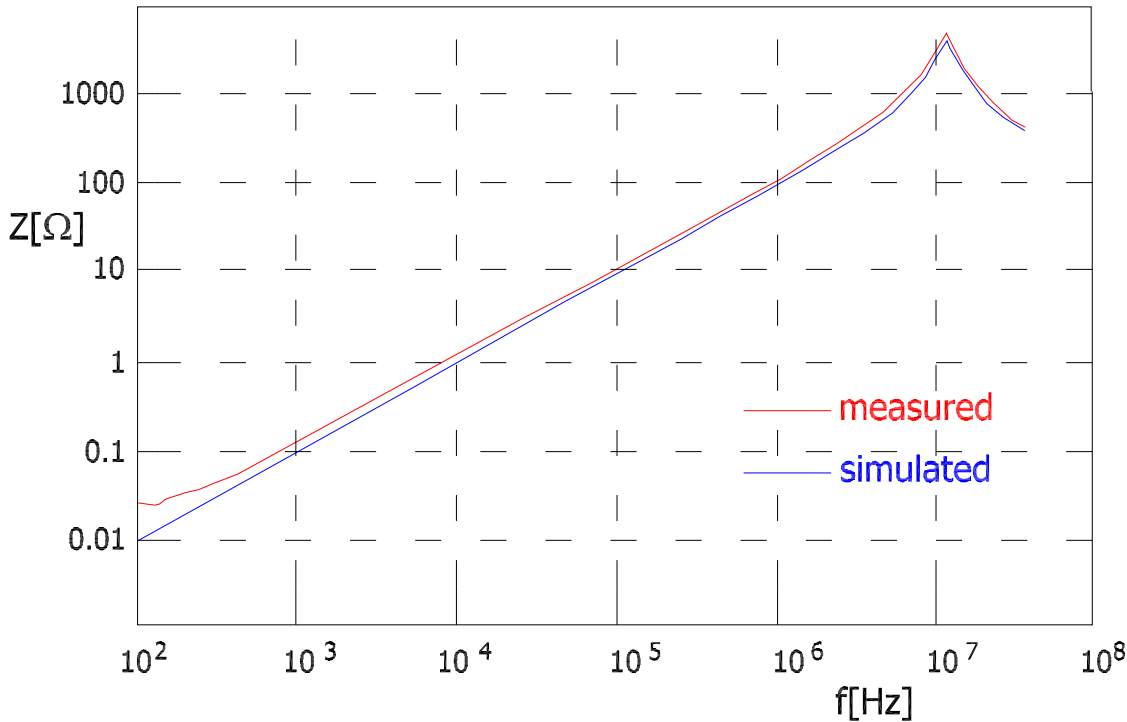


Figure 2.5: The inductor impedance measured and modeled

Table 2.1: The impedance of inductor

—	No load	$I_L = 8A$
$L_{datasheet}$ [$\mu\mathbf{H}$]	18.5	12.9
$L_{measured}$ [$\mu\mathbf{H}$]	16.2	14.7
\mathbf{R} [Ω]	5.5	3.96
\mathbf{C} [\mathbf{pF}]	13	13

about few nH ESL. Similarly, like for inductors, verification of manufactory data sheet of capacitors has been done using impedance bridge. In this case, results don't stay exactly with agreement to the data sheet. For example for ceramic capacitor, which values of capacitance in producer datasheet is 4[mF], has been modeled as series RLC circuit, where $R=28.4$ [$m\Omega$], $L=9$ [nH] and $C=3.9$ [mF]. Inductance and resistance of capacitors bonding have been represented by Saber macrocomponent, described in next section. In figure 2.7 impedance of real capacitor obtained from the HP 4194A, represents the RLC model as in figure 2.6.

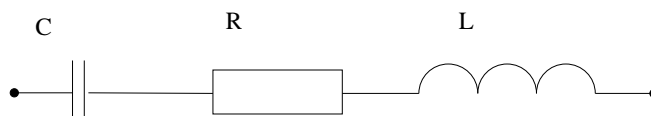


Figure 2.6: The capacitor model

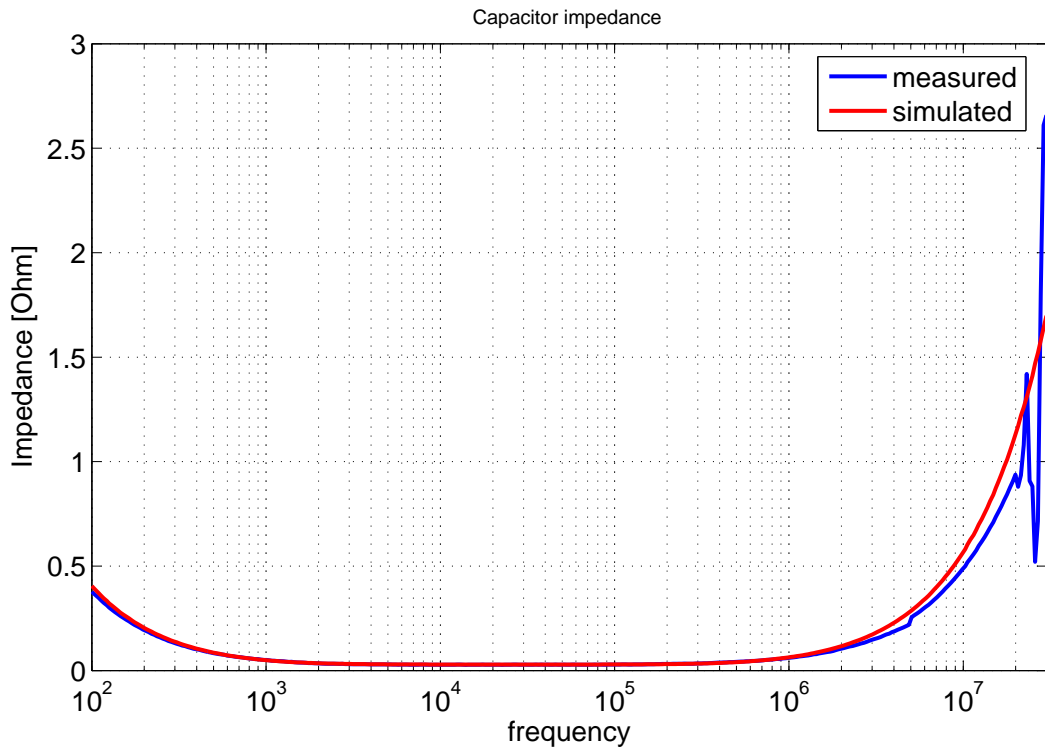


Figure 2.7: The comparative results of impedance measurement with HP 4194A and simulation of RLC model for input ceramic capacitor

2.4 Parasitic layout modeling

In power electronics application for the EMI simulations, models of all components are needed. Inductive and capacitive modeling of parts of circuit such as interconnections, tracks, semiconductors bonding or capacitor wires are necessary. The aim is to find dependencies between geometrical and physical properties of conductors and their RLC models. The resistance, capacitance and inductance values can be found using commercial software or can be calculated using electromagnetic field formulas. In the first case, results are obtained with high accuracy, but it usually demands a lot of programming and calculating time and computer power, in the second case RLC values can be fast estimated but without taking into consideration changing of current density, long line effect and etc.

Values of self and mutual inductance of copper tracks have been calculated using InCa [11] software based on Partial Element Equivalent Circuit (PEEC) method [67]. This method provides a very powerful approach to account for non-ideal behavior of conductors [50]. It is based on analytical formula to compute inductance and coupling, provided a uniform current density. However, due to bonding on copper tracks, current direction is unknown, and a complete inductive meshing must be used, contrary to other modeling used in the past. The density of the current is not constant in all conductor because of skin or proximity effects. The inductive mesh with partial self and mutual inductances guarantee

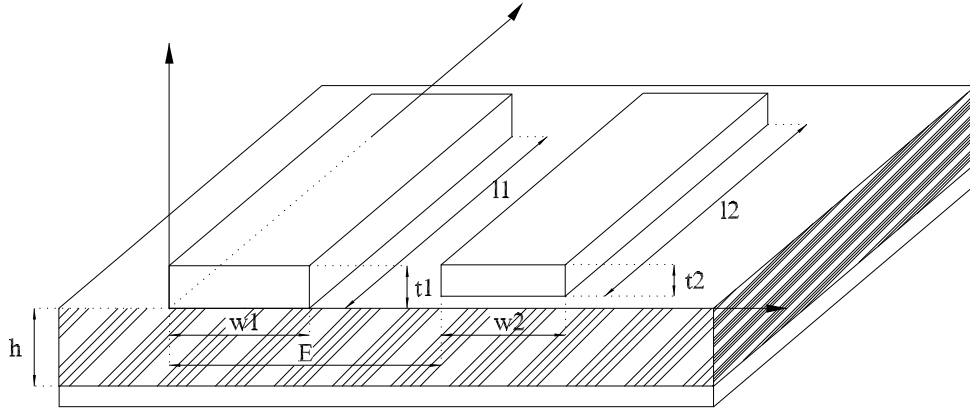


Figure 2.8: The geometrical description of 2 conductors for inductance calculation

correct modeling of this phenomena. The formula used in PEEC method, where as an input geometrical description of the printed circuit board and conductivity of conductors are given, is applied to calculated of the mutual inductance between two coplanar strips and also the self inductance of a micro strip. The inductance has been calculated with the following formula using variables described in Figure 2.8.

$$M_{p12} = \frac{1}{w_1 t_1 w_2 t_2} \sum_{h=1}^4 \sum_{i=4}^4 \sum_{j=4}^4 (-1)^{h+i+j+1} f(q_{h-1}, p_{i-1} o_{j-1}) \quad (2.3)$$

$$q(E, w_1, w_2) = \begin{pmatrix} E - w_1 \\ E + w_2 - w_1 \\ E + w_2 \\ E \end{pmatrix}, r(P, t_1, t_2) = \begin{pmatrix} E - t_1 \\ E + t_2 - t_1 \\ E + t_2 \\ E \end{pmatrix} \quad (2.4)$$

$$o(l_1, l_2, l_3) = \begin{pmatrix} l_3 - l_1 \\ l_3 + l_2 - l_1 \\ l_3 + l_2 \\ l_3 \end{pmatrix}$$

$$f(x, y, z) = (y^2 \frac{z^2}{4} - \frac{y^4}{24} - \frac{z^4}{24})x - \ln(\frac{x^2 + \sqrt{x^2 + y^2 + z^2}}{\sqrt{y^2 + z^2}}) + (y^2 \frac{x^2}{4} - \frac{y^4}{24} - \frac{x^4}{24})z -$$

$$\ln(\frac{z^2 + \sqrt{z^2 + y^2 + x^2}}{\sqrt{y^2 + x^2}}) + (x^2 \frac{z^2}{4} - \frac{x^4}{24} - \frac{z^4}{24})y - \ln(\frac{y^2 + \sqrt{x^2 + y^2 + z^2}}{\sqrt{y^2 + x^2}}) +$$

$$+ \left[\frac{1}{60}(x^4 + y^4 + z^4 + 3x^2 y^2 + 3z^2 y^2 + 3x^2 z^2) + \sqrt{x^2 + y^2 + z^2} \right] \quad (2.5)$$

$$+ \frac{(-1)xyz^3}{6} \arctg(\frac{xy}{z\sqrt{x^2 + y^2 + z^2}}) + \frac{(-1)xzy^3}{6} \arctg(\frac{xz}{y\sqrt{x^2 + y^2 + z^2}}) +$$

$$+ \frac{(-1)zyx^3}{6} \arctg(\frac{zy}{x\sqrt{x^2 + y^2 + z^2}})$$

Important thing is to choose correct way of the segmentation of conductors and their places in the circuit in order to assure correct modeling including phenomena such as skin effect or non-uniform current density [71]. Consequentially, inductive behavior of each conductor is represented in a simulation circuit by inductors mesh.

Using strictly results from PEEC method in circuit simulator is an undue burden on computer simulation. Therefore, a model reduction for inductive aspects has been proposed [44]. The points of connections between components and copper tracks have been apportioned - the idea is similar to scattering matrix from the microwave theory: the complete geometry is seen from input-output only. For each conductor linking several access, one is taken as reference (fig. 2.9). This referenced points have been linked to each other for the same connection. It allows to reduce the inductive representation of all conductors to minimum number of differential equations. The equations linking voltages (with respect to this reference point) to currents are deduced from global PEEC model as follows:

$$V_i = \sum_{j=1}^n \left[R_{ij} * I_j + L_{ij} \frac{dI_j}{dt} \right] \quad (2.6)$$

where R_{ij} , L_{ij} and I_j are resistance, inductance and current of partial branch.

This equation corresponding to the impedance matrix has been applied to generate *Saber*® macro component, which represent all self and mutual inductance behavior of all conductor tracks.

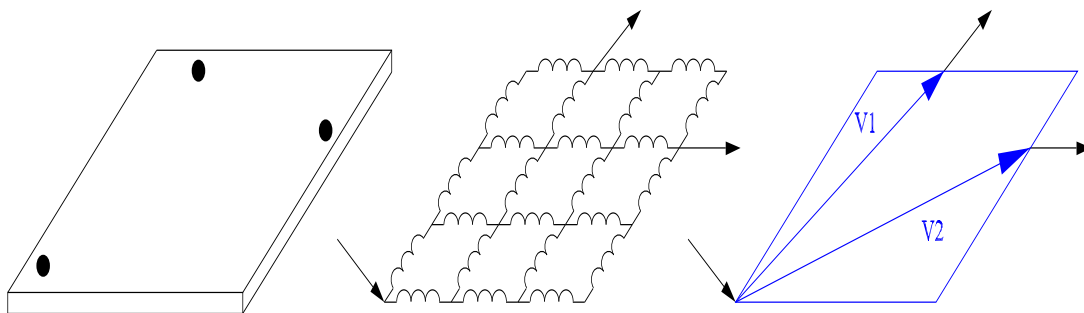


Figure 2.9: The reduction of PEEC inductive model for one interconnection

In this thesis, inductance calculations have been done with PEEC method, which gives the most accurate value and also formulas for inductance of micro strip by Paul, which allows to make fast estimation [55].

The parasitic capacitance behavior of layout is as important as inductive one and has impact on EMI spectrum. Values of parasitic capacitances are dependent on the geometry of physical structure. In general dielectric and insulate material properties (dielectric constants) thickness and width of conductors are known.

The formulas presented are well known but results of calculation have been checked and compared with measurements for few different structure of conducted tracks [48], what allows to confirm dielectric thickness and effective dielectric constant.

Parallel plate formula:

$$C = \epsilon_0 \epsilon_r \frac{w}{h} [F/m] \quad (2.7)$$

Wheeler formula [7]:

$$C = \frac{1.122 \epsilon_r}{\ln \left[1 + \frac{1}{2} \left(\frac{8h}{w_{eff}} \right) \left(\frac{8h}{w_{eff}} + \sqrt{\left(\frac{8h}{w_{eff}} \right)^2 + \pi^2} \right) \right]} [pF/m] \quad (2.8)$$

Wheeler/Schneider formula [7]:

$$C = \frac{1.122 \epsilon_{eff}}{\ln \left[1 + \frac{1}{2} \left(\frac{8h}{w_{eff}} \right) \left(\frac{8h}{w_{eff}} + \sqrt{\left(\frac{8h}{w_{eff}} \right)^2 + \pi^2} \right) \right]} [pF/m] \quad (2.9)$$

where ϵ - the dielectric constants, w, l and t - width, length and thickness of the track, h - the space between the track and ground and additionally coefficients have been defined as follow:

$$\epsilon_{eff} = \frac{\epsilon_r + 1}{2} + \frac{\epsilon_r - 1}{2} \left(1 + \frac{10h}{w} \right)^{-1/2} \quad (2.10)$$

$$w_{eff} = w + \frac{t}{\pi} \ln \left[\frac{4e}{\sqrt{\left(\frac{t}{h} \right)^2 + \frac{1}{\pi \left(\frac{w}{t} + 1.1 \right)^2}}} \right] \quad (2.11)$$

Paul formula [55]:

$$C = \frac{Z_c}{v} [F/m] \quad (2.12)$$

where for $w/h < 1$

$$Z_c = \frac{60}{\sqrt{\epsilon'_r}} \ln \left(\frac{8h}{w} + 0.25 \frac{w}{h} \right) \quad (2.13)$$

and for $w/h > 1$

$$Z_c = \frac{377}{\sqrt{\epsilon'_r}} \left[\frac{w}{h} + 1.393 + \frac{2}{3} \ln \left(\frac{w}{h} + 1.444 \right) \right]^{-1} \quad (2.14)$$

$$\epsilon'_r \cong \frac{1}{2} (\epsilon_r + 1) \quad (2.15)$$

2.4. PARASITIC LAYOUT MODELING

Then, all stray capacitances have been calculated using Wheeler/Schneider or Paul formulas. These formulas work pretty well and also appreciate edge effects. Additionally, Paul's method takes care about the width-to-height ratio and gives the most satisfied result.

According to PEEC method, a capacitive meshing can also be used. Parasitic capacitance to the ground for each track can be represented by capacitors mesh. Unfortunately this mesh is not the same like inductors one, so simplification has been made (fig. 2.10).

All capacitors from mesh can be replaced by equivalent one $\sum C_i$, if:

- all resonant frequencies $\frac{1}{2\pi\sqrt{LC_i}}$ for each pair of LC are greater than 30 MHz
- there is no long line effect in the conductor during normal operation.

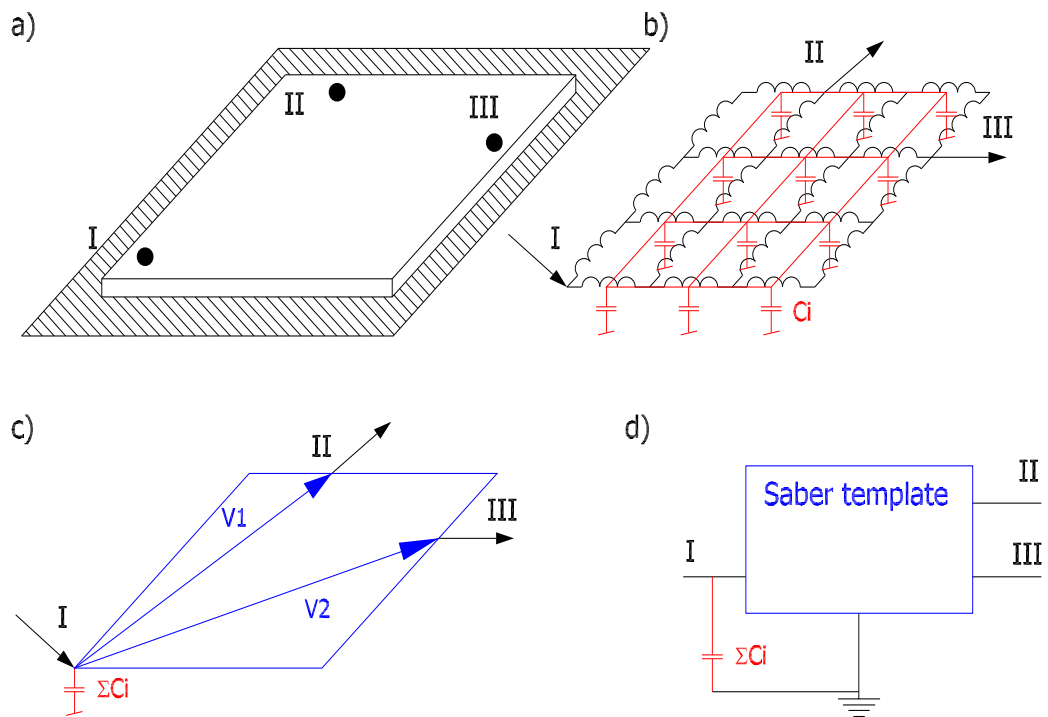


Figure 2.10: The reduction of PEEC capacitive model for one interconnection
 a) view of conductor b) inductive and capacitive meshes c) equivalent circuit
 d) *Saber*® template

The main input and output points of the circuit or points of main current input in copper tracks should be chosen as the reference points, where equivalent capacitor can be connected to as in figure 2.10.

Criteria of reference points selection:

- inputs and outputs point of supply voltage,
- inputs and outputs of passive components,
- point of connection a semiconductors is legs and the track,
- output points, where load connected.

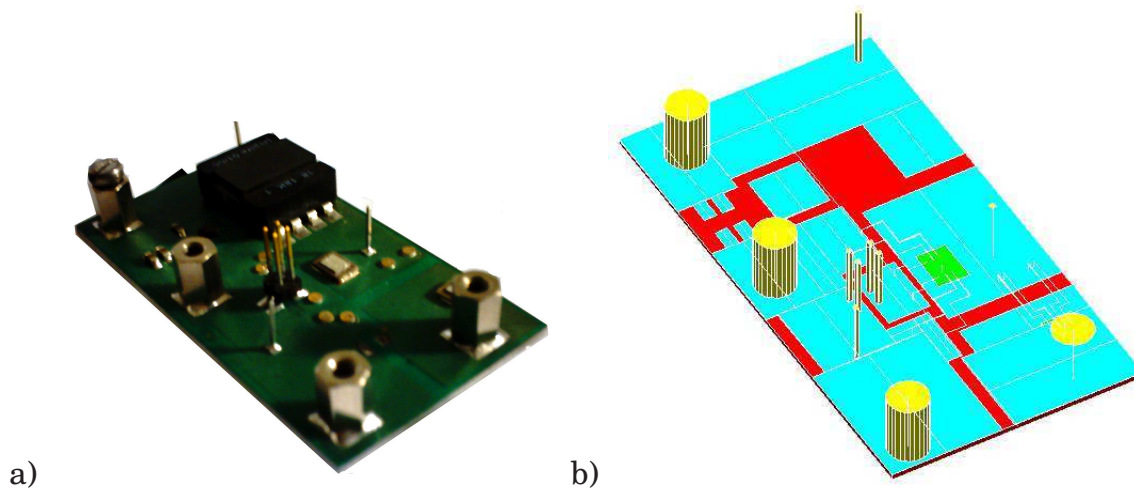


Figure 2.11: The boost converter a) view b) INCA model.

Chapter 3

DC-DC boost converter

Why speculate when you can calculate?

John Baez

3.1 Introduction

Investigations on conducted EMI of hard switching boost converter have been carried out. The converter is dedicated to transfer energy between 14V and 42V DC buses. It has been designed for typical automotive applications where these two levels of voltage can be found. This well known power electronics application [16],[62],[90], [86] was chosen because of electric structure simplicity. This enabled to relatively easily understand and simulate EMC - it contains only two active components - Schotky diode and MOSFET transistor. This DC-DC converter has been realized on the IMS (Insulated Metal Substrate) [4],[70]. This technology allows to obtain low inductive interconnections between components and also high value of surfacing capacitance (in range between 100 pF and 1000pF), thanks to proximity of the ground plane (70 μ m). Therefore, the generated disturbances level is quite low and common mode noise is dominated, that can cause the problems during measure process.

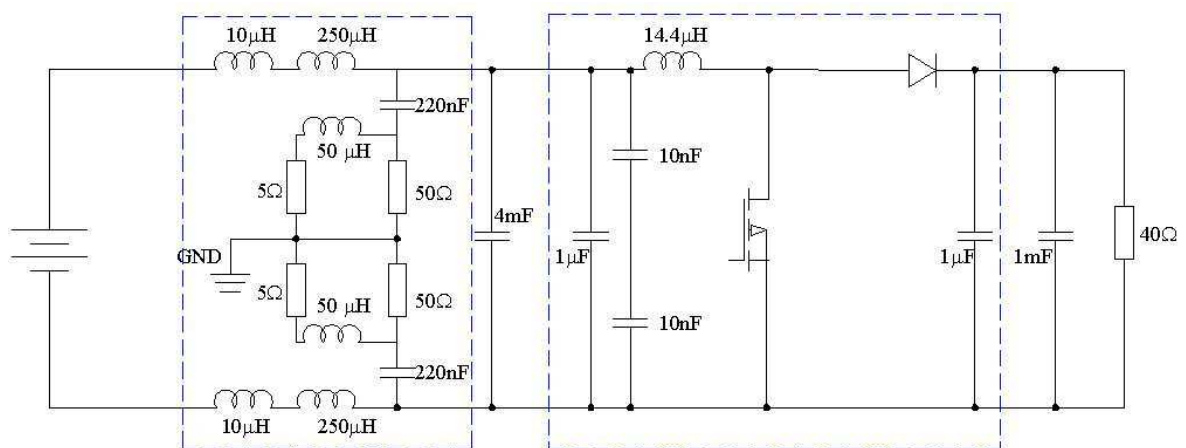


Figure 3.1: The fundamental schematic diagram of the boost converter including LISN

The base schema of testing system of DC-DC converter is presented in Figure 3.1. Switching frequency of MOSFET transistor is $f=100\text{kHz}$ with the duty cycle 0.75. Working application has been supplied from DC voltage source 12 V through LISN, as a load on output $2 \times 20 \Omega$ resistors were used. Decoupling input $C_{in}=4\text{mF}$ and output $C_{out}=1\text{mF}$ were added.

Voltage for MOSFET transistor driven was generated from the external auxiliary circuit. The transistor was driven in two ways:

1. Square wave generator was based on SG3524 regulating pulse width modulator which allows to change switching frequencies and duty cycle. Simply MOSFET driver was built with PNP (BD138) and NPN (BD137) silicon transistors, that allows to obtain the rise t_r or the fall time t_f in the range of few μs , what is similar to V_{ds} time changes. Driver schema is presented in figure 3.2. All control circuit has been placed on universal plate.
2. Special fast dedicated driver has been used, that allows to reach t_r and t_f in the range of μs fractions.

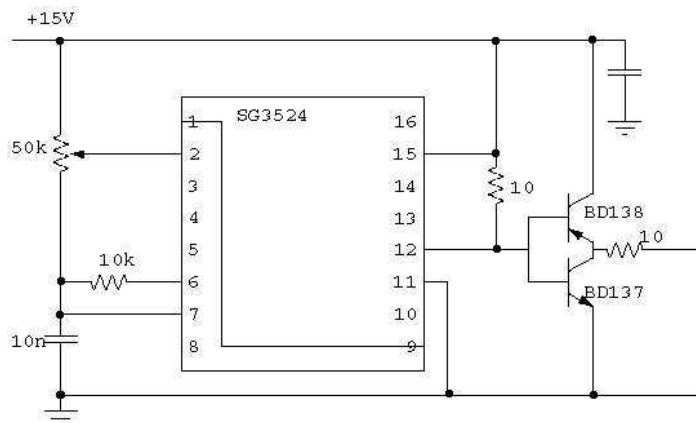


Figure 3.2: The simple driver schema

In order to decrease common mode current from control circuit, common mode filter (figure 3.3) has been added between driver and MOSFET. In this filter each winding of the inductor - wound on combinatorial core - is merged in series with the signal wired. The flux created by each winding cancels the flux in opposing winding. The insertion differential impedance of the inductor in the circuit is negligible small.

3.2 Accurate simulation

Simulations of complex model of the considered converter has been carried out using the circuit simulator [49]. Figure 3.4 presents equivalent *Saber*® scheme of the boost converter, the LISN and load. The models have been defined according to chapter 2. All interconnections of converter (IMS, screws and bondings)

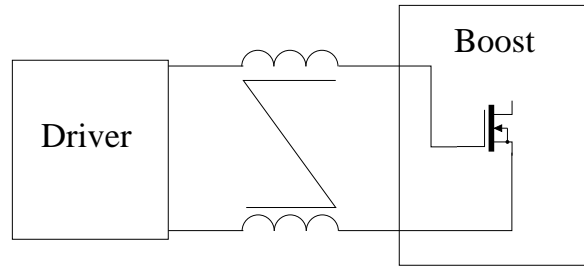


Figure 3.3: The common mode filter between driver and boost

have been modeled in InCa [44] and summarized into a single macro components, using differential equations. Additional blocks represent capacitors wires.

Simulations have been carried out using variable calculation step, in the range from 1 ps to 100 ns. It is possible to observed all currents and voltages, but in this thesis the waveforms connected with converter EMC behavior first of all are presented. The magnitude of FFT of noise generated in the boost converter and registered on LISN is presented in fig. 3.5. The analyses have been done using *SaberScope*® tools. The y-axis present normalized amplitude with respect to a volts reference, where normalization coefficient k depends on sampling frequency f_s , thus $[V/Hz]$ units are used.

$$dB [V/Hz] = \frac{1}{k(f_s)} \cdot 20 \cdot \log_{10} \left[\text{abs} \left(FFT \left(\frac{V}{1} \right) \right) \right] \quad (3.1)$$

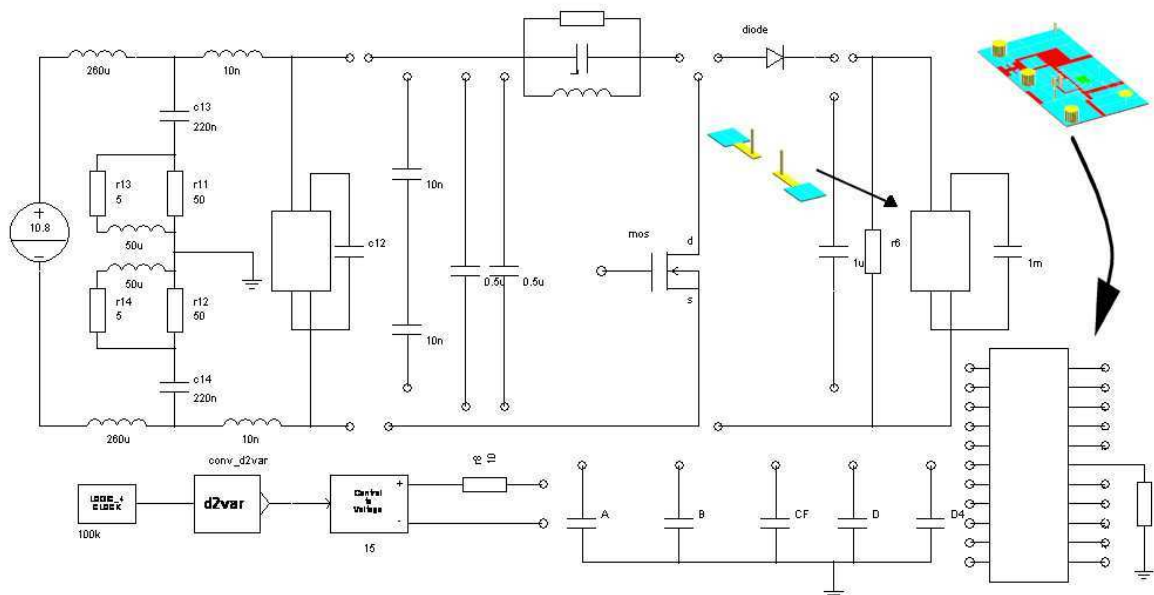


Figure 3.4: The Saber circuit including boost converter, LISN, supply, load and cabling

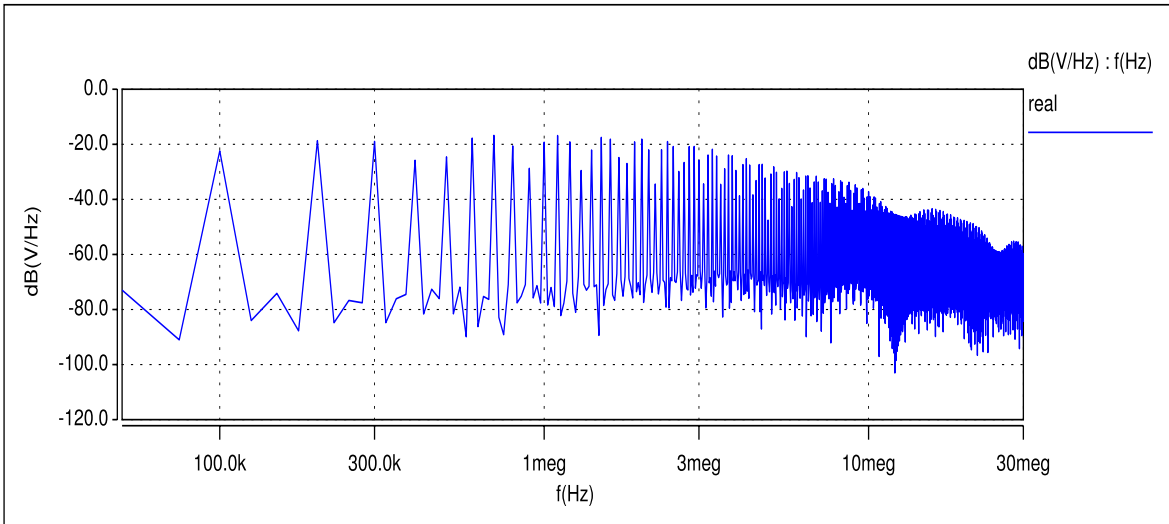


Figure 3.5: The LISN voltage spectrum obtained with Saber

3.3 Sensors influence

Two kinds of layout of DC-DC boost converter were taken into investigation. The first one is the typical application ready to apply in industrial, second one - similar to first but with specially designed extensions for currents measurement. The sensors have been added: the one - in MOSFET main current branch and the second in diode branch. It allows to measure currents in semiconductor devices, what is an important aspect for EMC analysis.

The simulations for this two layouts have been done to check influence of the sensors on level of global perturbation generated in the application. It is imposible to solve this problem during laboratory work, but it can be easily done with simulation. It is obvious that values of parasitic capacitances and inductances are different for this two structure. Those parameters have changed because new conductors were added and the shape of others have changed. It is the main reason of differences in the EMI spectrum.

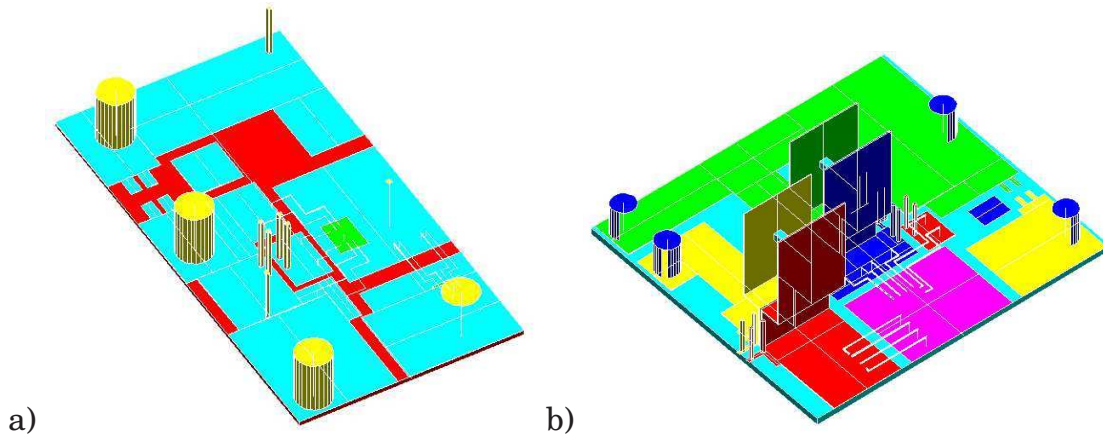


Figure 3.6: The layouts of DC-DC boost a) without sensors b) with sensors

3.3. SENSORS INFLUENCE

In order to calculate inductance, these two layouts have been described in InCa. The parasitic capacitances between tracks and ground have been calculated using the Wheeler/Schneider formula. Because the dimensions of these two structures are different, it can be noticed that values of parasitic inductances and capacitances are greater for boost with current sensors.

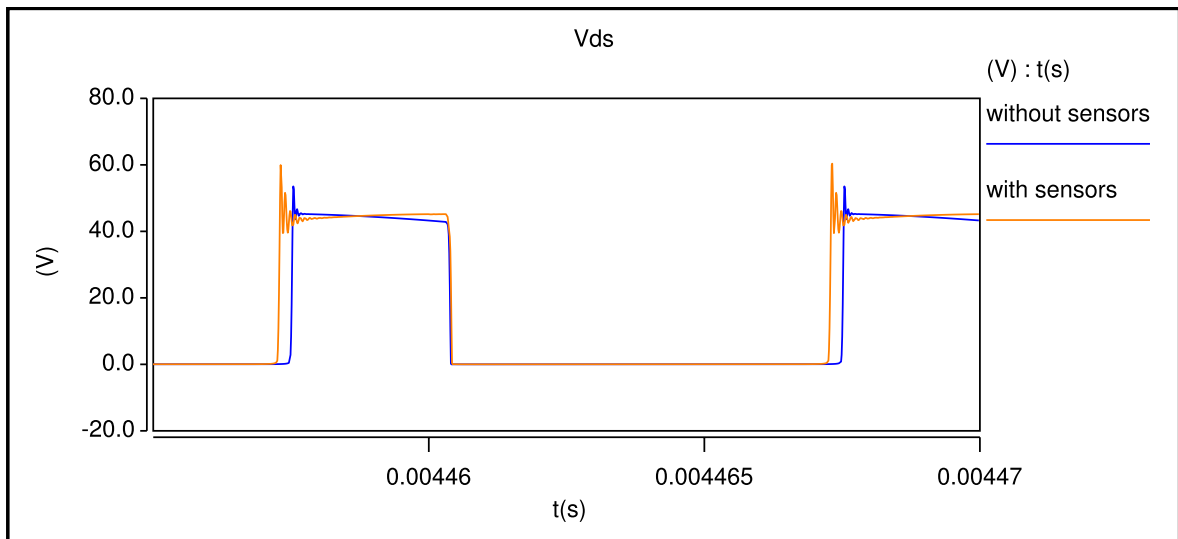


Figure 3.7: The comparison of MOSFET voltage V_{DS} for boost with and without sensors

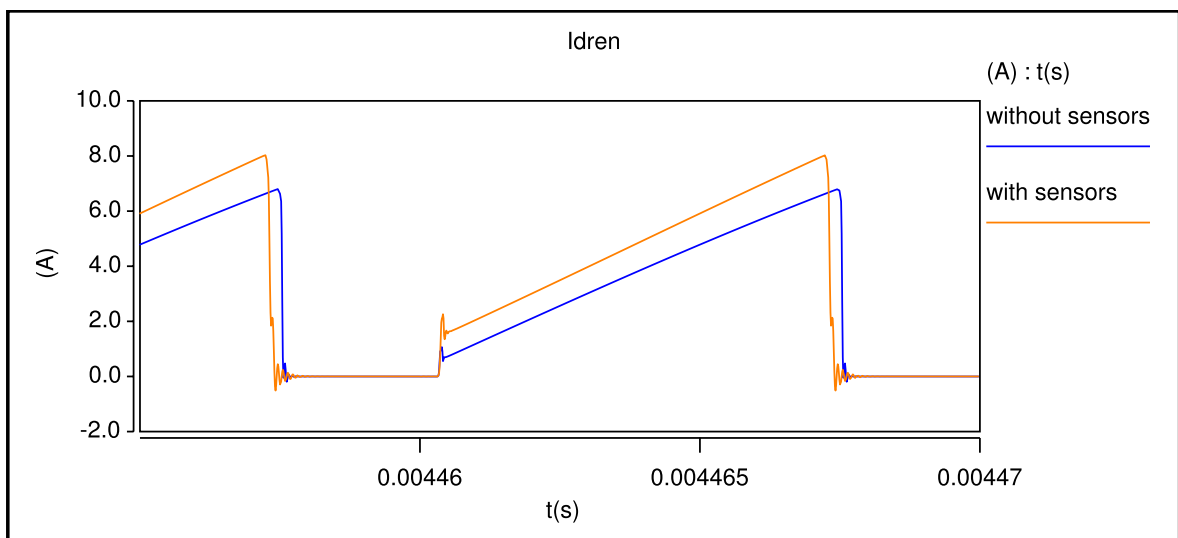


Figure 3.8: The comparison of MOSFET current (I_D) for boost with and without sensors

In order to compare these two layouts, two circuits have been simulated with Saber. The main schema of both applications were exactly the same (all main components, parameters and values), only geometrical shape and dimension of conductors were different, as it is shown in figure 3.6 what has an influence on values of parasitic capacitances and inductances. In simulation schema it was reflected by changes in Saber macrocomponents generated from InCa file for

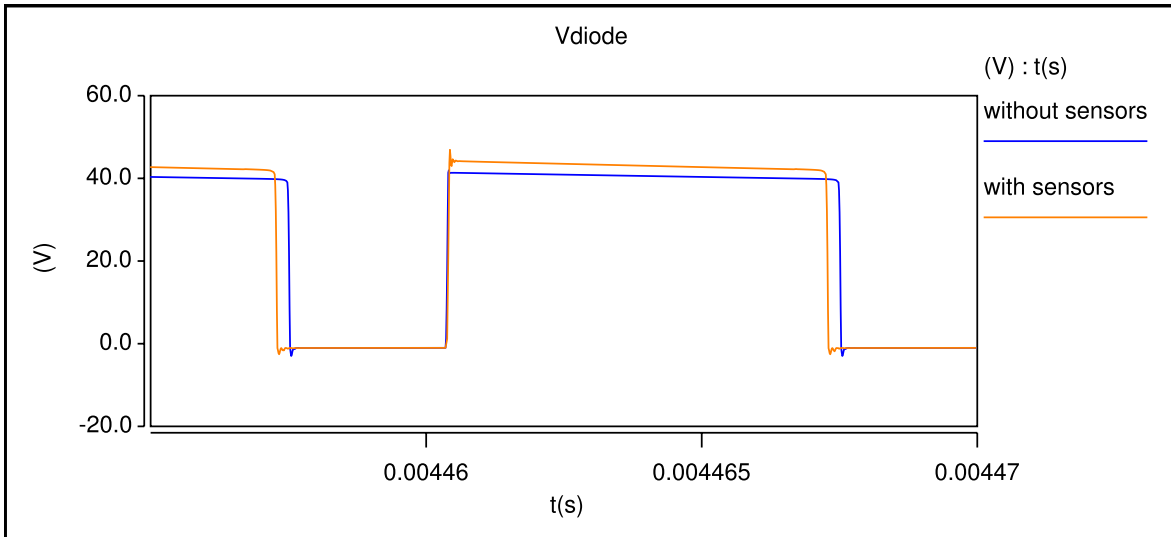


Figure 3.9: The comparison of diode voltage for boost with and without sensors

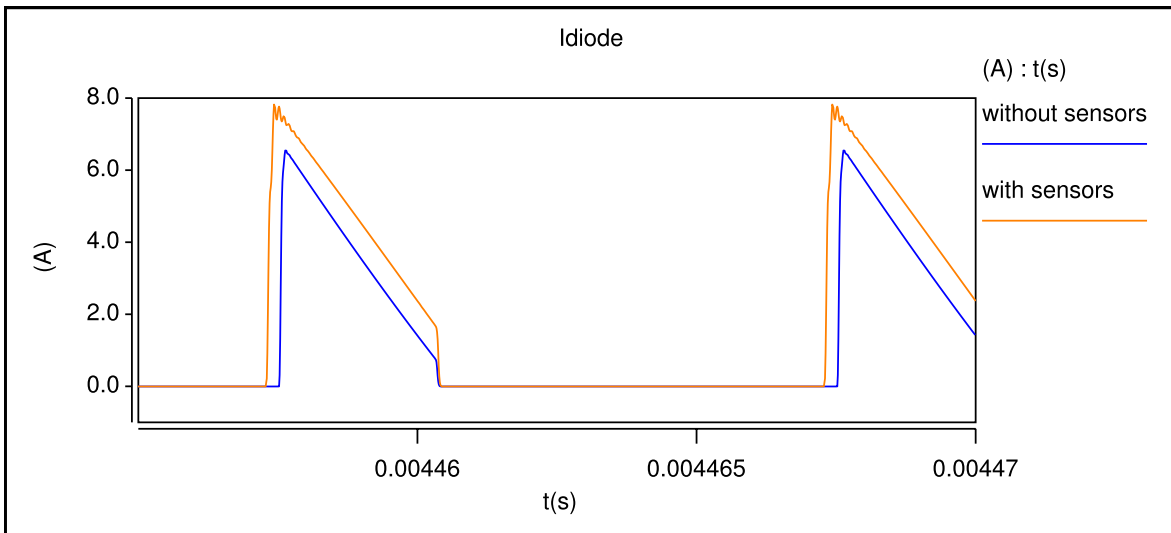


Figure 3.10: The comparison of diode current for boost with and without sensors

each layout and also values of parasitic capacitances represented by five capacitors. Moreover, simulations have been done with the same numerical method with the same conditions and parameters. Influences of it on power waveforms of semiconductor voltage and current obtained with simulations are illustrated in figures 3.7, 3.8, 3.9, 3.10. The different for those two layers are especially visible in waveforms, notably rise and fall time, oscillations and peak values during commutation. It confirms and proves that additionally parts like sensors or conductors affect on EMC behavior of converter. The generated perturbations have similar level for both circuits (fig. 3.11), only for frequency in range from 12 MHz to 25 MHz perturbation from DC-DC boost converter with sensors are smaller, because it can be more propagate inside the system what is consequence of additional electromagnetic linkages in sensors. Moreover, the amplitude of presented currents (figures 3.8 and 3.10) are different, because circuit with sensors

3.4. SENSITIVITY STUDY

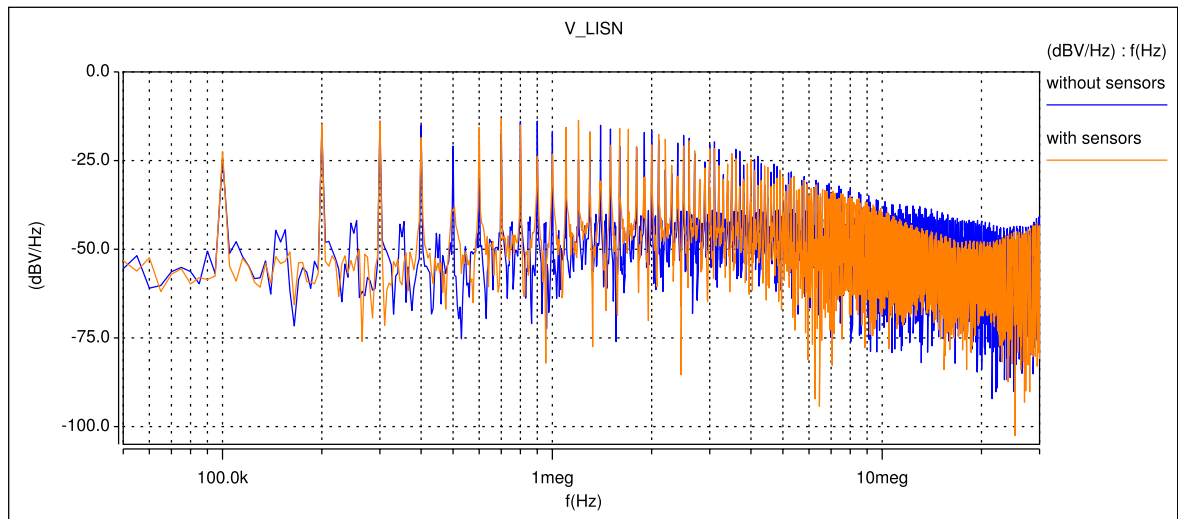


Figure 3.11: The comparison of generated perturbation from boost with and without sensors

contains resistors, which are placed series with MOSFET and diode.

3.4 Sensitivity study

In order to better understand the contribution of each parameter of the model to EMI spectrum, a sensibility study has been carried out. Each time, one element of the complete EMC model has been replaced with new one with ideal behavior. The comparison of this new result with the complete one allows to determine the influence of the modified component. In this study, the main goal is to determine the importance and the frequency range of chosen component (semiconductors, interconnections etc.) on perturbation level impact. This knowledge is very useful in design and optimization of layout geometry and properties and it allows to find the most appreciable parameters.

3.4.1 Semiconductors influence.

Model of the MOSFET transistor - including parameters presented in the chapter 2 - has been used in the complete simulation. It has been constructed with *Saber*® tool the Model Architect. In the next step, it has been replaced by ideal MOSFET model (...no charge storage & ideal, simple characteristics...) [1] and new simulations have been done. The LISN voltages from these two circuits are presented in fig. 3.12. The differences of spectrum envelope can be seen in a range above 5 MHz, which is connected with distinct turn on and off times of the MOSFET.

The dynamic parameters - responsible for turn on and turn off processes - play the main role in EMI of the MOSFET behavior. When the dynamic parameters of MOSFET are altered, envelope of spectra in mentioned range also

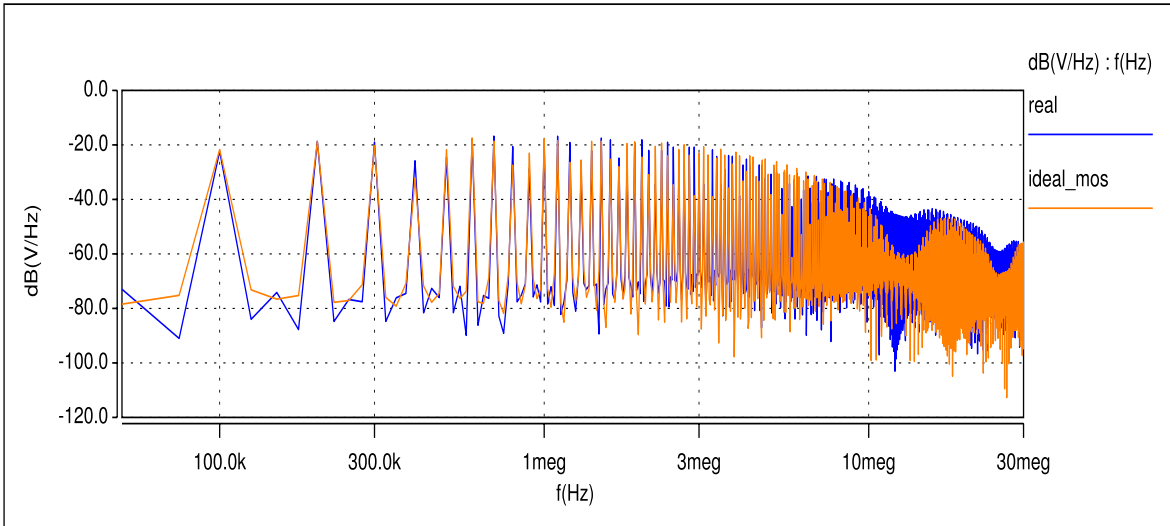


Figure 3.12: Influence of MOSFET parameters on LISN spectrum

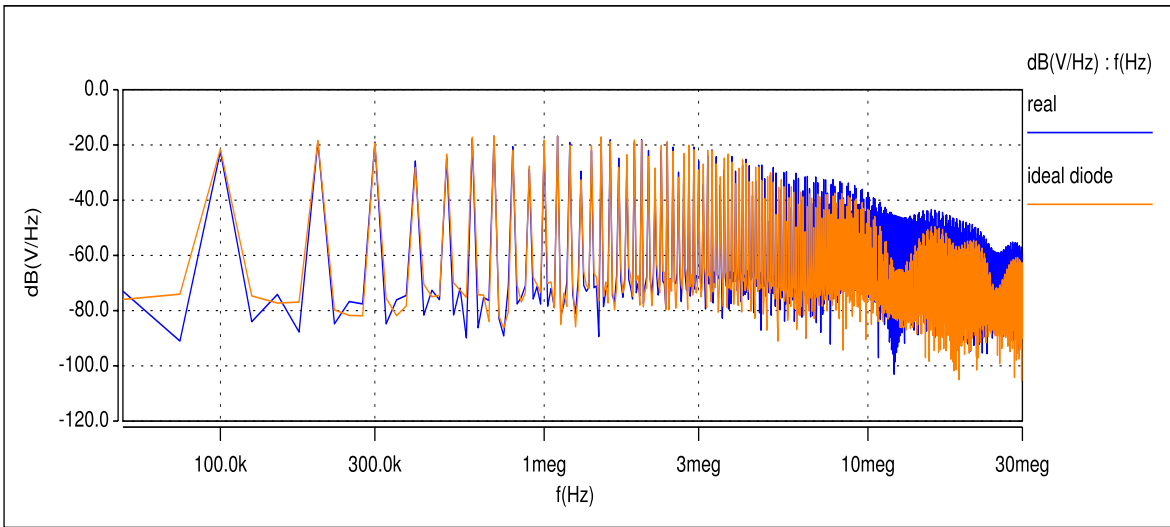


Figure 3.13: Influence of power diode parameters on LISN spectrum

changes. In the further works, investigation can be made, which semiconductor parameters are the most critical.

Other series of simulations have been made by replacing power Schotky diode model with ideal diode model. It can be noticed from the fig. 3.13, that the differences in EMI spectrum starts at 3 MHz, but is especially noticeable around 10 MHz. It is strongly connected with the junction capacitance. Concluding, semiconductor models have great importance in the high frequency part of the spectrum.

3.4.2 Layout influence

Inductive modeling of the tracks cannot be negligible in accurate EMI forecasting. Stray inductances play a great role in commutation and have an effect on voltages and currents in the circuit. In addition, because of resonance with

3.4. SENSITIVITY STUDY

capacitance, oscillations occur at frequencies depending on their values. The influence of stray inductance is shown in fig. 3.14, where comparison of results of simulation with and without parasitic inductances, represented by *Saber*[®] macro component generated in InCa, is presented. However in some cases, since layout provides low inductances (for example for IMS technology), stray inductance may be neglected without appreciable decreasing of simulation precision.

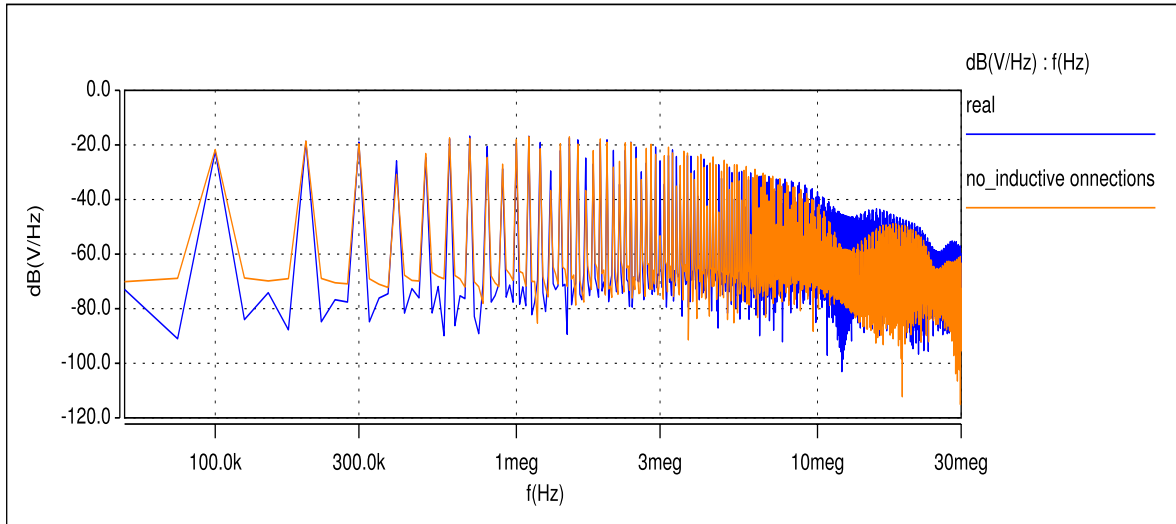


Figure 3.14: The influence of inductive connections on LISN spectrum

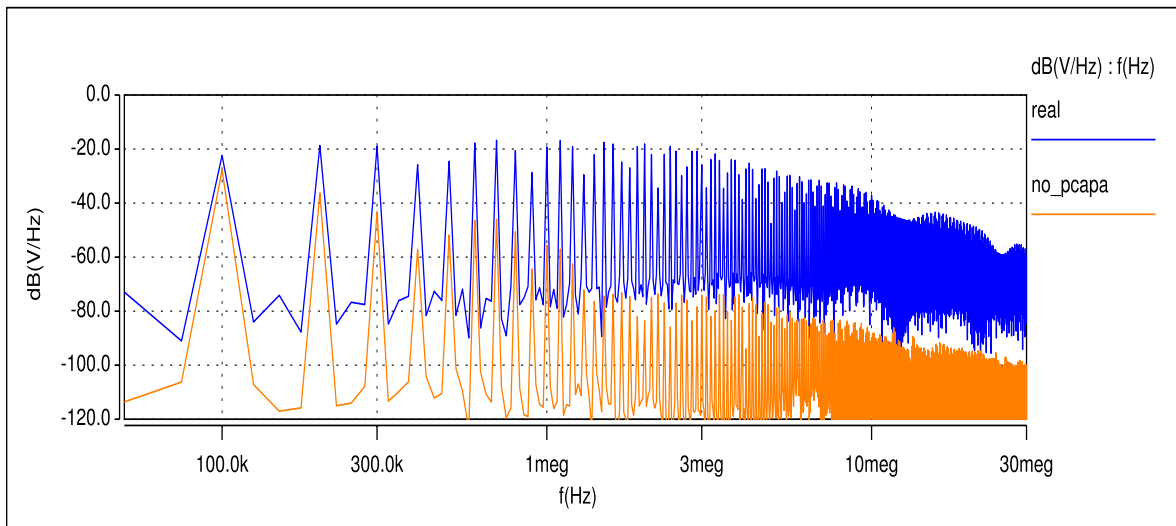


Figure 3.15: The influence of parasitic capacitances on LISN spectrum

On the other side, parasitic capacitance of copper track can be removed. For IMS circuit, stray capacitances have comparatively great values and their role is consequently significant. Removing parasitic capacitances give great difference on spectra for the whole frequency range of emitted EMI. It can be said that parasitic capacitance is an important parameter for EMC behavior description and it is important parameter in EMI forecasting. Using the same idea, it is easy to replace in simulation IMS substrate with conventional PCB (change

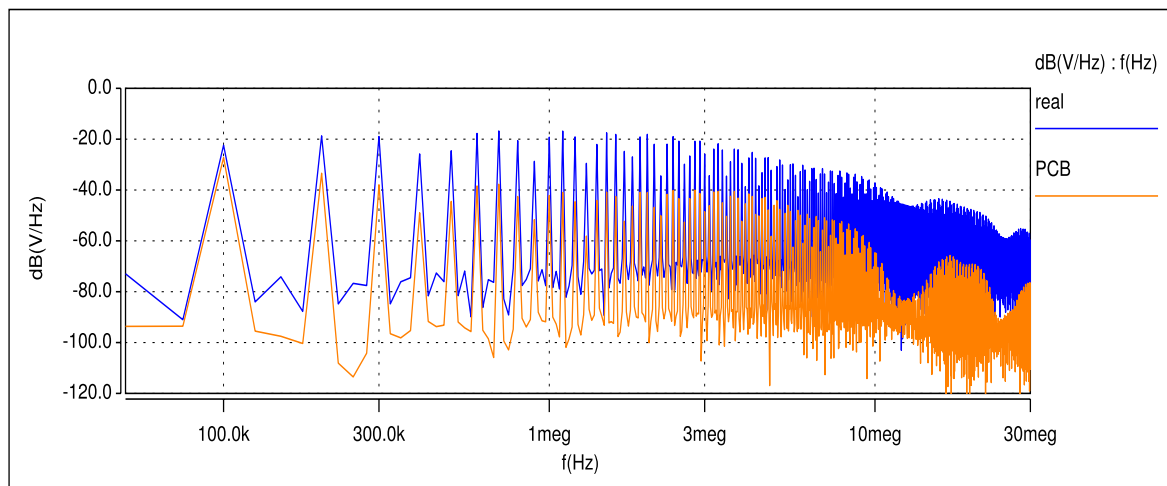


Figure 3.16: The spectrum of LISN voltages for PCB and IMS (real)

space between tracks and ground). This operation results in an increase of stray inductances, and a decrease of stray capacitances ($100 \div 1000$ pF for IMS and from $1 \div 50$ pF for PCB). This difference is due to the modification distance to the ground plane (1.3 mm for PCB and 70 m for IMS). The comparison of LISN spectrum for these two layout technologies is presented in fig. 3.16. Disturbances generated in PCB layout circuit are much lower than those from IMS, due to lower stray capacitance. Thus, it should be said that parasitic inductance and capacitance of conductors play an important role in EMI generation and every kind of forecasting calculation should contain these parameters.

3.5 Simplification of boost model for forecasting EMI

A better knowledge of EMC generation mechanisms has allowed the construction of a simplified circuit to forecast EMC behavior of the boost converter. Since inductive characteristics of the interconnections and the semiconductor switching characteristics act in the high frequency range mainly, the MOSFET and the diode have been replaced with a simple voltage source, and no inductive parameters have been taken into account for interconnections. On the contrary, all capacitive aspects were kept in the modeling. In this simple scheme (Fig. 3.17) can be found the LISN (C_n , R_n and L_n), the input capacitors (C_1 , C_2 and C_3), the input inductor (L , C_L , R_L). Two main parasitic capacitances due to the layout are also taken into account, which are taken from the complete capacitive model. This leads to a very reduced linear model, and therefore to fast calculations.

It can be implemented in a simple Mathcad document or with other computation languages and fast and easy calculations in the frequency domain. Spectrum obtained with Mathcad sheet is presented in fig 3.18. It can be noticed that in this particular case, for frequencies below 10 MHz results are similar to those

3.5. SIMPLIFICATION OF BOOST MODEL FOR FORECASTING EMI

from measurement (presented in the next section in figure 3.22) and *Saber*® simulation (fig. 3.5). Moreover, the differences above 10 MHz in shape are not greater than 10 [dB].

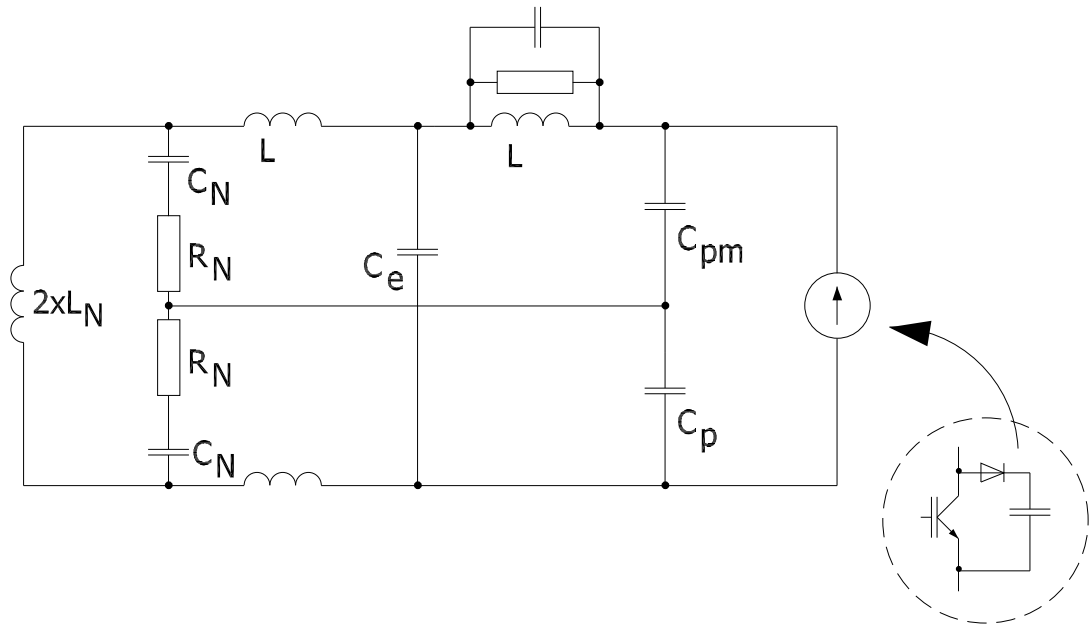


Figure 3.17: Schema of simplified boost converter model for EMI forecasting

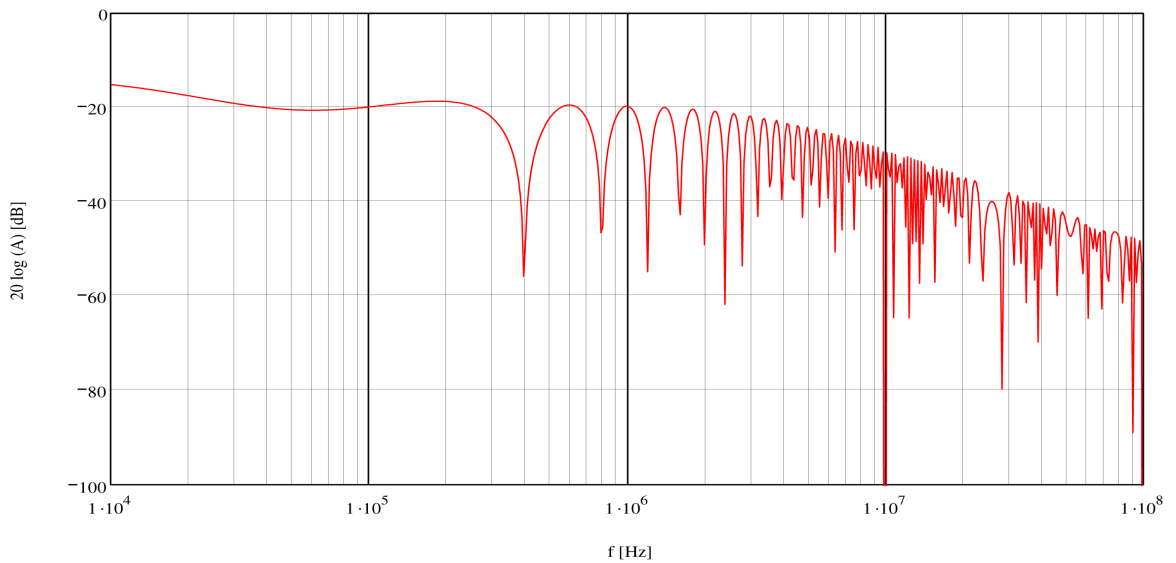


Figure 3.18: Spectrum of LISN voltages obtained with simplified Mathcad model

This scheme was presented in details in [16] and used to improve the capacitive layout of this converter, with respect to EMC constraints. The simple DC-DC boost converter model can be used in layout optimization because it allows to obtain correct results in the frequency range under 10 MHz. The modeling and prediction of conducted EMI using this model could be useful as a fast design and optimization tool for power electronic applications. The most important

parameters of parasitic capacitance and passive components, LISN parameters and simplify trapezoid shape of the voltage from the switch including true turn on and turn off times are only needed.

Moreover, this model also can be easily used to find the transfer function between semiconductor switch voltage from consider application and perturbation, in order to describe converter EMI behavior. The one from DC-DC boost converter is presented in figure 3.19.

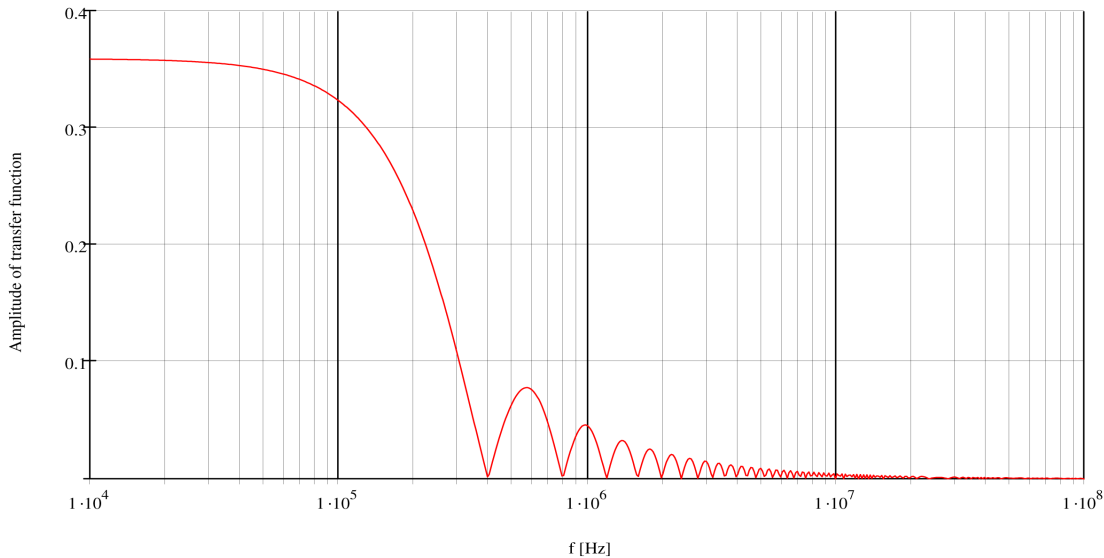


Figure 3.19: The transfer function between semiconductor switch voltage from DC-DC boost converter and perturbation

3.6 Experimental results

An experimental investigation on conducted EMI of DC-DC boost has been carried out. The converter has been connected to power supply through a LISN,



Figure 3.20: View of DC-DC boost converter, driver and LISN

where spectrum from 50 kHz to 30 MHz has been measured in typical conditions of work using spectrum analyzer HP 8560A. Many difficulties were encountered to achieve accurately this measurement. Indeed, great part of the emitted noise came from the driver. Voltage quick variations of the driver (15V) are synchronous with the one of power circuit (42V).

In spite of it, two kind of drivers have been used:

- 1) - simple, slow driver based on PNP and NPN transistors with low level of generated EMI noise,
- 2) - special dedicated for this kind of application, fast, controlled by square signal generator with high level of generated perturbation.

3.6. EXPERIMENTAL RESULTS

Comparison of simulations and measurements have been made for the first one. Reducing of noise emitted by driver has been realized using common mode filter and by disposing it far from the ground plane, but total decreasing of it was not possible.

The EMI level on the two legs of the LISN (DC+ and DC- legs) are exactly the same. This remark can be made in both simulation and measurement. This phenomenon can be attributed to the use of nearly perfect input capacitors (ceramic), which first contributes to differential mode cancellation, and second leads to a symmetrical path for common mode current through DC plus and DC minus tracks as it is shown in figure 3.21.

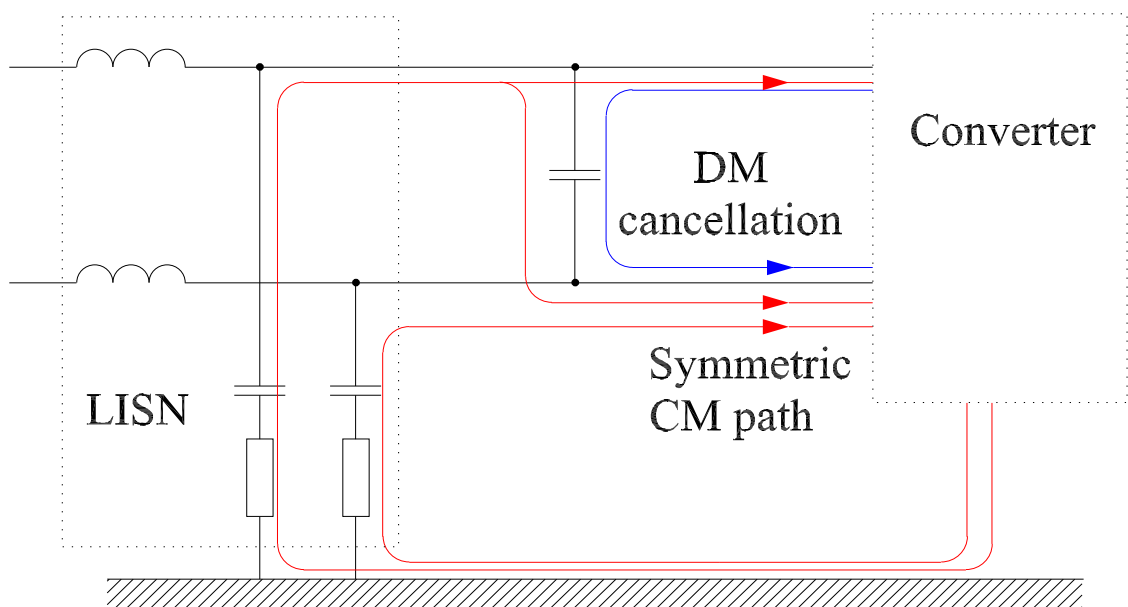


Figure 3.21: The differential mode cancellation and common mode current path

Regarding LISN spectra from measurement (Fig. 3.22) and simulation (Fig. 3.5) it can be noticed that shape of envelope is almost the same, but in the whole range there is the difference about 10dB. The reason can be from different FFT normalization coefficients used in the spectrum analyzer and *Saber*[®]. Another validation can be made by comparison of MOSFET or LISN voltage waveforms (Fig. 3.23). The correlation is very good, taking into account all measurement inaccuracies (the problem is that voltage cannot really be measured directly across the transistor).

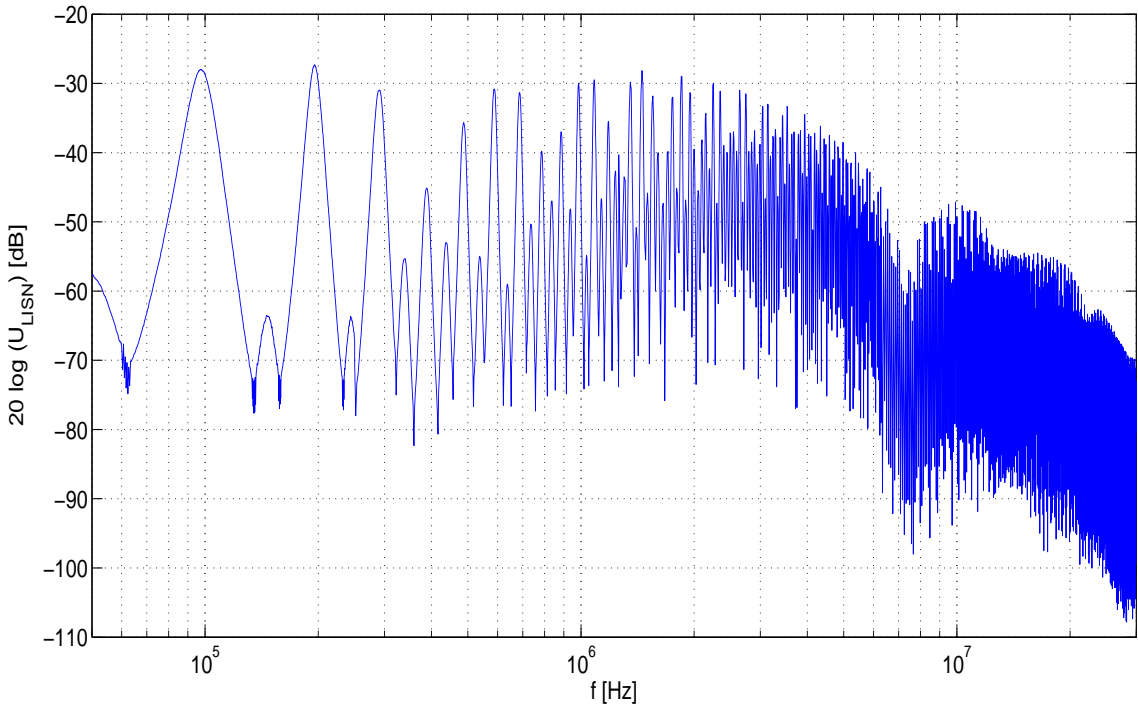


Figure 3.22: LISN voltage spectrum obtained with spectrum analyzer

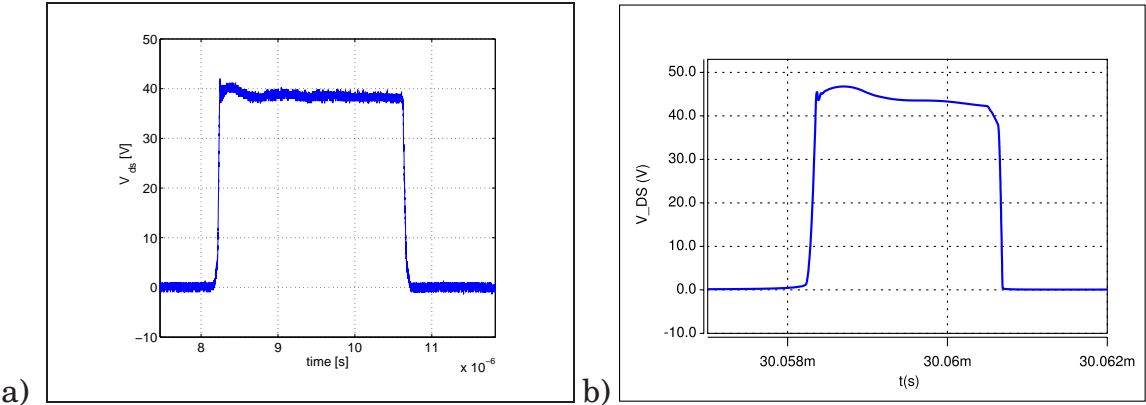


Figure 3.23: Temporary MOSFET voltage comparison a) measured b) simulated

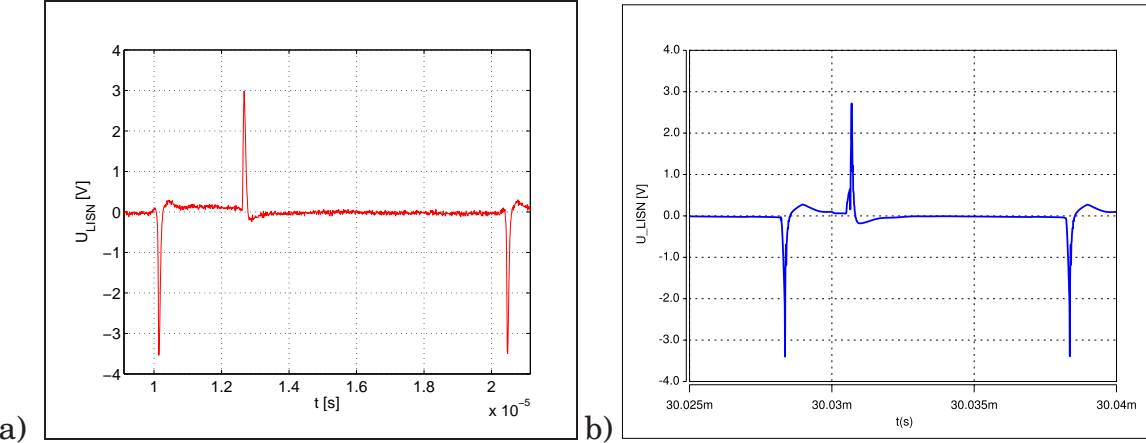


Figure 3.24: Temporary LISN voltage comparison a) measured b) simulated

3.7 Wiener filter

3.7.1 The converter state independent method

The transfer function or impulse response of Wiener filter can be use in describing EMI behavior of power electronic application (converter and LISN). The great interest of this method is that it does not necessitate any knowledge of the converter structure. It is an identification process, which considers the converter as "black box". The calculations of Wiener filter describing EMI behavior of DC-DC boost converter have been done using data from Saber simulation and measurement from real application with 4 - channel Tekxtronix TDS744 oscilloscope. In order to obtain correct and recurrent results, all data have been taken in steady state of converter. In the first step, a single filter was defined for the complete converter, whatever the semiconductor states (on or off). The calculations have been done for boost converter with two options of MOSFET driver (described in section 3.1). First - slow driver based on two PNP and NPN transistors - has been used. MOSFET and LISN (perturbation) voltage waveforms obtained from simulation and measurement have been compared with ones from Wiener filter. It is presented in figure 3.25. It easy to observe that reconstructed disturbances agree with real ones. There are some additional noises from another sources, resulting from imperfection of measure equipment or numerical method errors.

In order to find out which of the boost signal is sufficient to apply in this method, calculations of the WF have been made with different waveforms:

- MOSFET voltage
- MOSFET current
- diode voltage
- diode current
- MOSFET driver voltage.

In all above cases (with slow driver) system has been recognized with satisfactory precision, indicating that for power electronic application with low number of switching components one of voltage or current waveform of semiconductor arbitrary could be taken.

In presently used applications, drivers are much faster than main semiconductor devices. Simulation and measurement have been made with another MOSFET control driver. In fig.3.27 LISN voltage is presented. It can be noticed that level of disturbances changed, both amplitude and time of oscillations are much bigger than in previous case. The reconstruction works not so well as in the first experiment, in the estimated signal there are some additional peaks which cannot be found in real signal (denoted by green circle). It should be noticed that

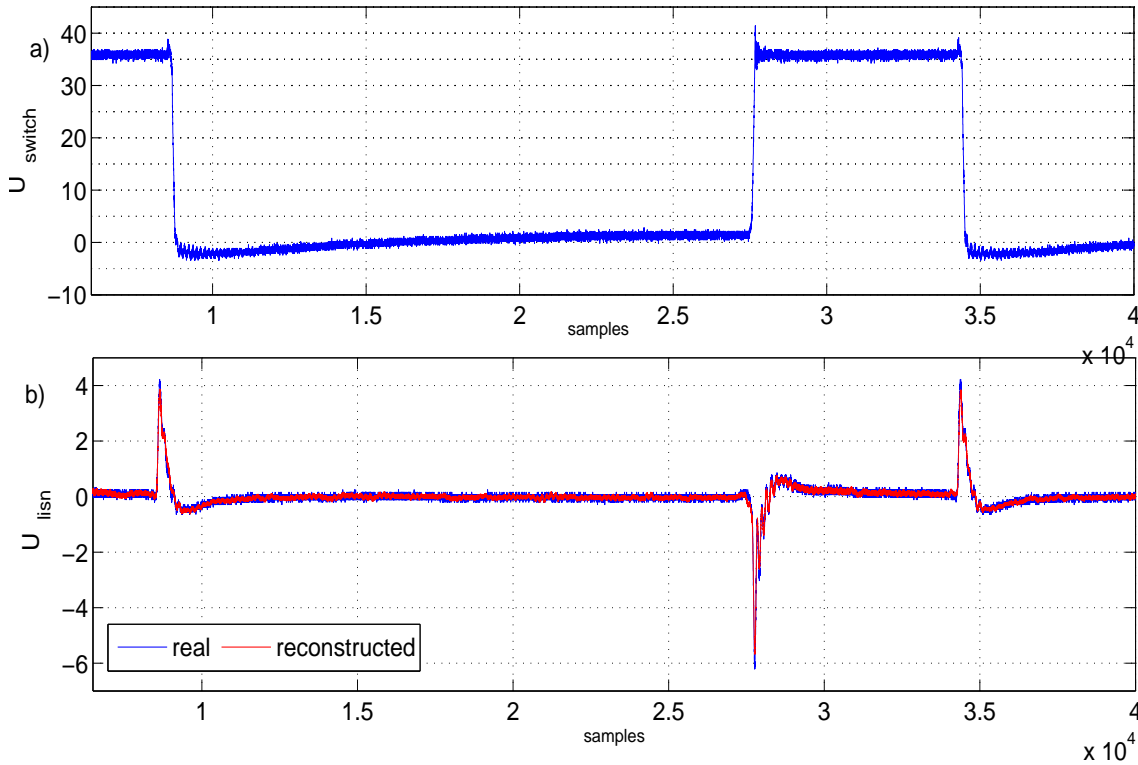


Figure 3.25: The perturbation reconstruction for MOSFET signal a) source of disturbances V_{ds} b) disturbances V_{LISN} real and reconstructed

there are some little divergence (Fig. 3.27) at the beginning of commutation process what can be produced by another external sources of disturbances e.g such as driver. The response of the boost and environment is longer than V_{gs} changes causing errors in WF structure. Thus, MOSFET driver voltage cannot be used as an input signal of Wiener filter. In this case, the waveforms of switch voltage are not correlated and relationship between them is not linear, what comes from delay and switching MOSFET transistors features. Moreover, transfer function of Wiener filter should change when state of all semiconductor devices changes, because propagation path of perturbation generated during switch turning on and off are different, what has not been noticed for slow commutations. Thus, the system containing two Wiener filters, which takes into account the converter state changes, has been proposed

3.7.2 Wiener filter with state detection

The disturbances source identifications have been developed, in order to remove all errors presented in previous subsection. The aim is to find Wiener filters for all converter states describing EMI behavior of DC-DC boost and allowing to reconstruct perturbations. The EMI behavior of the one switch in power electronic application has been described by identification of two systems - first for on state and the second for off state of the switch. The assignment of each

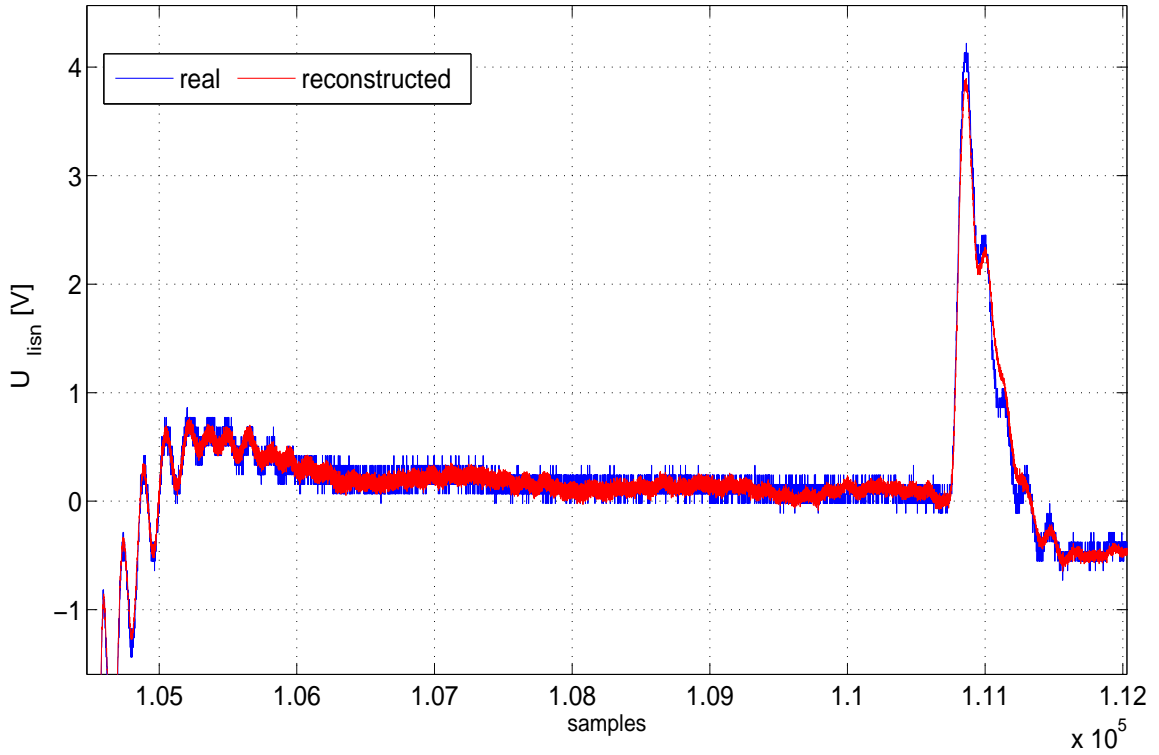


Figure 3.26: Zoom of V_{LISN} for „slow” driver **real** and **reconstructed**

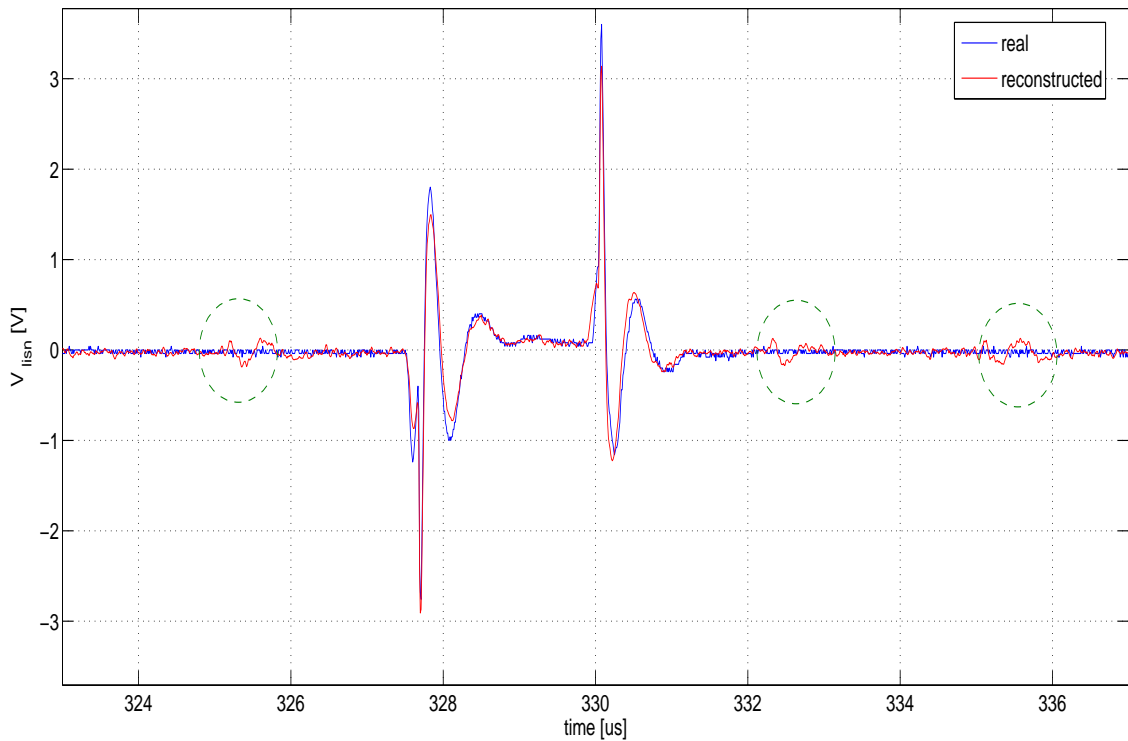


Figure 3.27: The perturbation waveforms V_{LISN} for „fast” driver **real** and **reconstructed**

Wiener filter to disturbance signals was determined by additional control signal - in this case it was V_{gs} gate-source voltage of MOSFET.

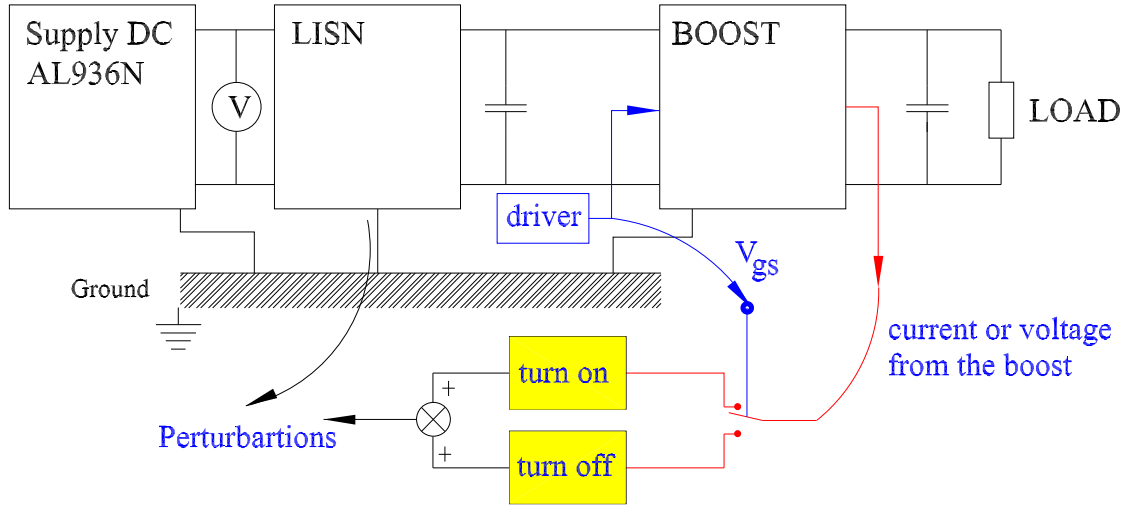


Figure 3.28: Two different systems for each state of the MOSFET

The new approach - based on 3 step calculation - has been apply using *Matlab*®.

- In the first step input and output signals are divided in time domain into two subsets and decomposed in two parts depending on the state of the switch. The moment of dividing can be determined by V_{gs} or derivative of V_{gs} by choosing suitable threshold. The threshold should be taken in a range which allows to make correct assignment of the each switch state for each system. For V_{gs} greater than threshold all signals are linked with first filter, if V_{gs} is smaller than threshold they are attributed to second filter (figure 3.29). In the consider DC-DC boost converter, an instant before commutation of MOSFET has been chosen. In some cases, when more accurate dividing is necessary, it is favorable to take two thresholds, different for turn on and turn off (figure 3.29 b).
- Two independent systems are identified in the second step - the first one for on-state and the second one for off-state of the switch. In each separately case, subset of V_{switch} and V_{LISN} , obtained in first step, are used in system identification. The Wiener filter transfer function calculation procedures for each state is similar to method approach for one filter described in section 3.7.2 . The results of this step are two independent Wiener filters for representation of EMI behavior of whole one switch power electronic circuit.
- Perturbation generated are reconstructed in the third step. Two systems are used to reconstruct the electromagnetic perturbations generated by

3.7. WIENER FILTER

the boost in both states of the switch. Next, obtained signals are composed to find all perturbations in time domain. Moreover, transfer functions between source (semiconductors) and perturbation (voltage measured on LISN) for each state of the switch can be found.

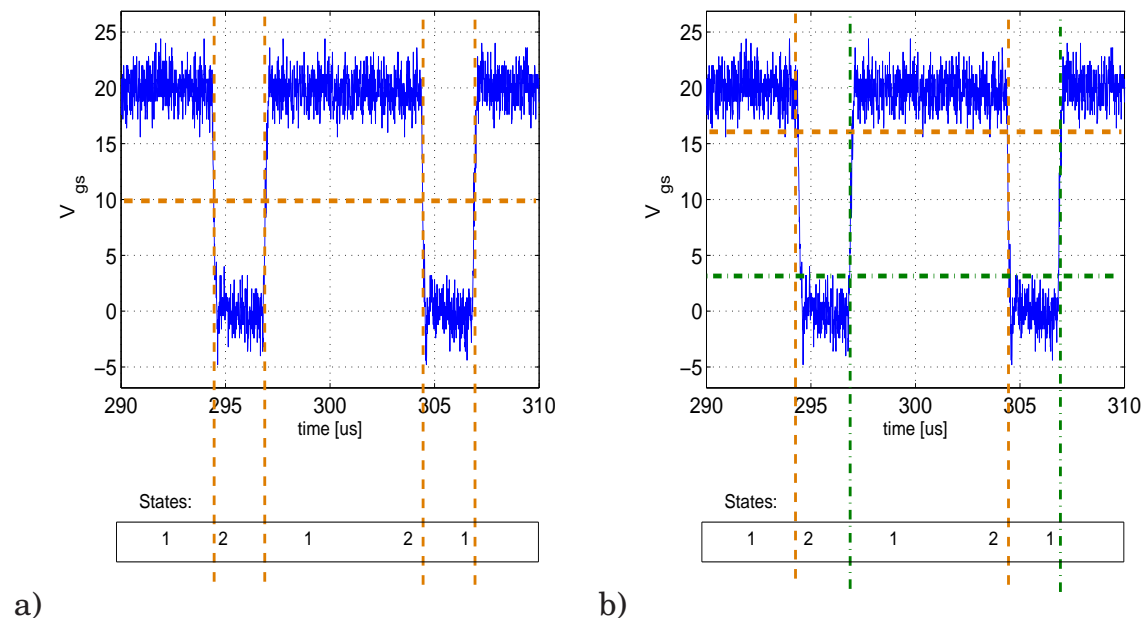


Figure 3.29: The signals dividing using a) one threshold b) two thresholds

Algorithm described in this section has been applied to identify disturbance sources in the DC-DC boost converter using simulation and measured data [51]. It is possible to identify transfer functions linking the voltage across the MOSFET to the voltage across LISN. Two different transfer functions have been identified, one for the on state, one for the off state (fig.3.28).

After the identification of the two systems corresponding to the boost, it is possible to reconstruct the EMI disturbances. The voltages registered on the LISN obtained with Saber time simulations in comparison with reconstructed signal, using the two Wiener filters, are presented in figure 3.30. As an input signal, MOSFET voltage V_{ds} has been used. The reconstructions mean error in this particular case is lower than 1 %.

Other semiconductors waveforms have been used for identification and reconstruction. However, measurement of the voltage across MOSFET was the most simple (compared to current measurement for instance).

The measured signal contains additionally noises from external sources and measure equipment, which are outcome of sampling inaccuracy. It can be noticed that the appeared noises are not reconstructed (Fig. 3.32), since they are not correlated with source of disturbances - V_{ds} . Thanks to the *Wiener filtering method*, it is possible to separate the contribution of the driver by choosing two different thresholds in dividing switch state (figure 3.29 b), so driver contribution can also be reconstructed (Fig. 3.32 b) or not (Fig. 3.32 a).

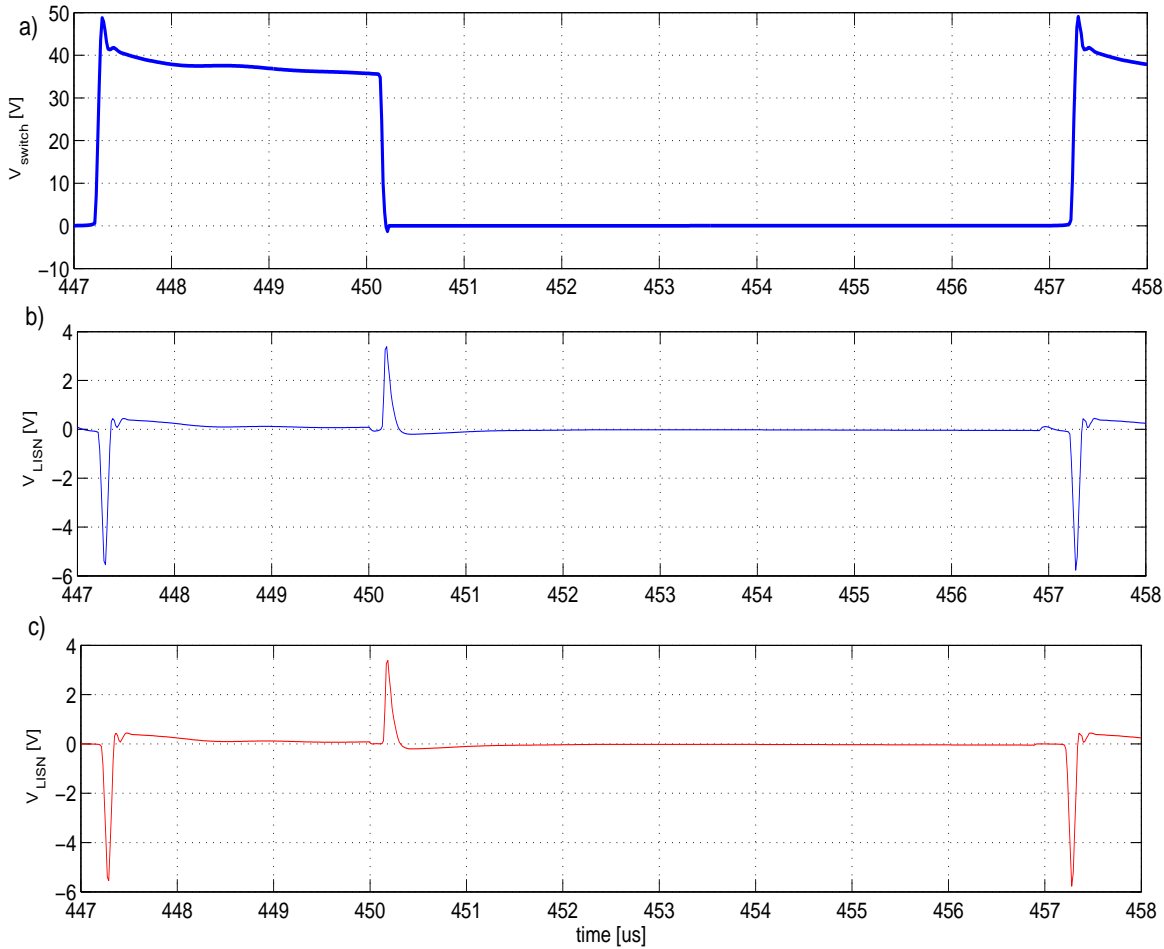


Figure 3.30: The voltage waveforms a) V_{switch} simulated b) V_{LISN} simulated with *Saber*® c) reconstructed by Wiener filter

Moreover, it is possible to divide perturbations in the groups for different converter state and propagations path - in figure 3.33 open state and close state perturbations are separated. If threshold is chosen incorrectly some perturbation from one state could be assigned to the second one, thus it can have influence on reconstruction process or transfer function calculation.

3.8 Conclusion

The EMI behavior of DC-DC boost converter has been investigated. The simulation has been done using accurate models of all components of the circuit, what allows to observe chosen voltage and current. The generation and properties of conducted perturbation have been analysed. The impact of chosen components on perturbation level has been presented. The results from simulation and measurement have been compared, the average error is smaller than 10 %. This knowledge allows to develop the simplified model of DC- DC converter for

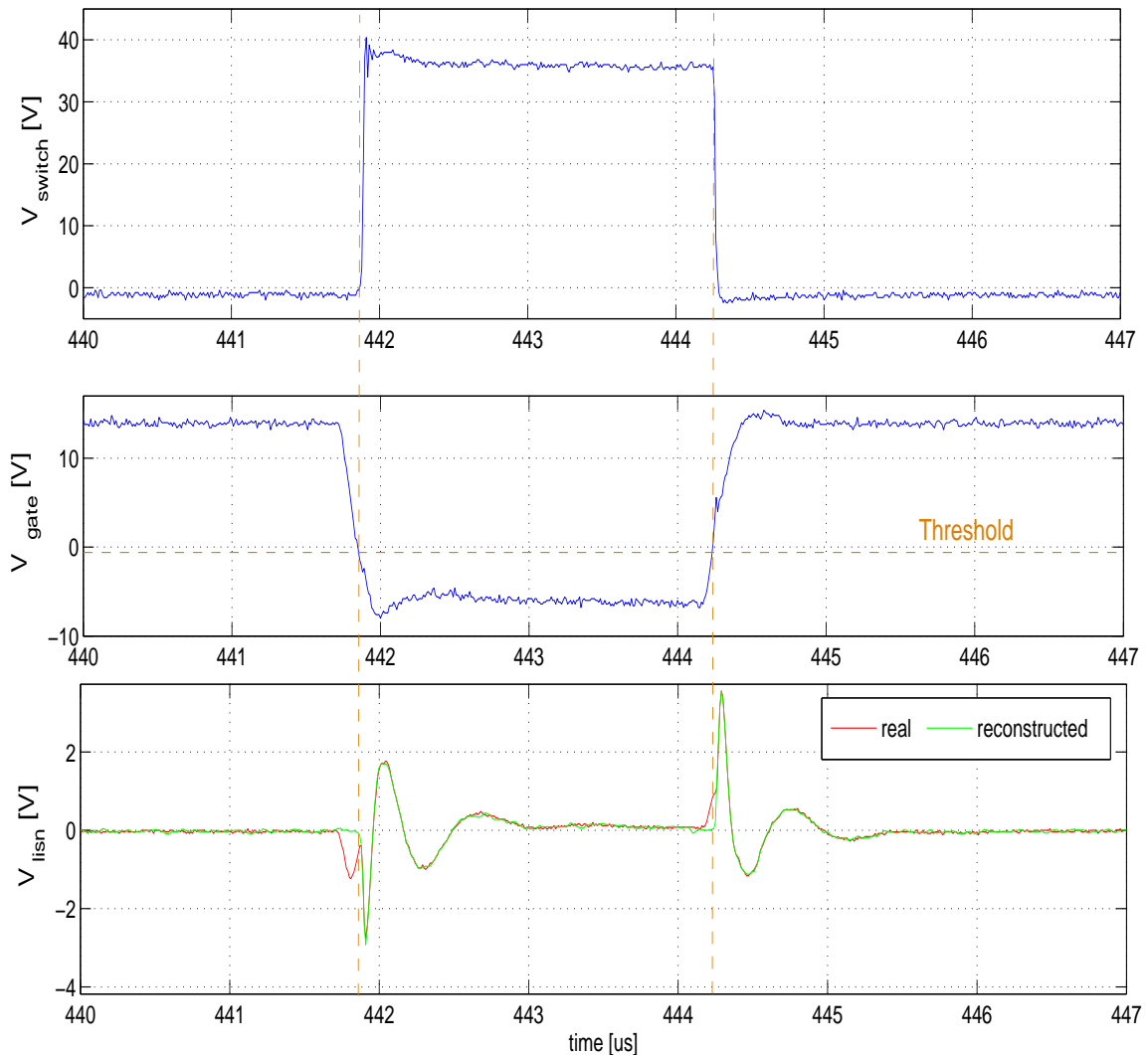


Figure 3.31: The voltage waveforms V_{switch} , V_{gate} and V_{LISN} measured and reconstructed with the WF

fast EMI estimation in frequency domain and it was used in validation of Wiener filtering method.

The "Wiener filtering" method has been applied to determine the main cause of EMI disturbance, originated from a power electronics converter and to identify the transfer function between source and perturbation. First, one filter has been used for state independent approach, next two filters have been distinguished for open and close state of MOSFET. It was proved that propagation paths for these two states are different. This time and frequency domain methods can be used with either measurement signals or simulations. It has been applied to the boost switching cell, where power MOSFET voltage is shown as the main EMC actor and reconstruction works quite good and fast. The average errors is in the range between 0.5 % and 10 %, depending on chosen threshold during state detection. The investigation has been done for two types of transistor drivers.

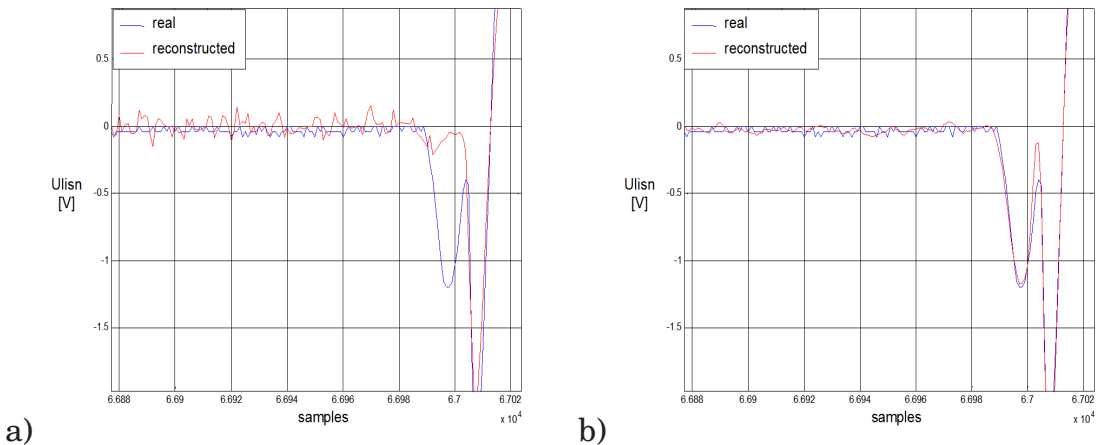


Figure 3.32: The V_{LISN} during commutation measured and reconstructed by Wiener filter a) separating of driver contribution b) reconstruction of driver contribution

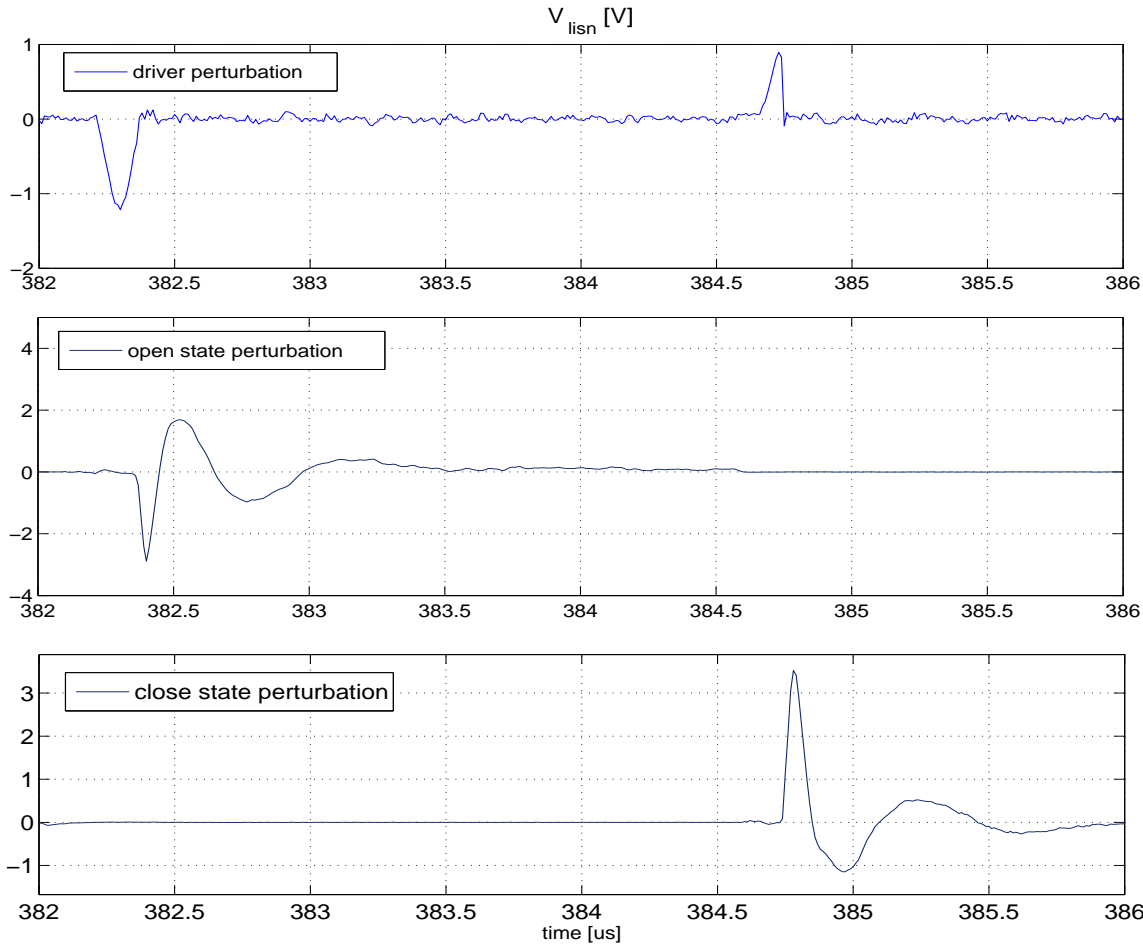


Figure 3.33: The perturbation divided for driver, open and close state of the switch

Chapter 4

Hard switching inverter

Science... never solves a problem without creating ten more.

George Bernard Shaw

4.1 Introduction

In this chapter the EMI forecast and analyze methods will be applied to various three phase hard switching inverters, which are traditionally used as three phase voltages sources in many applications. The study of the pulse width modulation (PWM) and pulse density modulation (PDM) inverters are presented in this chapter. These kinds of converters are complicated in terms of the control system, power stage, packaging and parasitic components. An essential part of such investigation is the modeling of the whole system using simulation and Wiener filter method. Moreover, the fundamental mechanisms of perturbation generation and propagation are analyzed with computer simulation and laboratory experiments. The successful EMI performance prediction is conditioned by accurate noise source and path information.

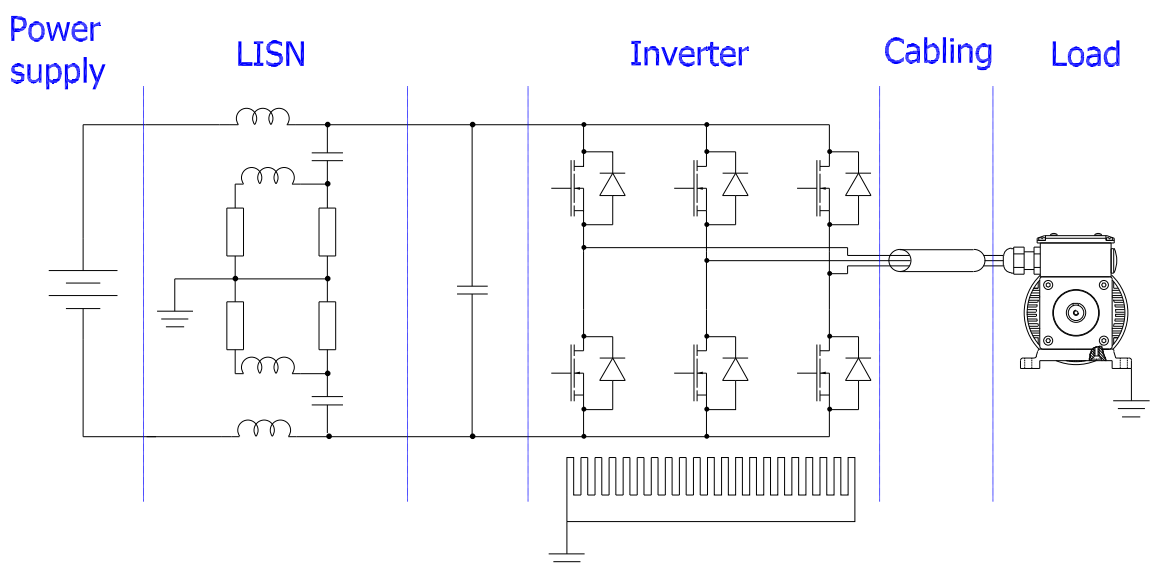


Figure 4.1: The DC/AC motor fed system

In the typical voltage source inverter, CM conducted emission are caused by currents that flow between the inverter and the earth of the system. In an inverter system, like in all typical power electronic devices, the combination of the rapidly switched voltages and the various stray inductances and capacitances, especially to earth, cause generation and propagation of conducted emission. The transistors are mounted on the metal base plate with an electrical insulating material. This insulating layer is normally made as thin as possible in order to make the thermal resistance small and the stray capacitance between the collector and the base plate tends to be large. CM current flows to the metal baseplate that is connected to the heatsink. The heatsink is normally grounded for safety reasons. It can be said, that the placement of circuit components and the load has strong impact on the level of CM noise.

EMI problems in hard switching three phase inverter have been discussed by many authors. A few ways of perturbation analyzes and forecasting can be distinguished. The equivalent circuit can be built using models of all components of inverter [38] [82]. Many paper can be found, where simplified models based on engineering knowledge are presented [58] [60], [89], to be applied for fast EMI estimation or where analytical solution can be carried out [56]. Models described in [27], [74], [88], don't only focus on an inverter, but take into consideration also DC source, load, motor and cabling.

4.2 Simulation

Accurate wide band model of inverter has been built in *SaberSketch*®. This model takes into consideration only inverter with PWM control and LISN. The very simple models of parts of system as voltage source, load and cabling are also included in simulation schema. The aim was to obtain model, that allow to analyze all phenomena connected with perturbation generation and propagation and to observe voltage and currents waveforms in the moment when switching occur. Thus, this model has not been constructed for accurate EMI forecasting, and that's why results don't exactly agree with ones from real application. In fact it can be used for the validation of the perturbation reconstruction method.

Models of all circuit components have been constructed as it is presented in chapter 2. The semiconductor models have been taken from *Saber*® library and corrected with parameters from producer data sheet. Insulated gate bipolar transistors (IGBT) are used as switching devices. The inverter layout is more difficult to modeling than boost connections, because of high complexity, however all main conductors are taken into consideration. Parasitic inductances have been subtracted with PEEC (formula 2.5) method and parasitic capacitances with Paul formula 2.12.

4.2. SIMULATION

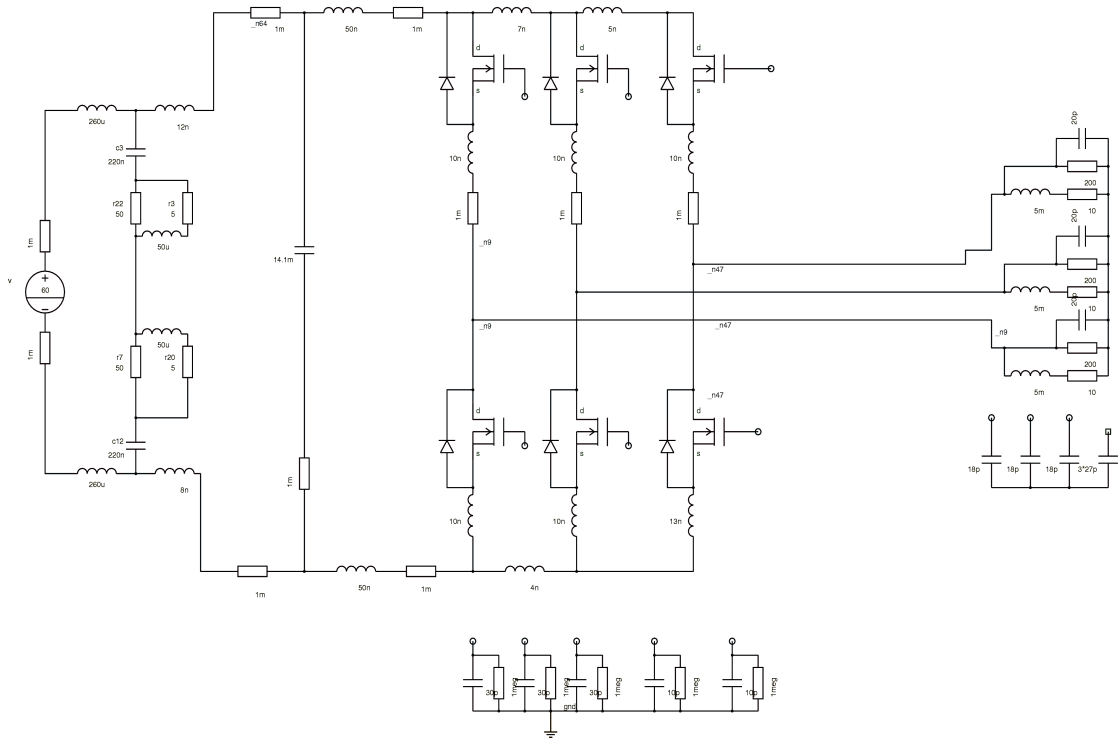


Figure 4.2: Inverter schema from SaberSketch

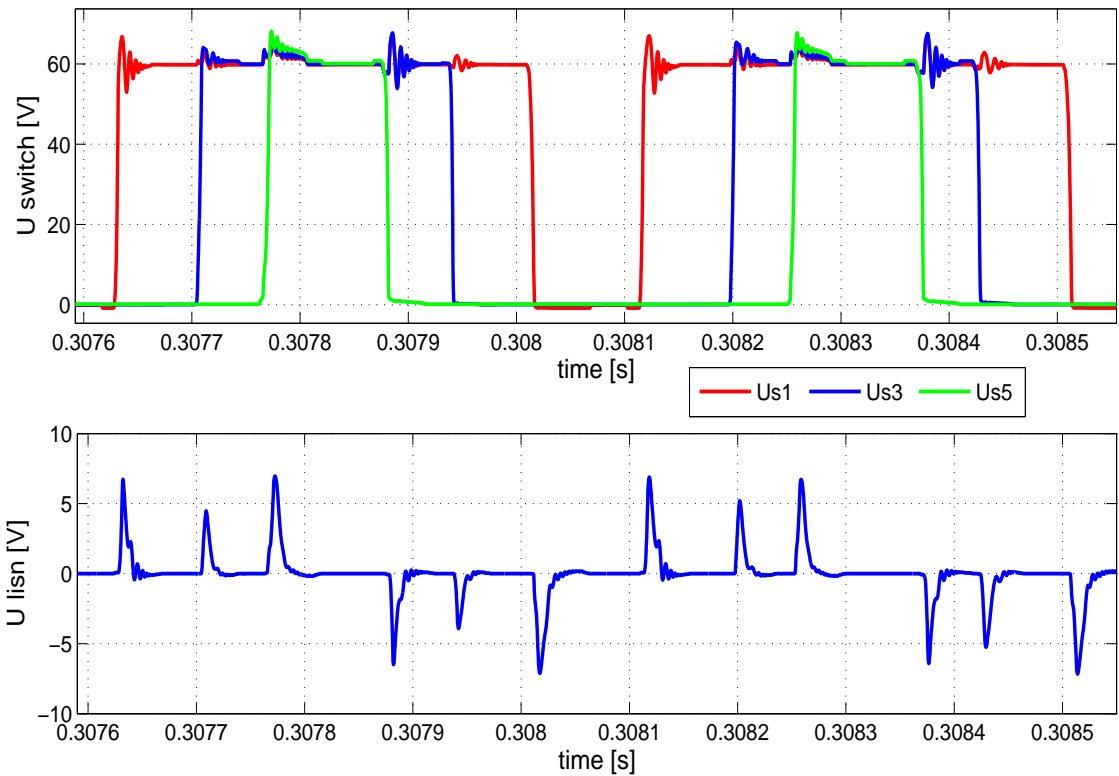


Figure 4.3: Voltages across the switches and LISN waveform obtained by simulation

Simulations of inverter EMC behavior is a process that needs a lot of time and computer power because of the high complexity of circuit and great discrepancy of time constants. Even with simply models of all components, it takes more than 3 hours for computer with Pentium 4, 2.00 GHz processor and 512 MB RAM. If more accurate models are taken, this time could be doubled.

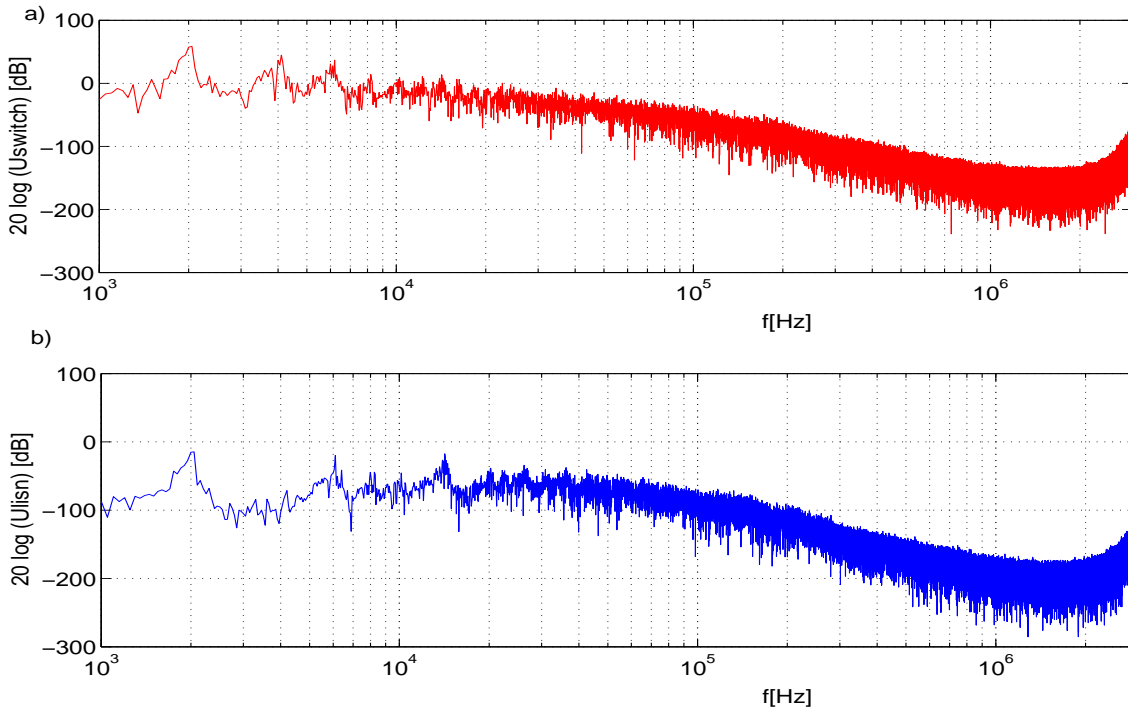


Figure 4.4: Voltages across the switches and LISN spectra obtained by simulation

Since in one leg of the considered inverter, sum of voltages across the upper and the lower switches is always equal DC link voltage, it is sufficient to observe commutations in three upper legs. Voltages waveforms across the three switches - the main sources of disturbances - and perturbation registered on 50Ω LISN resistor are presented in figure 4.3. It can be noticed that these signals are correlated (figs. 4.4 and 4.3). In the instants when transistors are turn on or off, perturbations occur. The oscillations after commutation have the same frequency in both waveforms. The perturbation amplitude is strongly dependent on semiconductor voltages velocity changes dV_{switch}/dt .

Moreover, it is possible to subtract common and differential mode noise (according chapter 1.1), but in this case, DM perturbation are infinitesimal, what is shown in figure 4.5. The cancellation of DM is mainly due to the filtering influence of input capacitor. It can be noticed, that CM perturbation have dominate role in the whole noise.

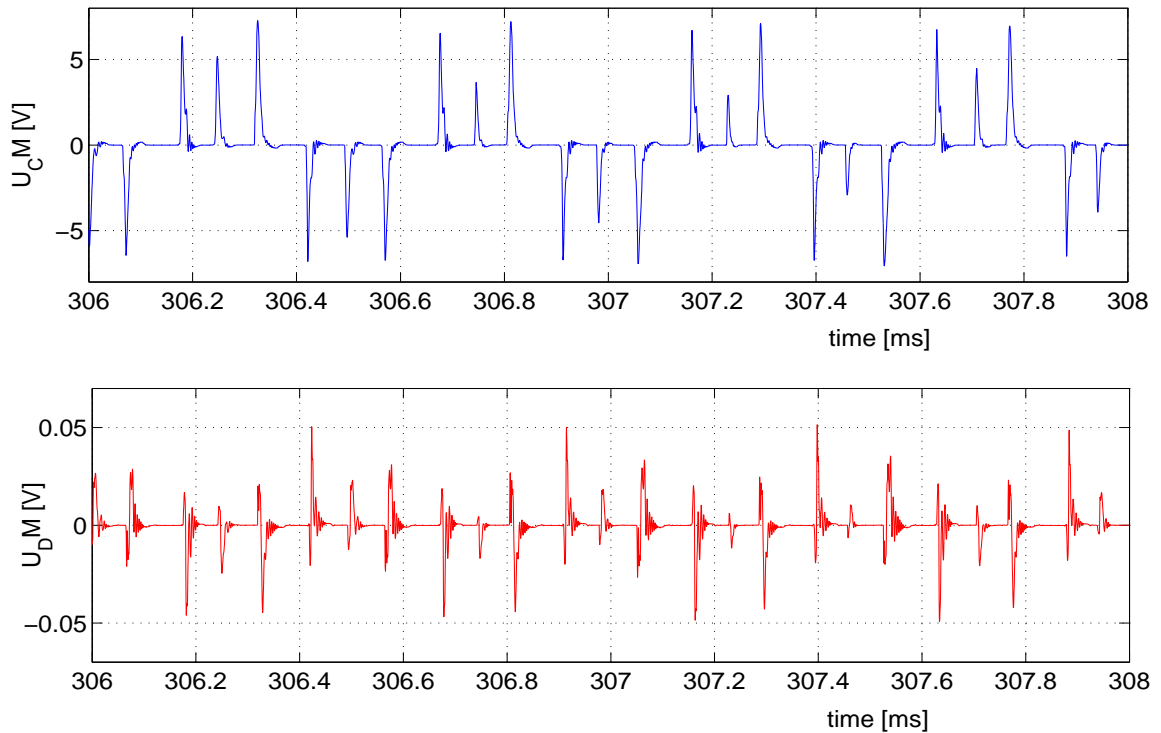


Figure 4.5: Differential-mode and common-mode separation

4.3 Wiener filter

In this thesis the new technique of fast EMI reconstruction and prediction, that allows fast and more accurate estimation of the perturbations for a power electronic inverter is presented. Starting from digital signal processing basis, we aim to determine the contribution of perturbations level, due to switch turn on and turn off. This digital signal processing method is based on powerful Wiener filtering approach (section 1.3), that links the source of disturbances and noise measured on LISN. The main aim is to find numerical representation of those components of circuit, which take a part in perturbation propagation. From the digital signal processing theory, transfer functions of unknown system describing EMI behavior of inverter are requested.

The perturbation from power electronic converters are generated during semi-conductors turn on or turn off. The fast rated changing voltage on one of circuit elements is the reason for perturbation that appears and can be registered on the LISN. Standardized LISN is typically used for perturbation measurements generated in power electronic applications. The level and waveforms of perturbations depend not only on voltage (dv/dt) and current (di/dt) rise or fall time, but also propagation path has an influence on it. Parasitics of all components can not be neglected, including parasitic capacitances and inductances of semi-conductors and passive components, inductance of connection and conducting tracks and also capacitances to the ground.

In this method, the following assumptions have been adopted:

- perturbation is the result of commutation of only one switch, but level and waveform of perturbations strongly depends on state of residual semiconductors,
- transistors in parallel branches cannot be switch in exactly the same time instant, what is quite typical in modern power electronic applications.

4.3.1 Specifying inverter states

In previous papers, in order to forecast perturbation, authors used only one transfer function between switch and the line impedance stabilization network (LISN) voltage [72], [9]. In author opinion, such a simplification is too strong and in some cases could lead to incorrect results. The perturbation paths can be different owing to various parasitics which take part in propagation. The waveform during commutation of first transistor, when neighboring switches are open, is not the same with closed ones. The inside junction capacitances of semiconductor device changes during inverte operation and have different values for open and close switch what make propagation paths different. The states of all semiconductor devices have influence on perturbation level. So, it can be concluded that the level of perturbation generated during commutation of one switch is strongly depended on states of all other inverter switches [52].

Therefore, the transfer function between source of perturbation and perturbation registered on the LISN depends on all circuit parameters and state of inverter. It can be also noticed that values of all components are time invariant during typical inverter operation, but only inverter state is changing.

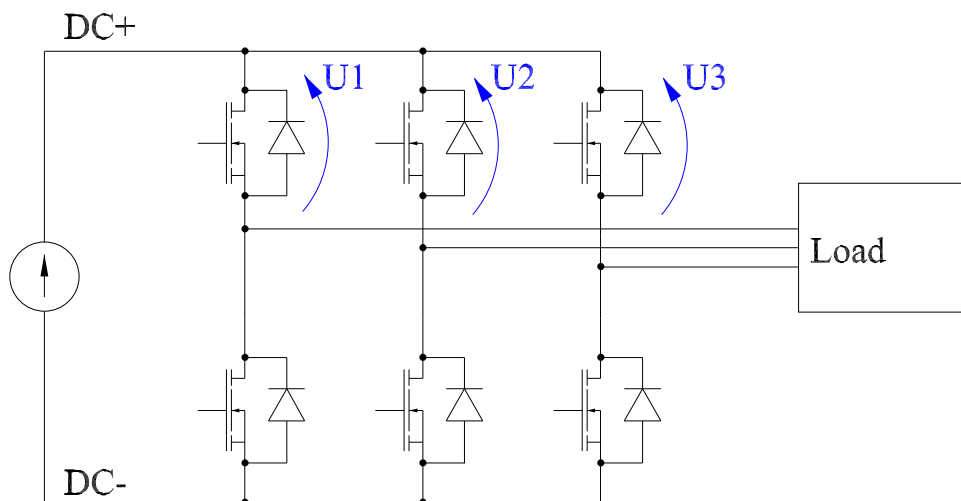


Figure 4.6: The voltages used to inverter state definition.

4.3. WIENER FILTER

Conventionally, the eight states of three phase bridge inverter can be defined in accordance with voltage space vector which is produced on the output of converter. However, this approach is not useful for EMI analyzes, because it is impossible to find which semiconductor device is a source of disturbances. Moreover, it is necessary to know previous state of inverter. In this thesis, definition of new method of states determination based on voltages between one of busbar DC+ or DC- and midpoints of three parallel inverter legs (fig. 4.6) is presented. These voltages can be easily obtained by computer simulations and they are available for measurement in a large majority of real applications. The proposed approach allows to define 12 states and to determinate of 12 transfer function linking voltages across the switches and the 50Ω LISN resistor, to forecast perturbation waveforms.

When commutation happens in the first leg (transistor or diode is turn on or turn off), the other semiconductor devices are on (low voltage) or off (high voltage). Regarding only U_2 and U_3 level, four different inverter states can be defined for one switch commutation ($dU_1/dt \neq 0$). These states are different because propagation path are different and intrinsic capacitances of semiconductors change.

Table 4.1: DC/AC hard switching converter states definition for U_1 change.

state	U_1	U_2	U_3
1	change	high	high
2	--	high	low
3	--	low	high
4	--	low	low

Table 4.2: DC/AC hard switching converter states definition for U_2 and U_3 change

state	U_1	U_2	U_3
5	high	change	high
6	high	--	low
7	low	--	high
8	high	--	low
9	high	high	change
10	high	low	--
11	low	high	--
12	high	low	--

Respectively, next states are defined for commutations in remaining legs, when U_2 and U_3 are changing (table 4.2). To conclude, for accurate forecasting of EMI perturbations generated in hard switching inverter, the 12 states should be distinguished for different propagation paths. Moreover, as perturbations spread in a different way, when the switch is turn on and turn off, it provides total number of states doubled, what finally leads to the 24 states.

This method can be used to reconstruct inverter perturbation waveforms, for all kind of modulation. There is no need to check, which semiconductor - transistor or diode - actually conducts the current in chosen inverter leg. Furthermore, dead time and delay phenomena are taken into account.

4.3.2 Validation of Wiener filter method

In order to forecast EMI disturbances in the particular DC/AC hard switching converter using Wiener filtering method (chapter 1.3), the 24 transfer functions should be calculated (fig. 4.7) for turn on and turn off for each of 12 inverter states (see tables 4.1 and 4.2). The aim is to better achieve two objectives: to estimate the system H , and the disturbance p_v by measuring only two signals.

- source of disturbances v (which is one of the voltages U_1 , U_2 or U_3 defined in figure. 4.6),
- total disturbance p , measured on the LISN.

The signal recorded on LISN is decomposed into blocks. One block contains samples from time period between two neighboring commutations. In order to apply Wiener filtering, each block is linked with one of 24 systems, depending on inverter state and direction of commutation. For each system, the voltages across the one switch (from the leg where commutation occurs) and LISN are used to calculate transfer function.

In order to apply the Wiener filtering method, the new software has been built in *Matlab*® environment (appendix A). The input signals are the inverter switch voltages U_1 , U_2 and U_3 (fig. 4.6), which are used first to detect inverter state and then to calculate perturbation. The total reconstructed signal is composition of signals achieved from all of 24 systems. The result of disturbances reconstruction is presented in figure 4.8.

It can be noticed that signals obtained by Wiener filtering are almost the same as the original ones. In this case, the normalized estimation error is 3.5%. The inaccuracy can be explained by perturbations not correlated with the input voltages, interfered from another sources as load, transistors drivers or control system. Moreover in many digital signal processing algorithms, not sufficient number of samples can be a problem. As the DC/AC converter can operate in some states for a short time, resulting in a low number of samples for these periods. In this case *Saber*® simulations have been effected with variable calculating step, producing non-regular number of samples per estimation period.

4.3. WIENER FILTER

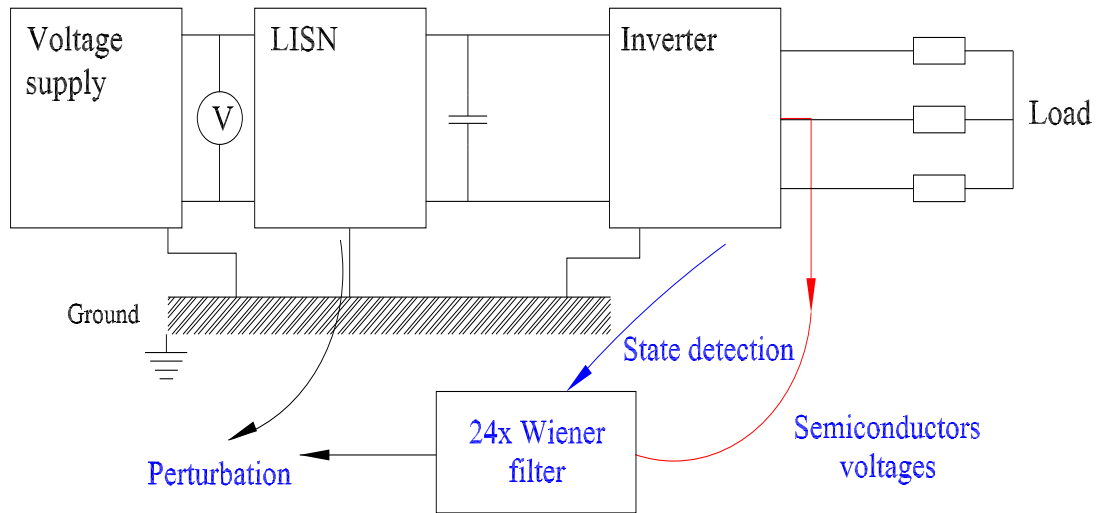


Figure 4.7: Wiener filters and the inverter

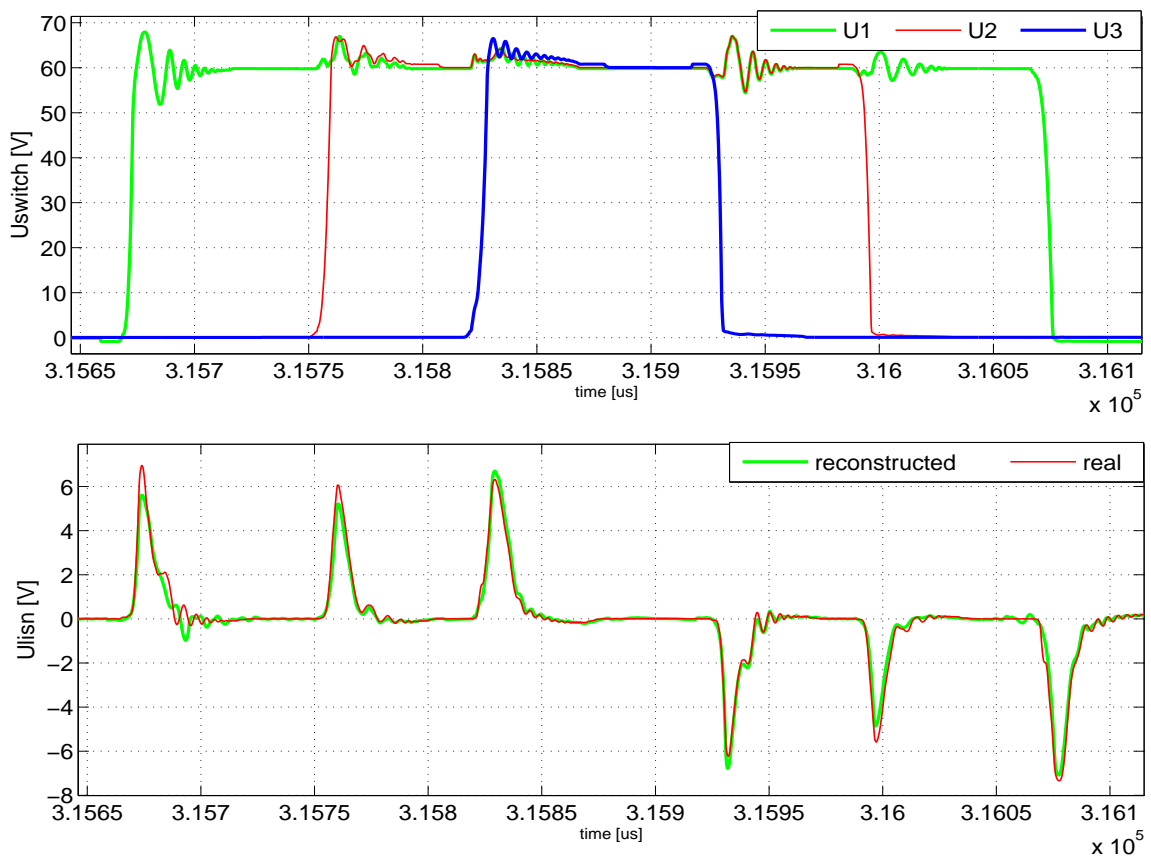


Figure 4.8: The semiconductors and LISN voltage waveforms obtained from simulation and Wiener filter

Furthermore, using data from measurement as input signals, suitable number of samples should be assured in measurement equipment.

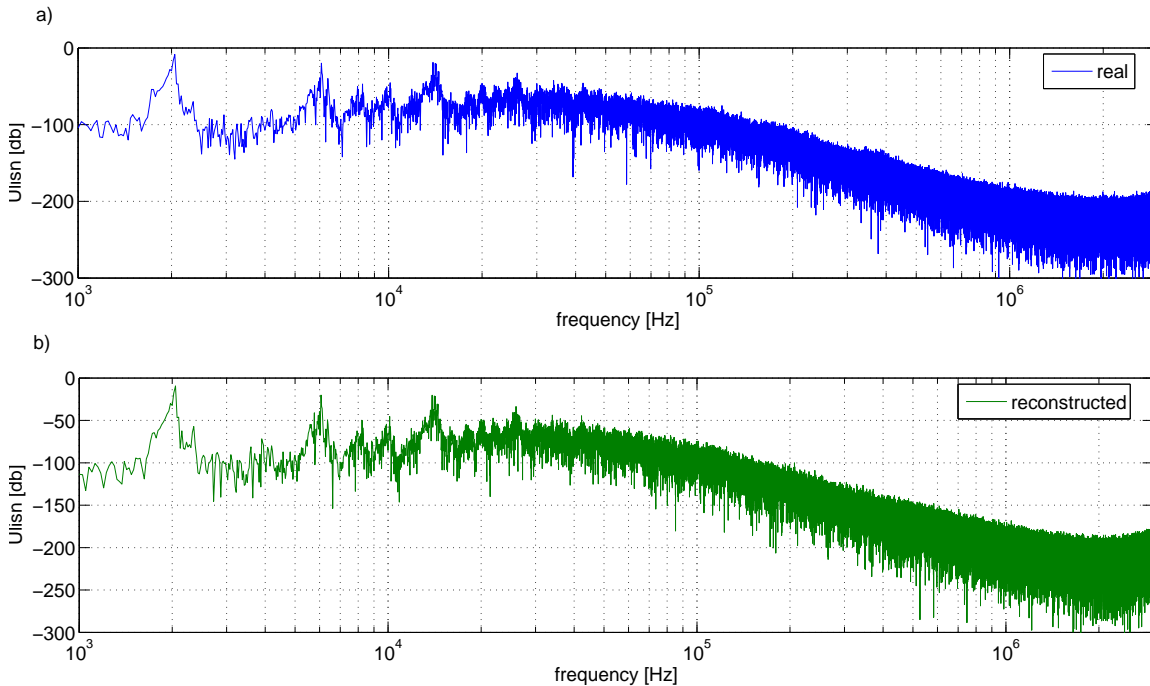


Figure 4.9: The LISN voltage spectra a) simulation b) estimation

Comparative evaluation of the EMI simulation and estimation by Wiener filtering in the frequency domain is shown in figure 4.9. In high frequencies range, above 10 MHz, is indicated approximate estimation error of 2%. In this case reconstruction of perturbations is quite precise, excepting this number samples discrepancy. In comparison with "typical" simulations, which need lots of computing time, powerful simulators and fast computers, Wiener filtering method is more effective as can be realized in a short time.

The identification of source disturbances can be obtained directly with this method: each part of perturbation waveform can be linked with the corresponding inverter switch commutation voltage (fig. 4.10). It allows to separate perturbation generated by each particular switch or make EMC analyzes for chosen state of inverter. The worse working condition can be found, when maximal level of perturbation occurs. This knowledge is useful to optimization for geometrical layout and reductions of EMI emissions.

The main circuit property changes during system operation. Components that take part in EMI propagation and their parameters have variable actions, so the level of perturbations depends on inverter state. Considering transfer functions of Wiener filter of only one switch (U_1), they are different for 4 inverter states (table 4.1). The shape of transfer function depends on propagation path and participation of all parasitics components which take a part in perturbations propagation. Although, all envelopes of impulse response are similar (fig. 4.12),

4.3. WIENER FILTER

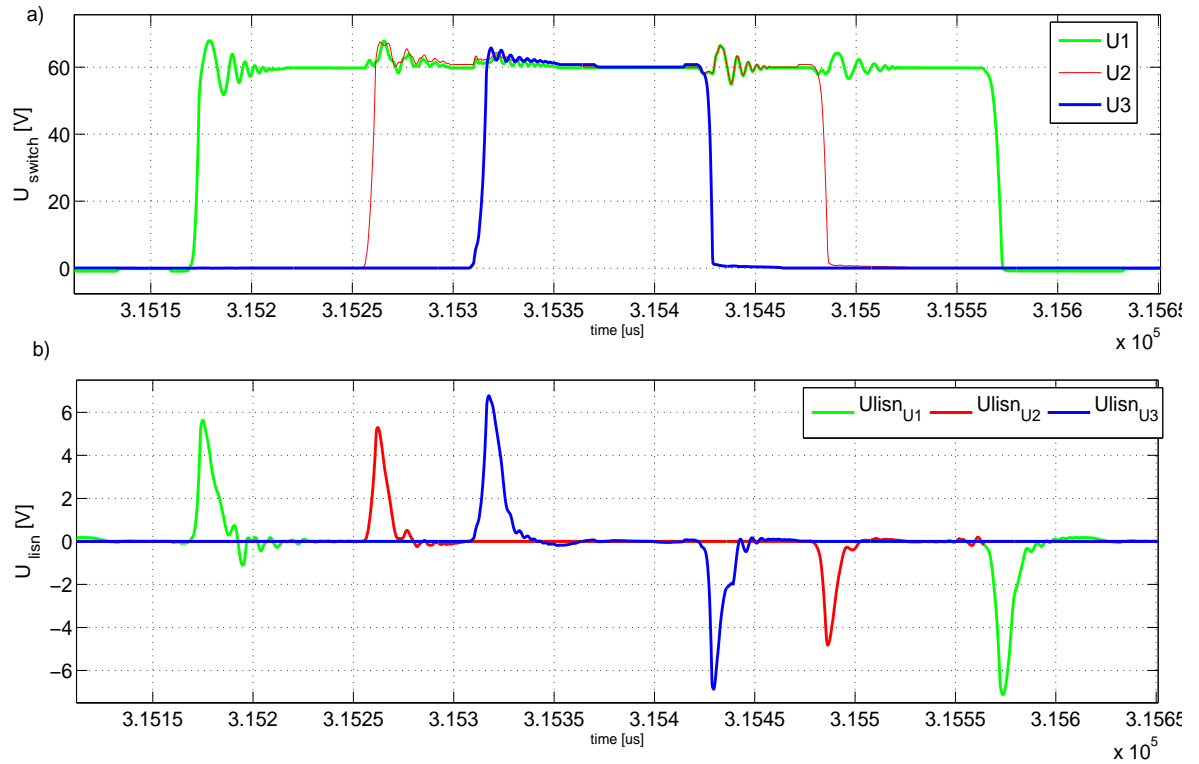


Figure 4.10: The perturbations source identification using data from simulation

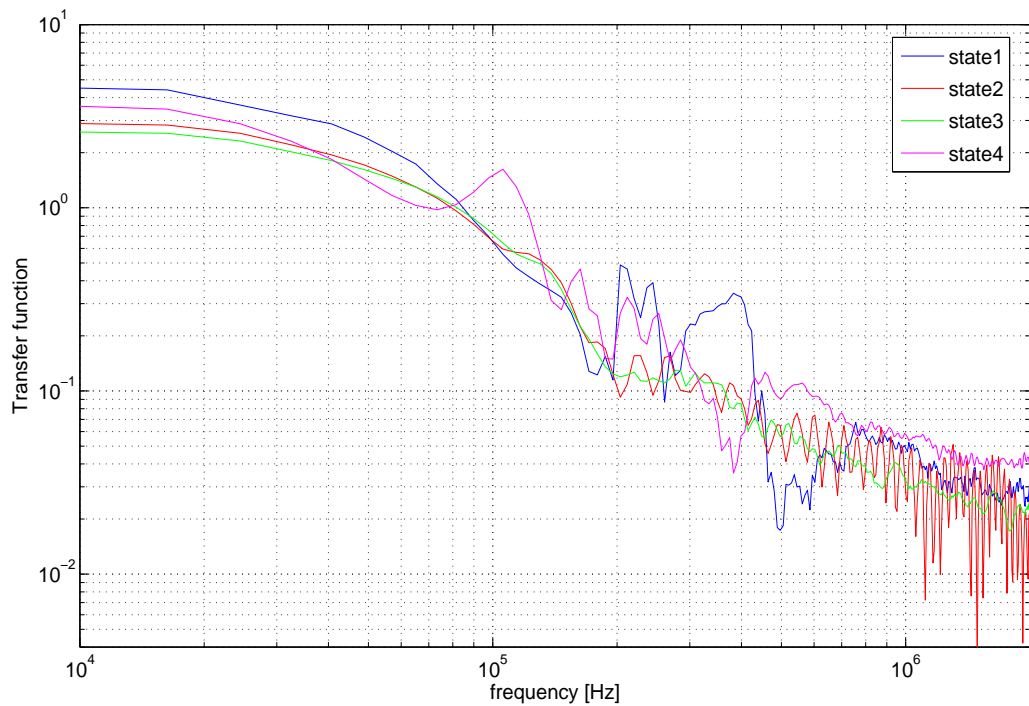


Figure 4.11: The transfer functions for different states of inverter obtained from Wiener filtering method using data from simulation (table 4.1 p1-4)

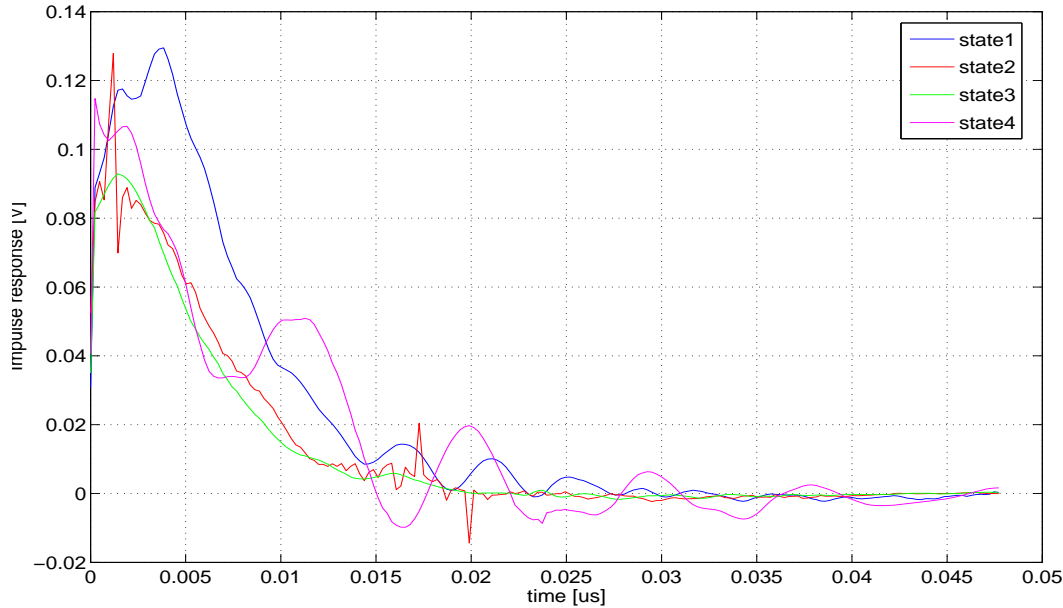


Figure 4.12: The impulse response for different states of inverter obtained from Wiener filtering method using data from simulation (table 4.1 p1-4))

the waveforms are completely different. In figure 4.11 it is also shown the different resonance frequencies which induce an amplification of electromagnetic perturbations in some particular frequency bands. Thus, the figures 4.11 and 4.12 are the proof, that level and propagation path of perturbations generated in inverter depend of his state.

To verify results obtained with simulation data in the above section, the conducted EMI of hard switching inverter has been measured. The perturbations reconstruction and source identification have been done using data from measurement. The hard switching inverter was supplied from traction battery 120V through the LISN. The induction machine was used for a load. The measurement was realized with 4 channel oscilloscope Textronix TDS5034B with high voltage differential probes.

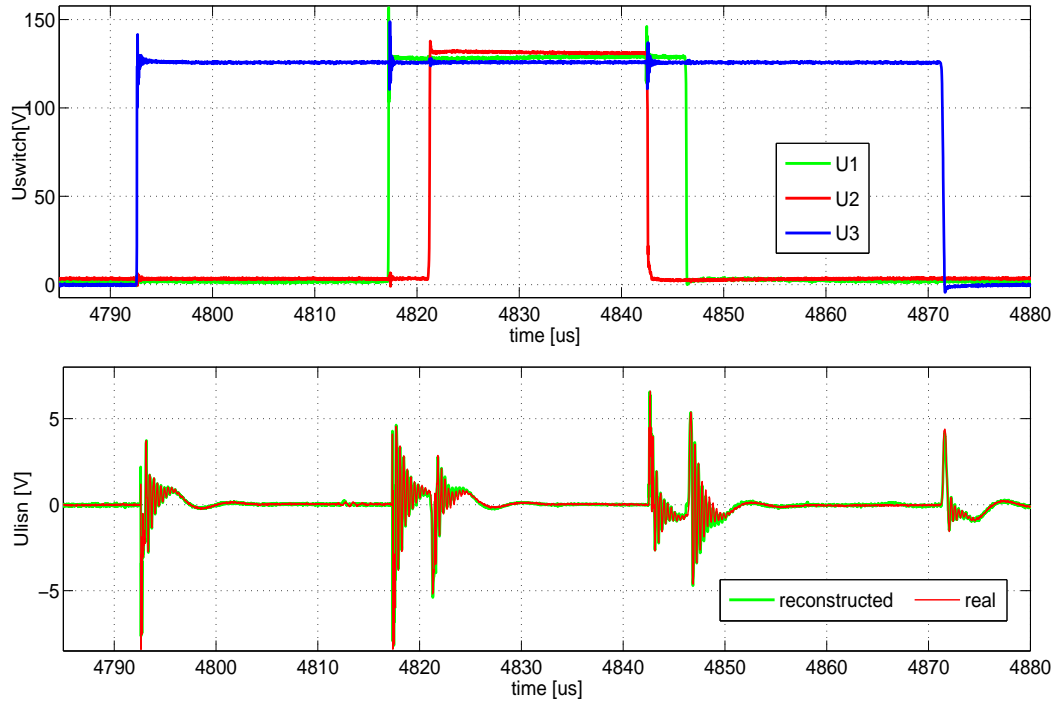
The waveforms have been registered with sampling frequency 50 MHz. The EMI generation for two kinds of modulation was carried out by:

- PWM - pulse width modulation
- PDM - pulse density modulation (sigma - delta)

The reconstruction of perturbations, generated by hard switching inverter with PWM modulation, using Wiener filtering works correctly, what is shown in figures 4.13 and 4.15, where waveform and spectra of the measured LISN voltage iare compared with the calculated one. The approximate estimation error is 3.3%. It should be noticed that in real applications not all inverter states occur, but it does not influence on reconstruction accuracy. Moreover, it can be noticed that, perturbations from inverter control system are not reconstruct, because they are not correlated with source of inverter.

4.3. WIENER FILTER

a)



b)

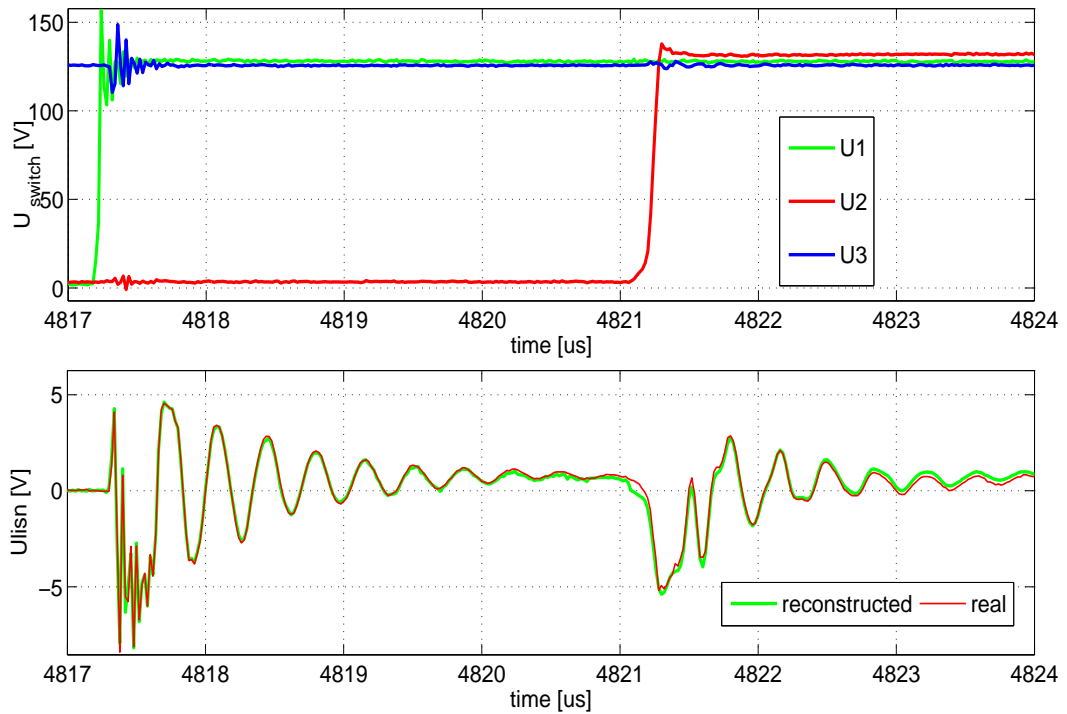


Figure 4.13: The measured voltage of semiconductors and LISN waveforms for PWM modulation b) zoom

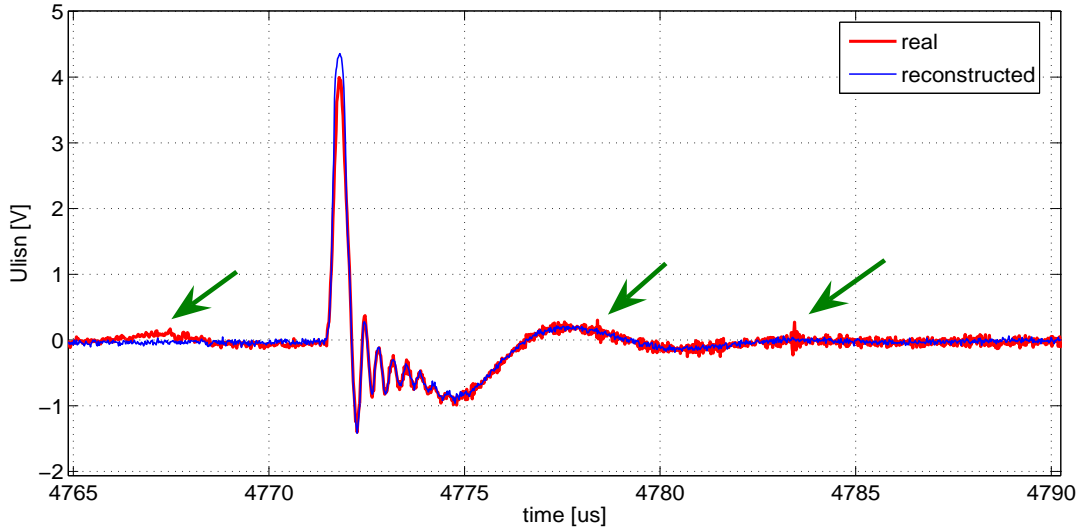


Figure 4.14: The measured voltage of LISN waveforms for PWM modulation - separation noise from other sources

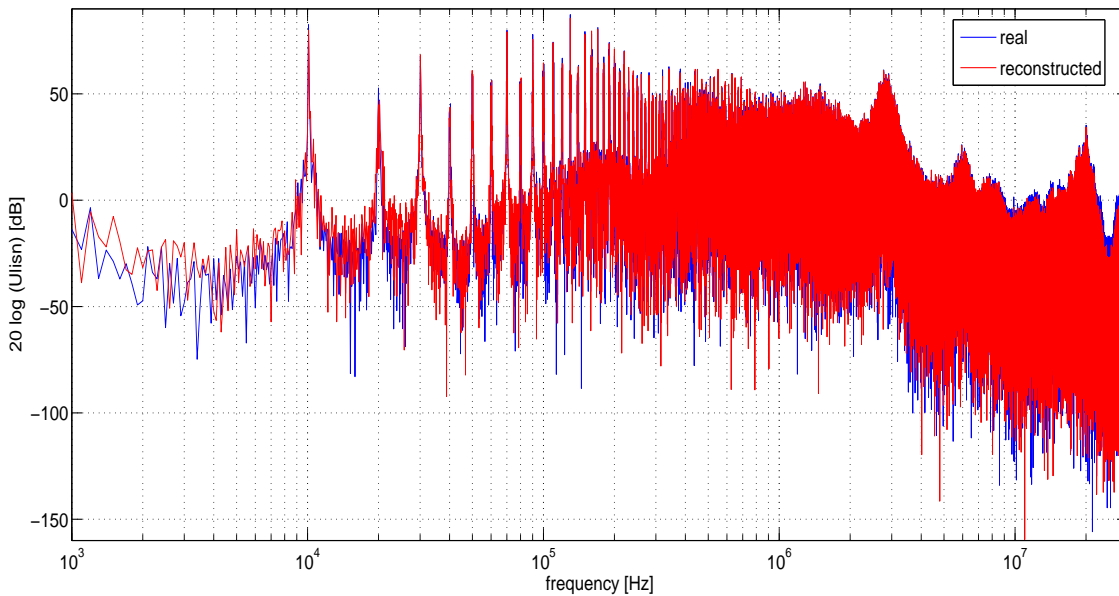
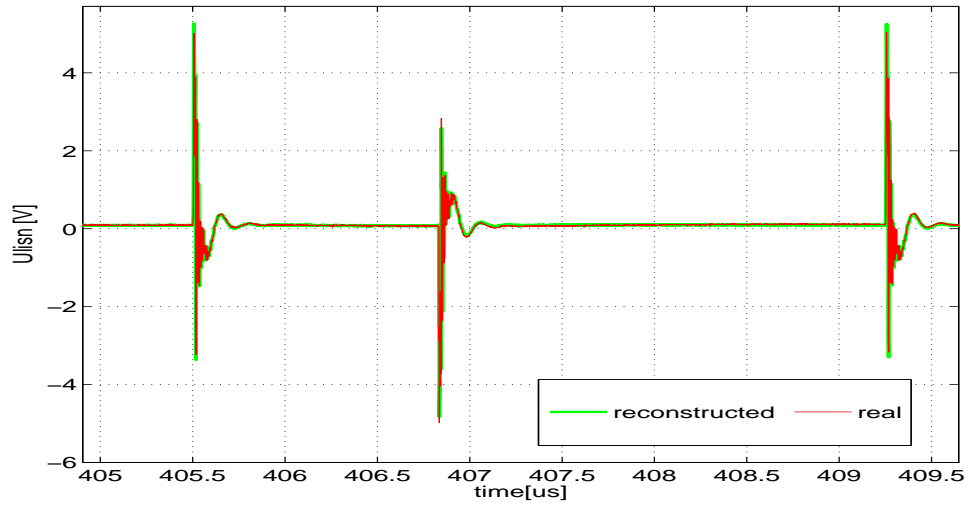


Figure 4.15: The LISN voltage spectra for PWM modulation a) measured b) Wiener filter estimation

The results of Wiener filtering of signals from the inverter with PDM modulation are depicted in figure 4.16. The reconstruction accuracy is also very high. The approximate estimation error does not exceed 3.7%, the calculation time was less than 4 min. in the whole emitted perturbation range (fig. 4.17). Moreover, this kind of modulation is a reason of signal processing problem: intervals between commutations are irregular, thus errors in transfer function calculation are slightly increased because of different number of samples for irregular inverter states.

4.3. WIENER FILTER

a)



b)

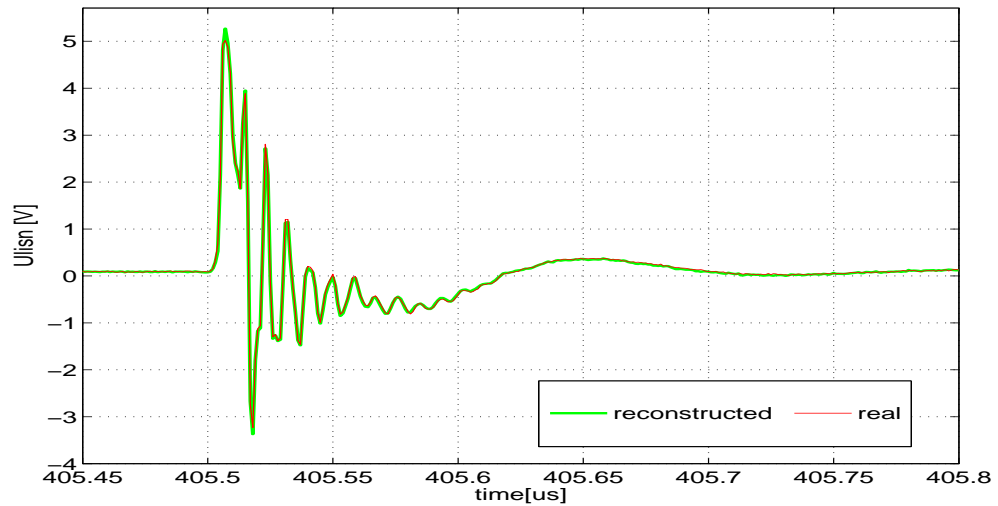


Figure 4.16: The measured and reconstructed voltage of LISN voltage waveforms for PDM modulation b) zoom

For perturbations estimation in hard switching inverter it is necessary to use several Wiener filters, because the level and waveform of perturbations strongly depend on system state. The analysis confirms that propagation path and contribution of inverter components are different for different state of inverter. Identification of commutation disturbances allows to link voltages across switches with perturbations. It is then possible to derive transfer function (impulse response in time domain) determining a relationship between the cause and effect of disturbances, that allows better understanding of EMI behavior of DC/AC hard switching inverter.

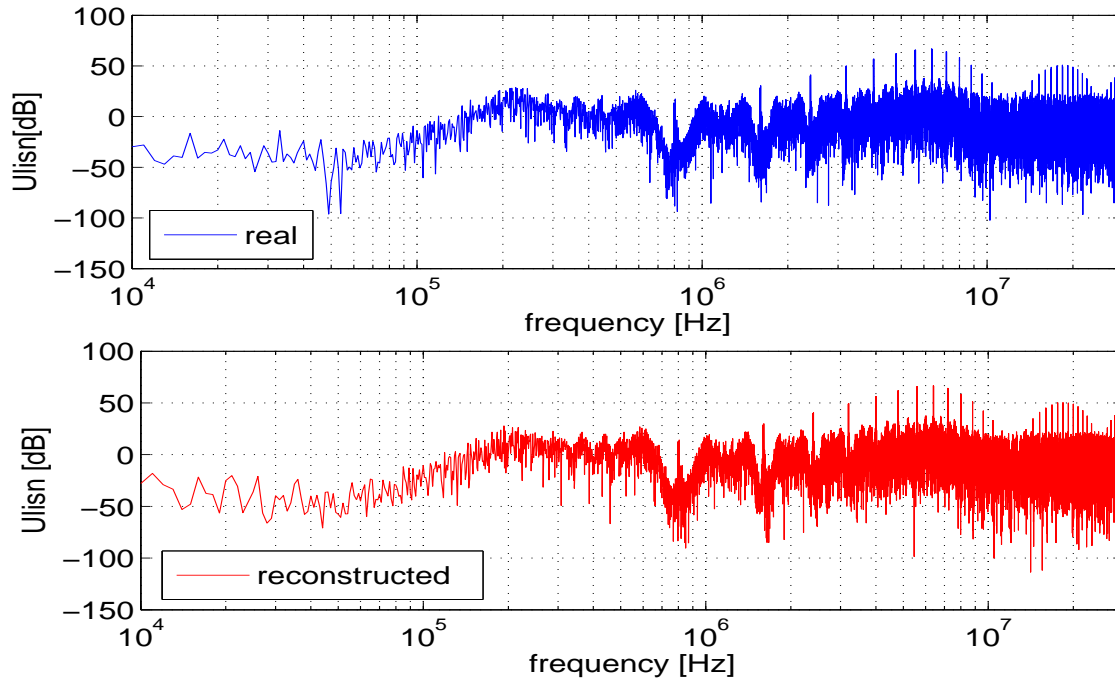


Figure 4.17: The LISN voltage spectra for PDM modulation **measured** and **Wiener filter estimation**

4.4 Conclusion

In this chapter, EMI behavior of hard switching inverter analysis has been presented. Accurate simulations, using complex models of all circuit components, have been used to observe currents and voltages during perturbation generation. The propagation paths have been investigated and new definition of inverter states has been proposed. The Wiener filtering method has been applied, where transfer function and/or impulse response for each state has been calculated using only voltages from inverter. However, if the differential mode noise takes greater part in total perturbation than in cases presented in this thesis, inverter currents variation also should be take into consideration. It can be said, that there are differences between transfer functions, what is the confirmation that the perturbation propagation path changes for each inverter state. This knowledge allows to built new tool for fast EMI perturbation estimation and separation noise from other sources. The validation has been done with data from simulation and measurement for two kinds of modulation.

Chapter 5

Soft switching inverter

A theory has only the alternative of being right or wrong. A model has a third possibility: it may be right, but irrelevant

Manfred Eigen

5.1 Introduction

A soft switching technique has been developed to alleviate an impact of EMI. The Zero - Voltage - Switching (ZVS) and the Zero - Current - Switching (ZCS) allow to reduce level of generated perturbation, especially for high frequency. Many authors present different topology structures of this kind of application [17], [34], [36], [69]. The soft switching inverter has less influence on perturbation generation because of lower dv/dt and di/dt and also allows to decrease voltage stress across the semiconductor devices, which are used as the power switches, what is attractive for high frequency and high power application [75], [77], [92]. The EMI generation mechanisms and the effects of soft switching technique on perturbation level is needed. In this thesis, ZVS parallel quasi resonant dc link voltage inverter (PQRDCLI) [41], [42] (Fig. 5.1), forcing the dc link voltage to zero during inverter switch commutation, is taken into consideration.

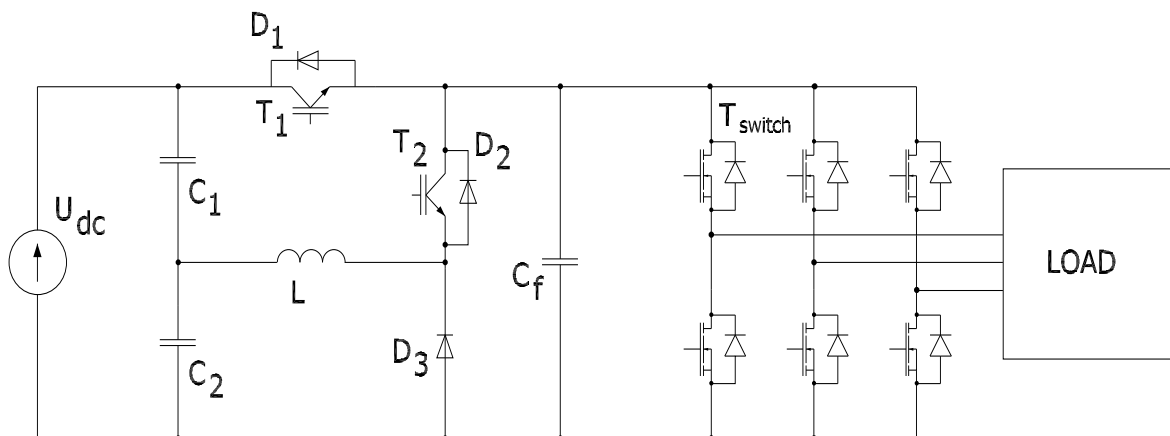


Figure 5.1: PQRDCLI circuit topology

The auxiliary resonant circuit is used to provide soft switching for the entire inverter. The state on inverter can only be changed at zero link voltage. In considered inverter, the PWM modulation is used, where a sine wave is compared with triangle waveform. The parallel quasi resonant circuit is located in the dc link of indirect frequency converter. Every commutation in the inverter is predated by reloading resonant circuit in order to discharge of the input capacitor C_f . Hence, transistors of the inverter bridge are switched in ZVS conditions.

The EMI behavior of soft switching inverter analysis has been investigated using simulation and Wiener filtering method, similar as it was done for hard switching inverter in chapter 4. The main source of electromagnetic perturbation is changing of the DC link voltage V_f . The rise and fall time of this voltage is much lower than in hard switching inverter and it depends on auxiliary resonant circuit parameters and operation conditions. Thus, the level of generated perturbation depends on geometrical and physical properties of circuit and transient operation of the semiconductor devices. It can be said, that the perturbation propagation path doesn't change significantly, as it is for hard switching inverter case (chapter 4.3.1), because state of all inverter semiconductor devices is always the same (ZVS) when commutation occurs. However, in the PQRDCLI, there are some differences in propagation path when voltage V_f rises up and falls down, so only two states of whole inverter are distinguished, what is connected with charging and discharging of C_f capacitor.

5.2 Simulation

The accurate wide band model of the quasi DC link resonant voltage inverter has been built in *SaberSketch*®. The circuit has been constructed using the same modeling procedure as for hard switching inverter (chapter 4.2). Furthermore, wide band models of all components, parasitics from auxiliary resonant and control circuit have been added. In spite of the simulation schema is not very accurate, because of simplified load, cables and power supply models, it is very useful for an inverter EMI behavior analysis and principle of operation. The simulation schema is presented in figure 5.2.

Using results of simulation, it is possible to observe all voltages and currents from the circuit. In figure 5.3, in the author opinion, are the most important waveforms for EMC analysis of considered inverter. It can be said, that the changing of DC link voltage and the inverter switches currents are the main source of perturbation and the first of these signals contains all necessary information to reconstruct V_{LISN} waveform. In figure 5.4 spectra of DC link voltage V_f (voltage accros capacitor C_f) and perturbation are presented, where it can be seen that these two signals are correlated. Moreover, some noise comes from T2 commutation, when it is switch on with non-ideal zero current condition.

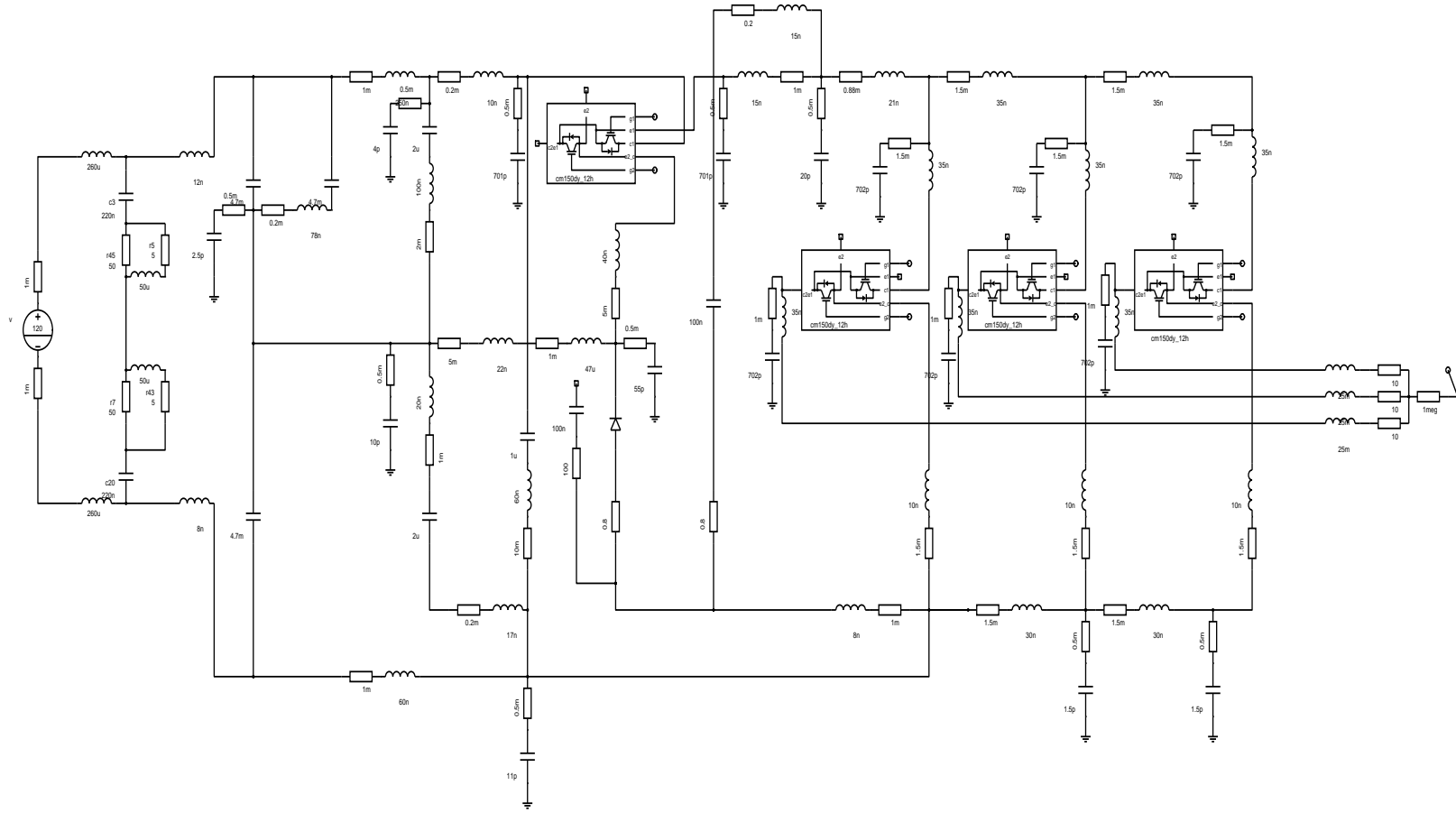


Figure 5.2: The quasi resonant dc link voltage inverter schema from SaberSketch

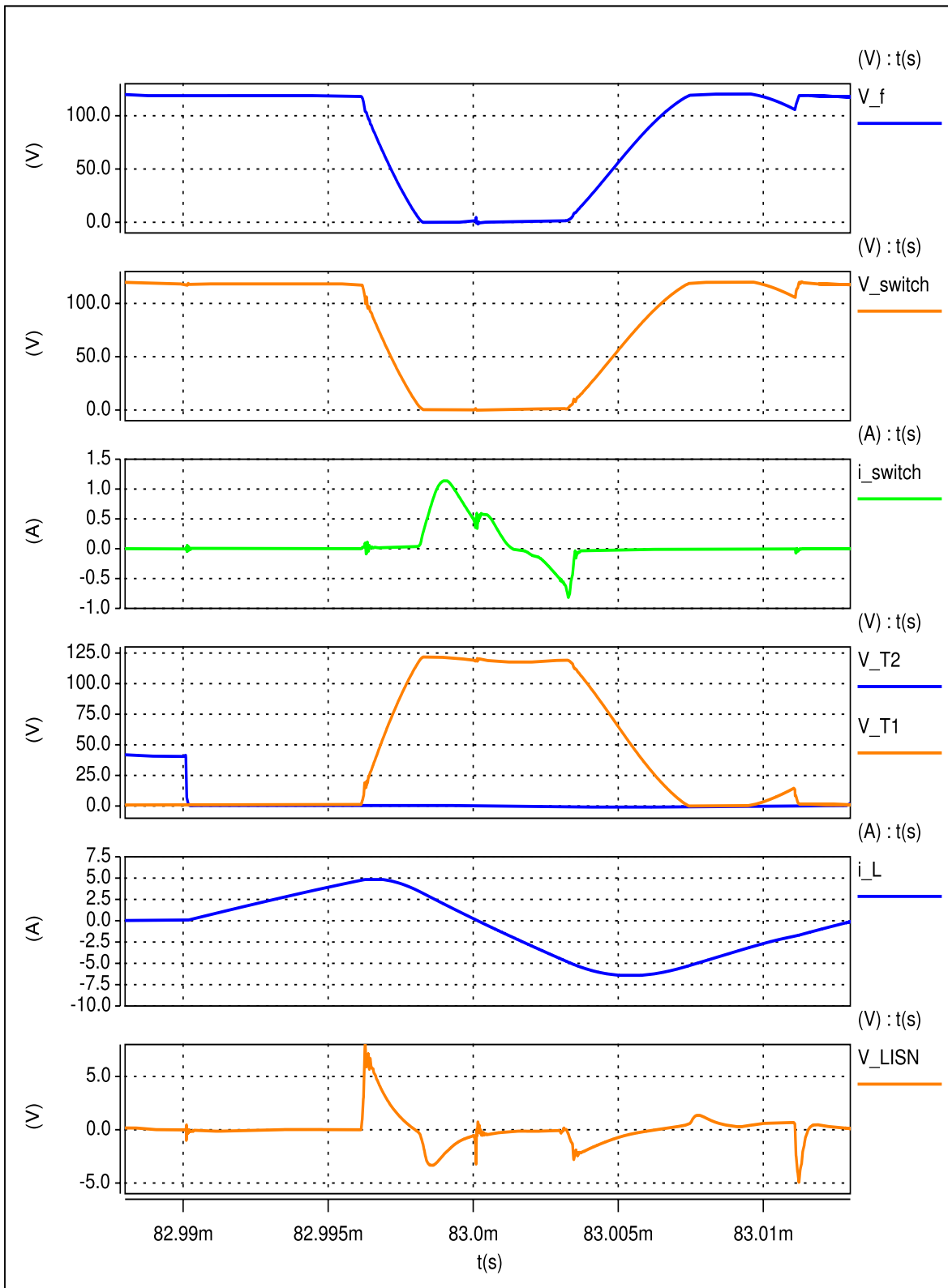


Figure 5.3: The simulation waveforms: V_f DC link voltage, V_{switch} - voltage across the one of inverter switches, i_{switch} - the one of inverter switch current, V_{T1} , V_{T2} - voltages across the T1 and T2 transistors, i_L - inductor L current, V_{LISN} - perturbation registered on LISN

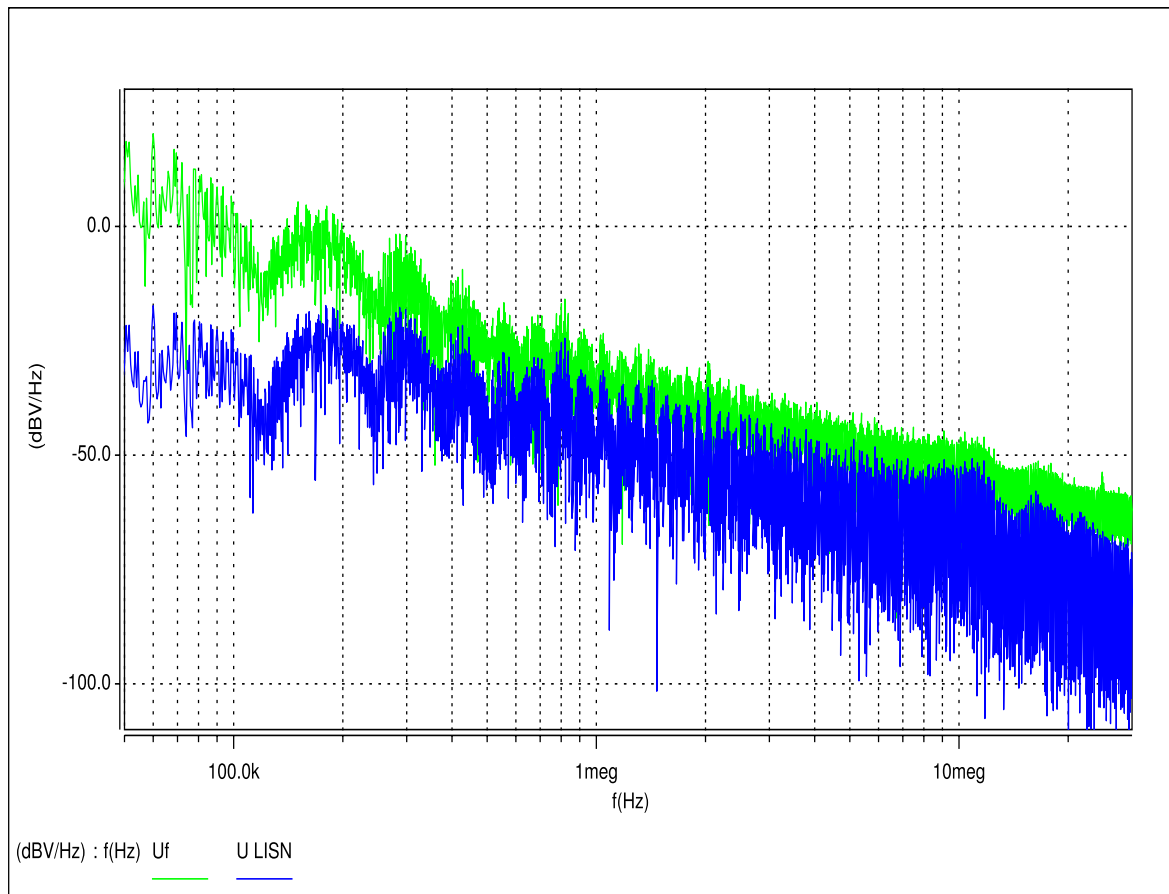


Figure 5.4: The spectra of **DC link voltage** and **perturbation** obtained from simulation

The time dependencies between all semiconductors turn on and off, in considered circuit, have an impact on the shape and the level of generated perturbation. The computer simulation allows to investigate influence of all parameters of an inverter and load. For example, all inverter transistors are turned on during some time t_{switch} , when DC link voltage is closed to zero voltage condition. If this time t_{switch} is changed, the dV_f/dt and amplitude of i_{switch} are also changed, what has influence on perturbation V_{LISN} . In figure 5.5, waveforms for two different times ($t_{switch1} > t_{switch2}$) are presented.

Moreover, it is possible to compare common and differential mode noise (according chapter 1.1). In this case - similar as for hard switching inverter (chapter 4.2), DM perturbation are much smaller in the whole conducted perturbation frequency range, what is shown in figure 5.6.

In order to show impact of the auxiliary resonant circuit on perturbation level, simulation of consider circuit have been done for hard switching. The transistors T1 was permanently turned on and T2 turned off - all operation of resonant circuit was stopped. In figure 5.7 perturbation spectra for soft and hard switching are compared. As it is known, resonance implies higher peak current an voltage, and thus higher disturbances in the low frequency range, whereas it generates lower high frequency perturbations due to smoother commutations.

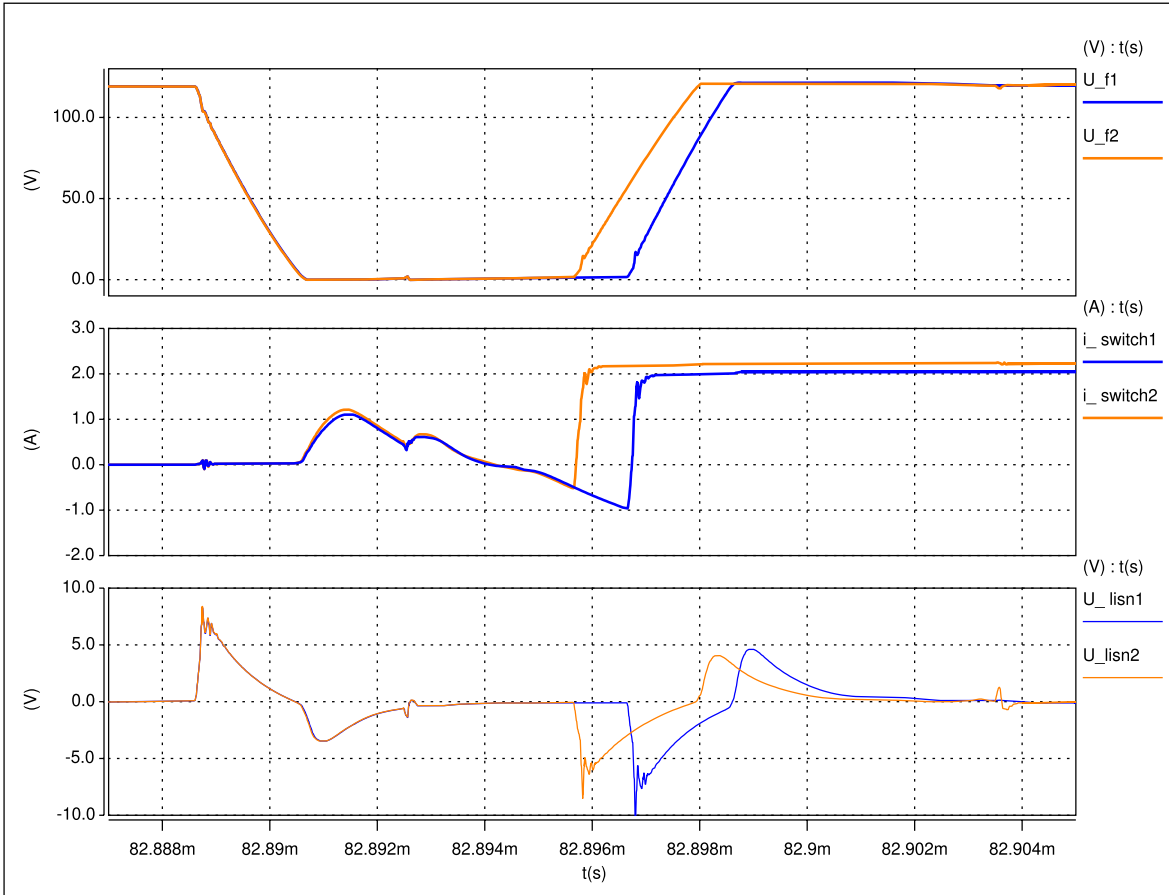


Figure 5.5: The comparison of the generated perturbation for two different times $t_{switch1} > t_{switch2}$

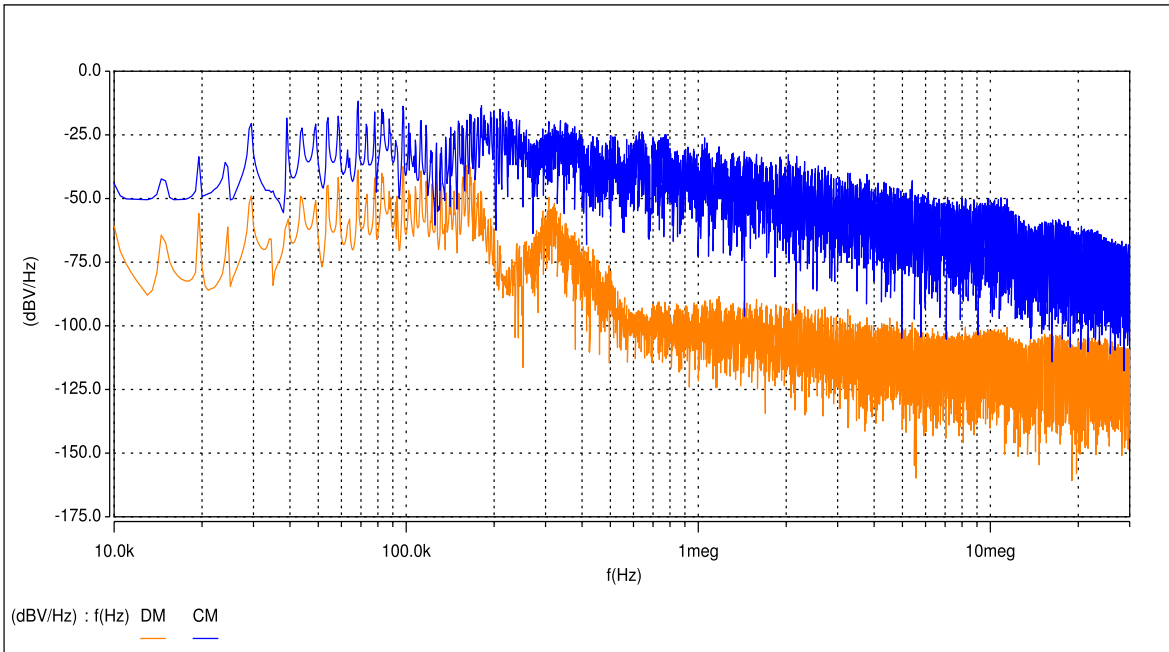


Figure 5.6: The differential-mode and common-mode noise comparison

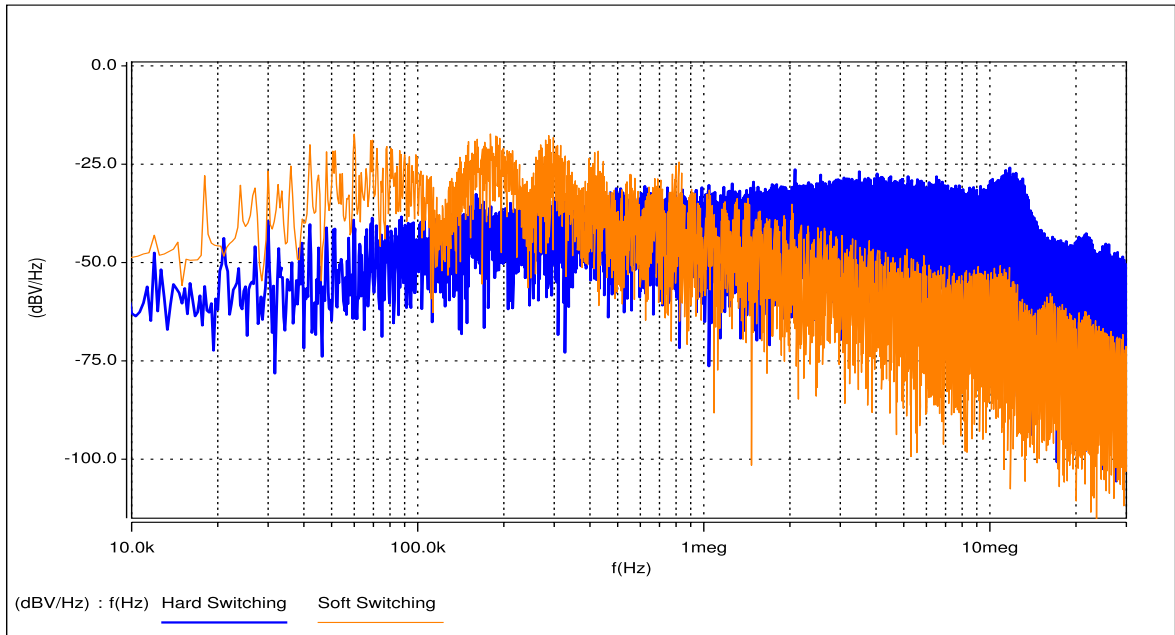


Figure 5.7: The comparison of the perturbation spectra for **soft** and **hard** switching inverter inverter

5.3 Experimental results

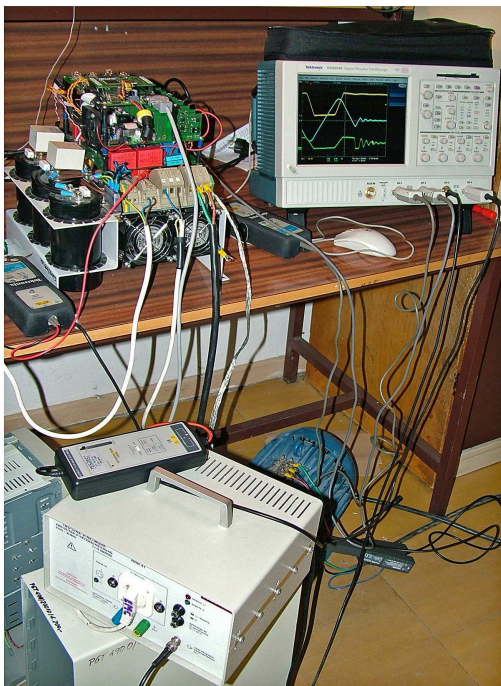


Figure 5.8: View of the quasi resonant DC link voltage inverter and LISN

An experimental investigation on conducted EMI of the quasi DC link resonant voltage inverter has been carried out. The converter has been connected to the power supply through the LISN (Schaffner NNB 41), where voltages has been registered in typical conditions of operation using the oscilloscope Textronix TDS5034B with high voltage differential probes. The sampling frequency was 250 ns. The converter load was an induction machine SZJe 34a, 220/380 V, 3 KW. The measurements have been done for different conditions of operation, load current and power factor and time dependencies, which were changing. In figure 5.9 one of the measurement results is shown. It should be said, that it doesn't precisely agree with the simulation, but the level, operation periods and voltage

slop shapes are similar. Moreover, the laboratory circuit contains additionally circuits like control system supply from DC/DC converter, which also generate perturbation, what can be seen in figures 5.9 and 5.13.

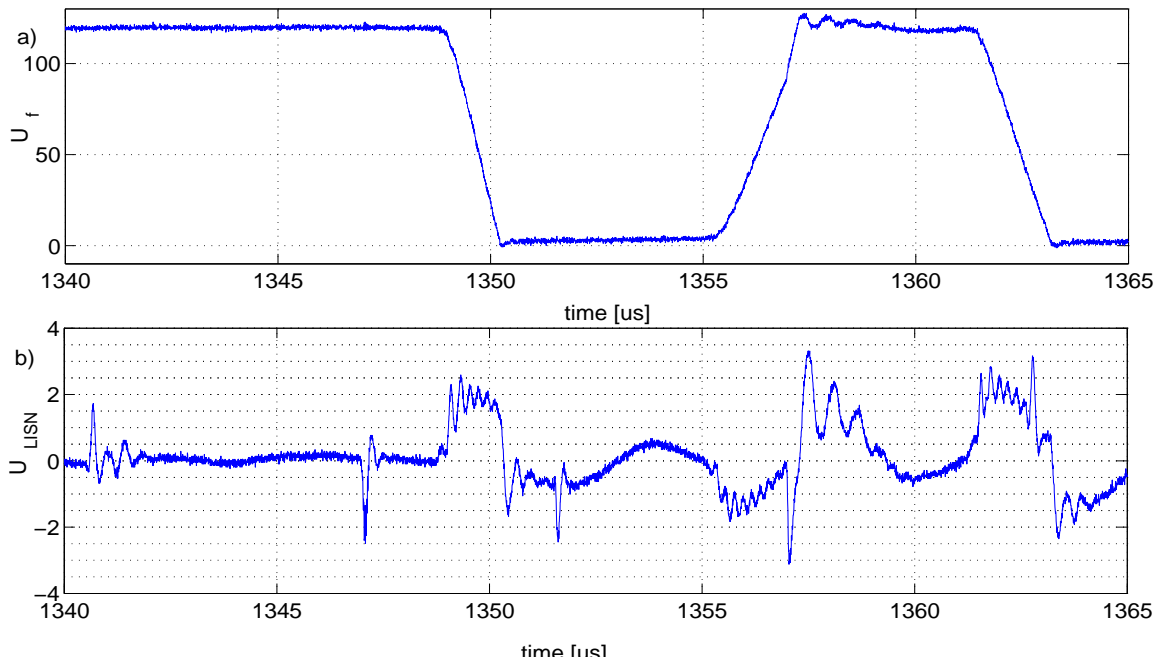


Figure 5.9: The measured transient waveforms a) V_f - DC link voltage, b) perturbation registered from LISN

5.4 Wiener filter

The computer based EMI analysis tools are required to aid better understanding and improving performance of soft switching inverters. The essential part of this thesis is to identify sources of disturbances and find transfer function between them and the generated perturbations. In order to calculate this transfer function, Wiener filtering method has been used. In the circuit, there are few source of disturbances, but the most significant one is the DC link voltage, which is changing when inverter switches state is to be changed. For all these operations, inverter state is always the same - all semiconductors are turned on, when the DC link voltage is zero volts. When DC link voltage comes from zero to V_f inverter can be in 8 different states, depend on all semiconductors state after commutation, but it has not significant influence on perturbation propagation path. However, the whole system is non stationary and perturbation propagation paths are different for DC link voltage rise up and fall down. Thus, in this case Wiener filter is synchronized on the changes of this system and two Wiener filters are used to described EMI behavior of the considered inverter. First, the data obtained from simulation has been used to calculate Wiener filters. Results are shown in figure 5.10, where source of disturbances is present. The perturbation from simulation and reconstructed with Wiener filter are compared. The average reconstruction errors is 4.3 %. One can notice that, the perturbation caused by T_2 transistor commutation are not reconstructed correctly (figures 5.13 and 5.12).

5.4. WIENER FILTER

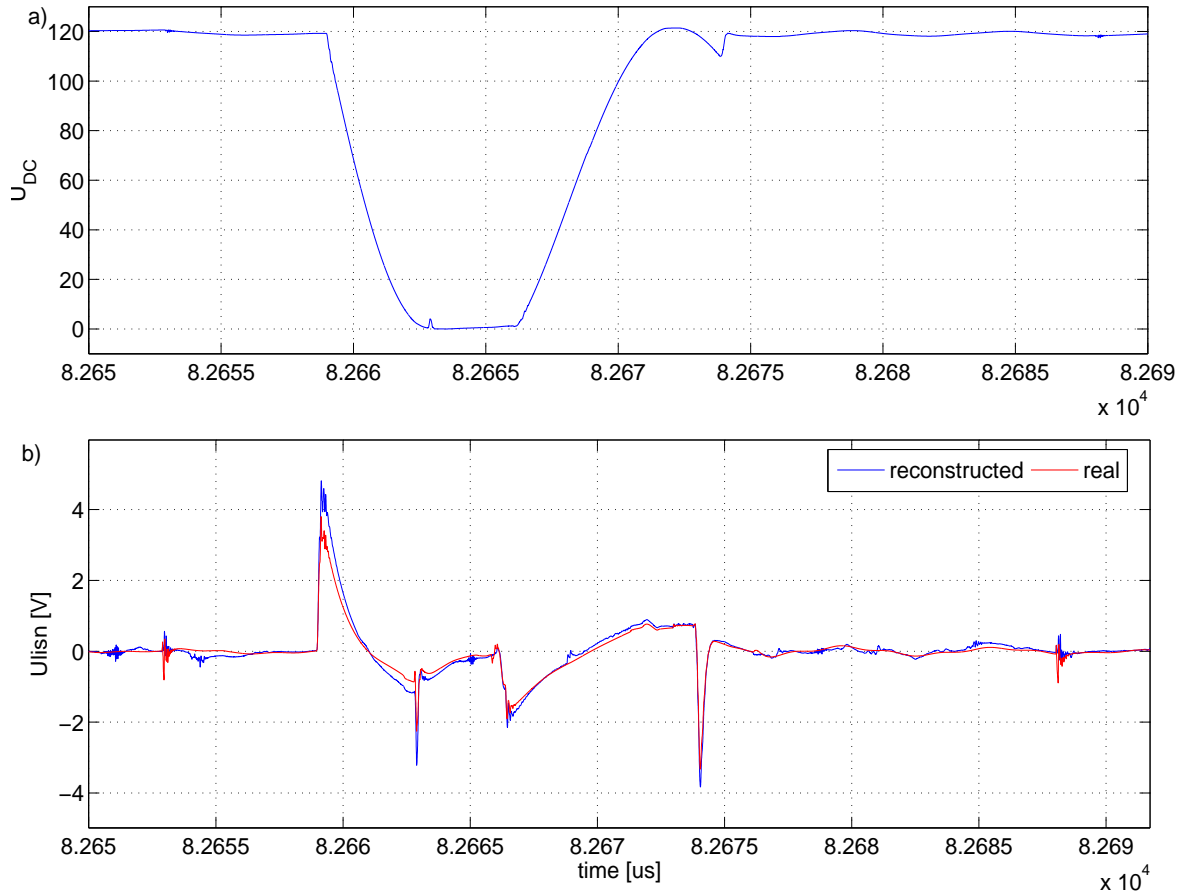


Figure 5.10: The DC link (a) and LISN voltages (b) waveforms from **simulation** and **Wiener filter reconstruction**

The propagation path depends on auxiliary circuit state. Fundamentally, the two states can be distinguished, one when DC link voltage rises up and the second when it falls down. The transfer functions for these two states are presented in figure 5.11. It can be confirmed, that spectra are completely different in the frequency range above 10 MHz, what proves the thesis of this work, that the level and propagation paths are depended on system state.

The Wiener filtering method has been also used with data from measurement. The reconstructed waveforms (Figure 5.12) don't agree precisely with measured ones as from simulation data, because the perturbation signal contains more noise, which is uncorrelated with DC link voltage. Moreover, in the figure 5.6, it can be observed that propagation path for DM and CM noise is completely different, what can be an explanation of Wiener filtering method accuracy. However, referring to spectra in figure 5.15, it can be found that in this case Wiener filtering method also works well. In figure 5.13, influence of the external DC/DC converter and T_2 commutation on total perturbation waveform is shown. These two signals are not correlated with the avowed source of disturbance signal (DC link voltage), hence the impact of them in reconstructed signal is not observabled.

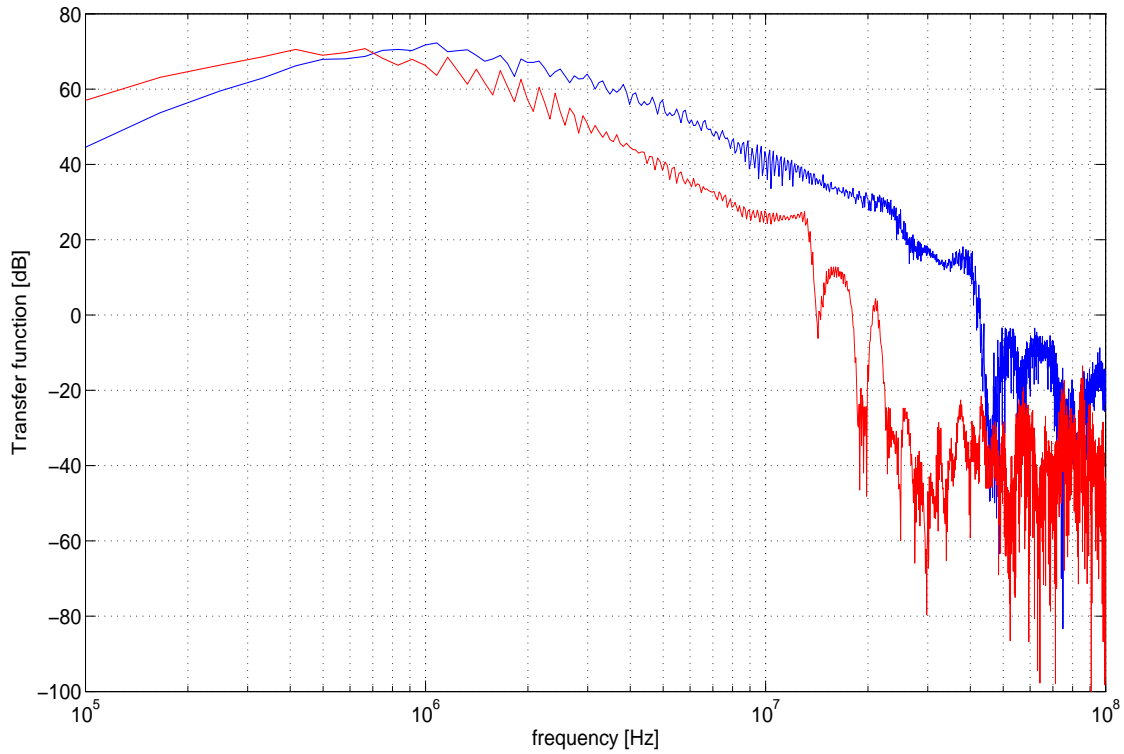


Figure 5.11: The Wiener filter transfer functions for two states of inverter

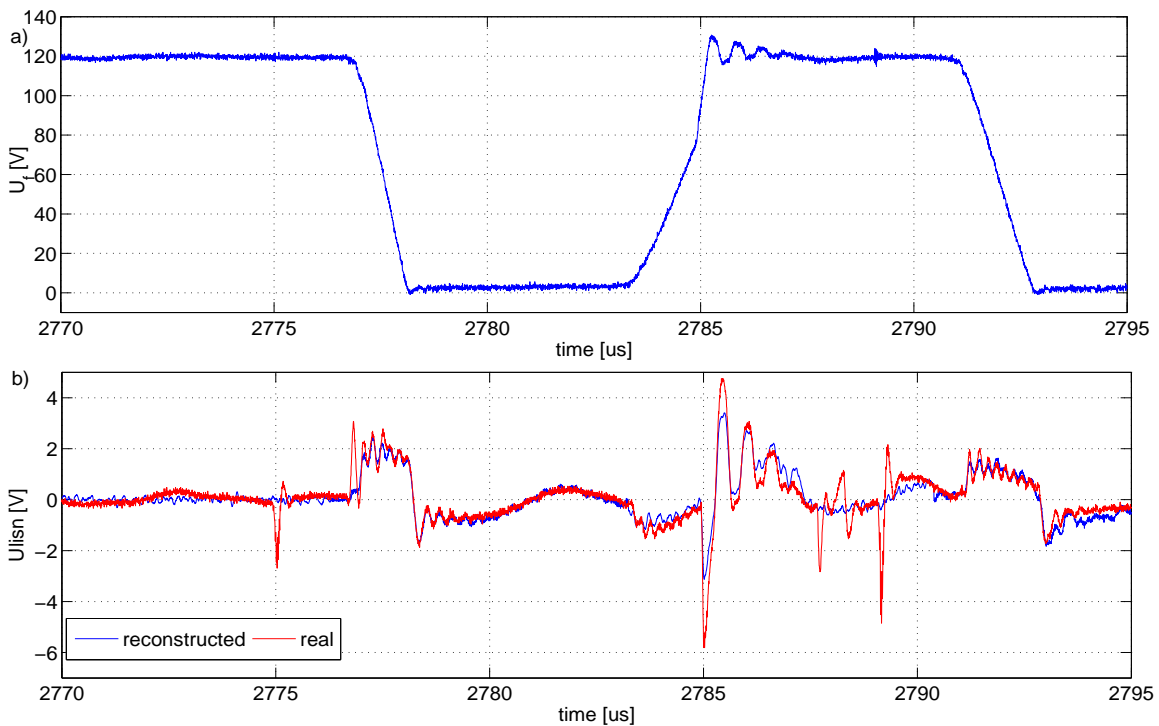


Figure 5.12: The DC link (a) and LISN voltage (b) waveforms from **measurement** and **Wiener filter**

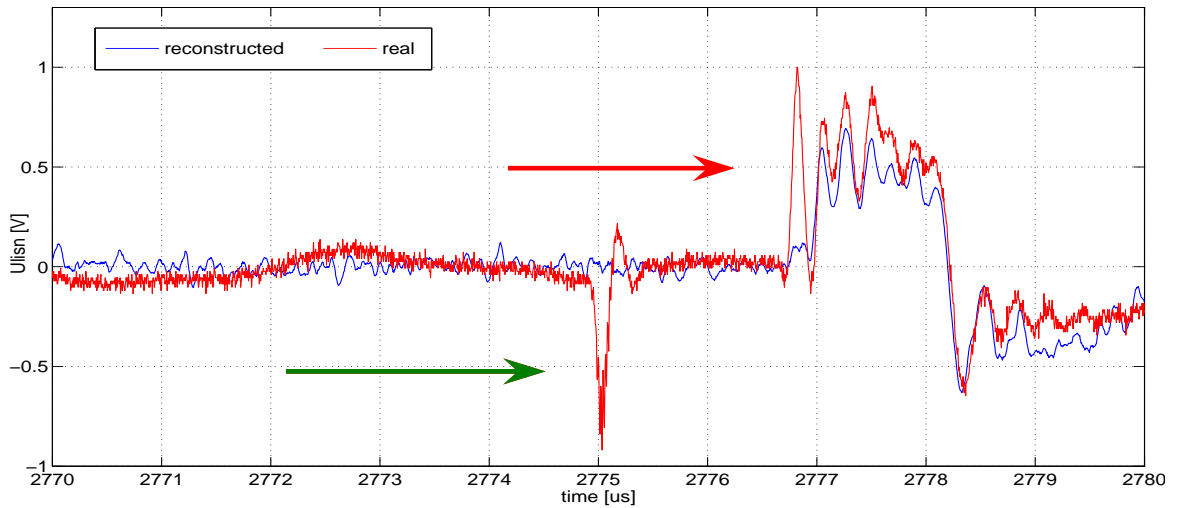


Figure 5.13: The LISN voltage waveforms from measurement and Wiener filter - influence of external DC/DC converter -> and T_2 commutation ->

Moreover, it is possible using Wiener filtering method to separate noise from external converter providing its input signal to Wiener filter, during adaptation process. In the figure 5.14 waveform of total perturbation (a) is divided to ones from the inverter and the external DC/DC converter. The spectra of these signals are presented in figure 5.15. These kind of results can be useful for reduction and analysis of EMI in real application, where signal from LISN contains perturbations from more than one source.

5.5 Conclusion

In this chapter, EMI behavior of soft switching inverter analysis has been presented. Using data obtained from simulation, the main sources of disturbances have been identified. In this particular case, changes of DC link voltage V_f and currents in inverter semiconductors are the main reason of generated perturbation. The perturbations are also generated because of the operation of T_2 and external sources. The Wiener filtering method, using two filters, have been applied. The validation has been made for data obtained from simulation and measurement. This method allows to separate noises from different sources in time or frequency domain.

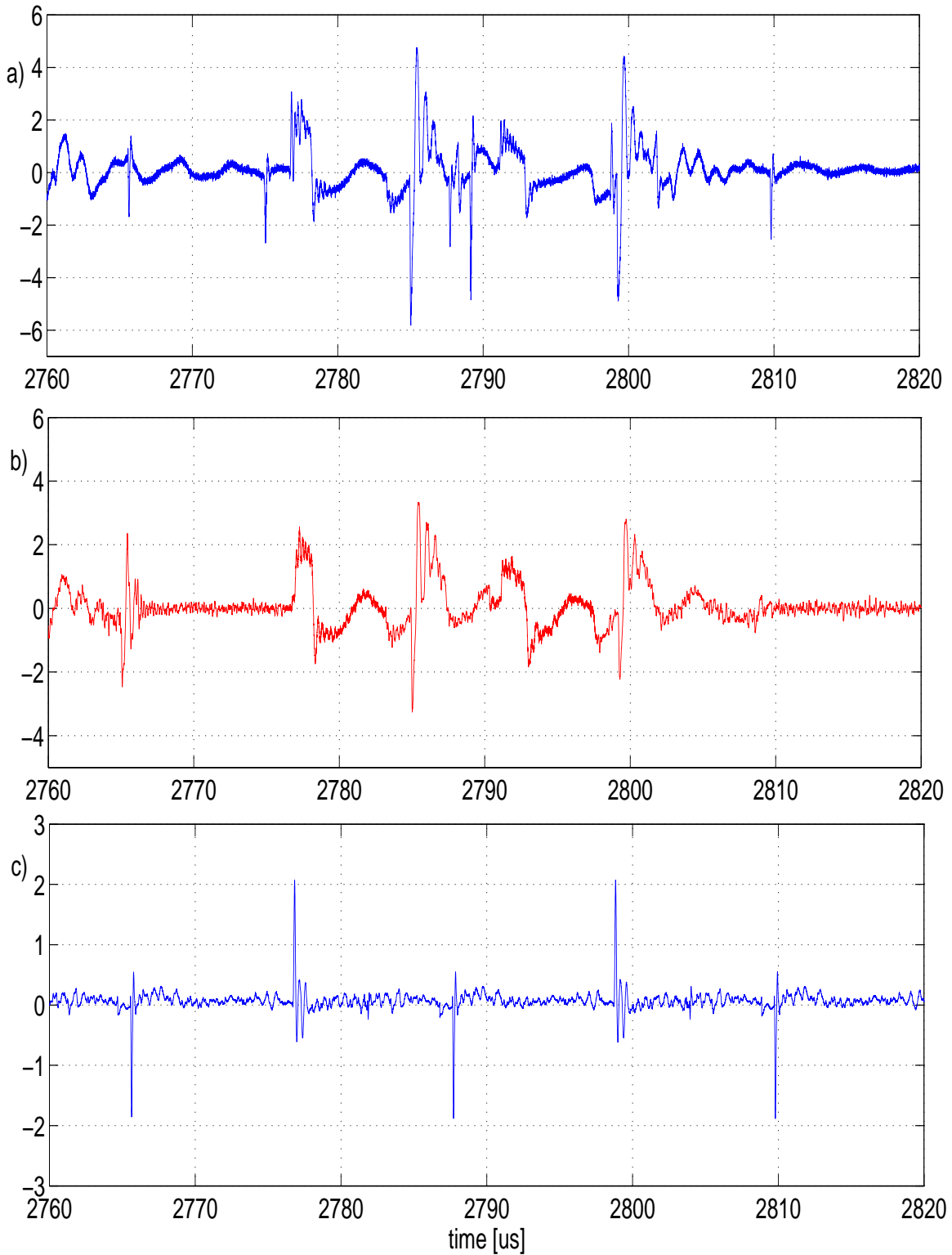


Figure 5.14: The LISN voltage waveforms from measurement and Wiener filter - separation of perturbation from external DC/DC converter a) voltage measured b) perturbation from inverter c) perturbation from external DC/DC converter

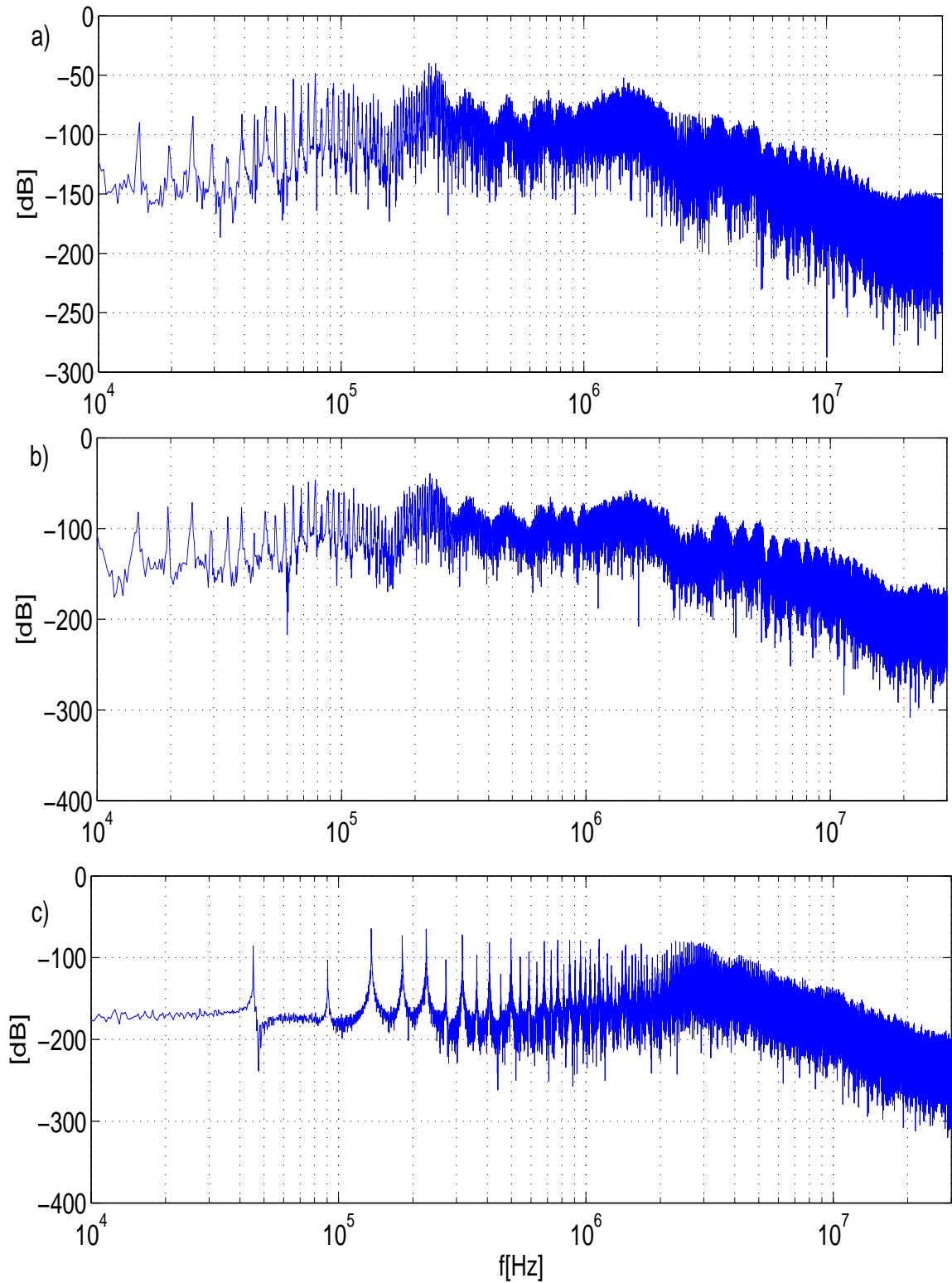


Figure 5.15: The LISN voltage spectra from measurement and Wiener filter - separation of perturbation from DC/DC converter a) voltage measured

b) perturbation from inverter c) perturbation from external DC/DC converter

There are no answers, only cross-references

Norbert Wiener

6.1 Summary and overview

This thesis gives a step to better understand phenomena connected to conducted perturbations generation. EMI behavior of power electronics converters has been investigated using computer simulation and digital signal processing method - Wiener filtering. In the simulation study, the most accurate presently available models of components of circuit have been used and improved. The layout equivalent circuit of considered applications, for capacitive behavior, has been proposed. The results allow to observe all currents and voltages from the system and to analyze phenomena connected with perturbation generation and propagation. This methodology is very useful in design process, when a cost of optimization is relatively low. Moreover, the sensitivity of circuit parameters have been checked. As it has been shown, the most important are values of parasitics, especially capacitance to the ground. The results of calculation have been verified by measurements. However, the disadvantages of simulation are as follows: building of simulated circuit needs much work and time, powerful computer and simulation program. There are difficulties with finding correct component models and values of circuit parameters.

The proposed Wiener filtering method is very useful for identifying the transfer function between source and generated perturbations. It allows to identify the source of perturbations - fast changing rate of voltages or currents of semi-conductors in the circuit. In order to reconstruct perturbations of considered converters, n Wiener filters have been used, where n depends on number of converter states. The main thesis contribution was to prove a proper representation number and choice of filter for three categories of converters:

1. DC/DC boost converter ($n = 2$)
2. DC/AC hard switching inverter ($n = 24$)
3. DC/AC soft switching inverter ($n = 2$)

The transfer functions for all inverter states are different, resulting that the level of perturbations generated in power electronics converters depend on their actual state. The analysis confirmed that propagation path and contribution of inverter components are different for different state of inverter. The identification of commutation disturbances allows to link voltages across switches with perturbations. It is then possible to derive transfer functions (impulse responses in time domain) determining a relationship between the cause and effect of disturbances. Using this approach, it is possible to reconstruct perturbation waveforms or spectra with very high accuracy or predicting EMI with different command laws, without any real implantation or time consuming simulation.

Furthermore, the comparison of soft and hard switching of inverter has been effected. It can be noticed, that soft switching technique allows to reduce perturbation in high frequency range, but it has minor impact on perturbation level for low frequencies. Thus, soft switching technique can be mainly use in order to reduce the high frequency perturbation.

6.2 Future work

Can we evaluated the implications of identifying the transfer function between source and generated perturbations, using Wiener filtering method ? In the author's opinion, it allows to reconstruct generated perturbation, what can be particularly useful in:

- optimization of operation condition of already existing system, for example in investigation of modulation strategy or finding optimal shape of waveform of voltages across the switches
- building the inverter models for fast EMI estimation in electronics simulation, but first the separate Wiener filters for differential-mode and common-mode perturbation should be calculated
- reduction of EMI perturbation in design process by layout optimization
- EMC filter design
- development of new inverters topologies and models.

Bibliography

- [1] *SaberBook online documentation Synopsys 06.2006.*
- [2] B. Allard, H. Garrab, W. Mi, K. Ammous, and H. Morel. Switching parameter maps-a new approach to the validity domain of power device models. 3:1220–1225, 2003.
- [3] B. Archambeault. Concerns and approaches for accurate EMC simulation validation. In *Electromagnetic Compatibility, 2003 IEEE International Symposium on*, volume 1, pages 329–334, 2003.
- [4] S. Asai, M. Funaki, H. Sawa, and K. Kato. Fabrication of an insulated metal substrate (IMS), having an insulating layer with a high dielectric constant. *Components, Hybrids, and Manufacturing Technology, IEEE Transactions on [see also IEEE Trans. on Components, Packaging, and Manufacturing Technology, Part A, B, C]*, 16(5):499–504, 1993.
- [5] D. Berning and J. Hefner, A.R. IGBT model validation for soft-switching applications. *IEEE Transactions on Industry Applications*, 37(2):650–660, 2001.
- [6] M. Besacier, J. L. Schanen, J. Roudet, P. Suau, and J. Crebier. PSPICE-compatible electrical equivalent circuit for busbars. In *Applied Power Electronics Conference and Exposition, 2000. APEC 2000. Fifteenth Annual IEEE*, volume 2, pages 846–851, 2000.
- [7] E. Bogatin. Design rules for microstrip capacitance. *Components, Hybrids, and Manufacturing Technology, IEEE Transactions on*, 11(3):253–259, 1988.
- [8] E. Bogatin. A closed form analytical model for the electrical properties of microstrip interconnects. *Components, Hybrids, and Manufacturing Technology, IEEE Transactions on*, 13(2):258–266, 1990.
- [9] M. Cacciato, A. Consoli, G. Scarcella, S. De Caro, and A. Testa. High frequency modeling of dc/ac converters. *EPE 2005*, Sept. 2005.
- [10] M. Cacciato, A. Consoli, G. Scarcella, and A. Testa. Reduction of common-mode currents in PWM inverter motor drives. *IEEE Transactions on Industry Applications*, 35(2):469–476, 1999.

-
- [11] E. Clavel. *INCA manual*. LEG/ENSIEG.
- [12] D. Cochrane. *Passive Cancellation of Common-Mode Electromagnetic Interference in Switching Power Converters*. PhD thesis, Virginia Polytechnic Institute, 10 2001.
- [13] B. Cogitore, J. Keradec, and J. Barbaroux. The two-winding transformer: an experimental method to obtain a wide frequency range equivalent circuit. *IEEE Transactions on Instrumentation and Measurement*, 43(2):364–371, Apr. 1994.
- [14] F. Costa, E. Laboure, F. Forest, and S. Lefebvre. Quantification and minimization of conducted interferences generated in hard switching and zero current switching cells. pages 615–621, 1994.
- [15] J. Crebier, J. Roudet, and J. L. Schanen. Problems using LISN in EMI characterization of power electronic converters. In *Power Electronics Specialists Conference, 1999. PESC 99. 30th Annual IEEE*, volume 1, pages 307–312, 1999.
- [16] J.-C. Crebier, J. Roudet, and J. L. Schanen. EMI analysis of single phase pfc boost rectifier in the frequency domain. *Revue Internationale de Génie Electrique*, 2, Issue: 2:215–241, Feb. 1999.
- [17] D. Divan and G. Skibinski. Zero-switching-loss inverters for high-power applications. *IEEE Transactions on Industry Applications*, 25(4):634–643, July/Aug. 1989.
- [18] J. Ekman. Experimental verification of PEEC based electric field simulations. In *Electromagnetic Compatibility, 2001. EMC. 2001 IEEE International Symposium on*, volume 1, pages 351–355, 2001.
- [19] J. Ekman, G. Antonini, and A. Orlandi. 3d PEEC capacitance calculations. In *Electromagnetic Compatibility, 2003 IEEE International Symposium on*, volume 2, pages 630–635, 2003.
- [20] J. Ferreira, P. Willcock, and S. Holm. Sources, paths and traps of conducted EMI in switch mode circuits. In *Industry Applications Conference, 1997. Thirty-Second IAS Annual Meeting, IAS '97., Conference Record of the 1997 IEEE*, volume 2, pages 1584–1591, 1997.
- [21] W. Fischer and H. Mecke. Application of data sheet based dynamic semiconductor models in the simulation of inverter welding power sources. In *Power Conversion Conference, 2002. PCC Osaka 2002. Proceedings of the*, volume 3, pages 1369–1374, 2002.
- [22] M. Gitau. Modeling conducted EMI noise generation and propagation in boost converters. In *Industrial Electronics, 2000. ISIE 2000. Proceedings of the 2000 IEEE International Symposium on*, volume 2, pages 353–358, 2000.
- [23] J. Guichon, J. L. Schanen, J. Roudet, and B. Meille, R. and Revol. Design of a PWM inverter regarding conducted EMC and losses: influence of some key parameters. In *Industry Applications Conference, 2005. Fourtieth IAS Annual Meeting. Conference Record of the 2005*, volume 3, pages 1855–1859, 2005.

- [24] K. Gulez, N. Mutoh, M. Ogata, F. Harashima, and K. Ohnishi. An approximation to improve EMI passive filter condition with triple-LISN for EMI noise problem. In *SICE 2002. Proceedings of the 41st SICE Annual Conference*, volume 2, pages 929–934, 2002.
- [25] J. He, J. Jiang, J. Huang, and W. Chen. Model of EMI coupling paths for an off-line power converter. In *Applied Power Electronics Conference and Exposition, 2004. APEC '04. Nineteenth Annual IEEE*, volume 2, pages 708–713, 2004.
- [26] J. Hu, J. von Bloh, and R. De Doncker. Typical impulses in power electronics and their EMI characteristics. In *Power Electronics Specialists Conference, 2004. PESC 04. 2004IEEE 35th Annual*, volume 4, pages 3021–3027, 2004.
- [27] X. Huang, E. Pepa, J.-S. Lai, J. Hefner, A.R., D. Berning, S. Chen, and T. Nehl. EMI characterization with parasitic modeling for a permanent magnet motor drive. In *Industry Applications Conference, 2003. 38th IAS Annual Meeting. Conference Record of the*, volume 1, pages 416–423, 2003.
- [28] K. Iwan, P. Musznicki, M. Turzyński, and P. J. Chrzan. Modelowanie i symulacja zaburzeń przewodzonych z zastosowaniem programów Saber i TCad. *Nowa Elektrotechnika*, 5(9):27–28, 2005.
- [29] K. Iwan, P. Musznicki, M. Turzyński, and P. J. Chrzan. Modelowanie i symulacja zaburzeń przewodzonych z zastosowaniem programów saber i tcad. In *PPEE'2005 XI Sympozjum Podstawowe problemy energoelektroniki i elektromechaniki*, 2005.
- [30] K. Iwan, M. Turzyński, and P. J. Chrzan. Szerokopasmowy model uogólnionego łącznika energoelektronicznego. In *Sterowanie w Energoelektronice i Napędzie Elektrycznym SENE 2005 : VII Krajowa Konferencja Naukowa*, 2005.
- [31] M. Jin, M. Weiming, Z. Lei, and Z. Zhihua. Identification of essential coupling path models for conducted EMI prediction in switching power converters. In *Industry Applications Conference, 2004. 39th IAS Annual Meeting. Conference Record of the 2004 IEEE*, volume 3, pages 1832–1839, 2004.
- [32] A. Kempster. *Elektromagnetyczne zaburzenia przewodzone w układach napędów przekształtnikowych*, ISBN: 83-89712-70-9. Monografie, T. 5. Oficyna Wydaw. Uniwersytetu Zielonogórskiego, Zielona Góra, 2005.
- [33] A. Kempster, R. Smolenski, and R. Strzelecki. Common mode current paths and their modeling in PWM inverter-fed drives. In *Power Electronics Specialists Conference, PESC 02. IEEE 33rd Annual*, volume 3, pages 1551–1556, 2002.
- [34] M. Krogemann and J. Clare. A soft switching parallel quasi resonant DC-link inverter with modified asynchronous space vector PWM. In *Power Electronics and Variable Speed Drives, 1996. Sixth International Conference on (Conf. Publ. No. 429)*, pages 208–213, Sept. 1996.
- [35] M. Kumar and V. Agarwal. Power line filter design for conducted electromagnetic interference using time-domain measurements. *IEEE Transactions on Electromagnetic Compatibility*, 48(1):178–186, 2006.

-
- [36] M. Kurokawa, Y. Konishi, and M. Nakaoka. Evaluations of voltage-source soft-switching inverter with single auxiliary resonant snubber. *IEE Proceedings- Electric Power Applications*, 148(2):207–213, Mar. 2001.
- [37] J.-S. Lai, X. Huang, E. Pepa, and T. Shaotang Chen and Nehl. Inverter EMI modeling and simulation methodologies. In *Industrial Electronics Society, 2003. IECON '03. The 29th Annual Conference of the IEEE*, volume 2, pages 1533–1539, 2003.
- [38] J.-S. Lai., H. Xudong, E. Pepa, C. Shaotang, and T. Nehl. Inverter EMI modeling and simulation methodologies. *IEEE Transactions on Industrial Electronics*, 53(3):736–744, 2006.
- [39] Q. Liu, F. Wang, and D. Boroyevich. Model conducted EMI emission of switching modules for converter system EMI characterization and prediction. In *Industry Applications Conference, 2004. 39th IAS Annual Meeting. Conference Record of the 2004 IEEE*, volume 3, pages 1817–1823, 2004.
- [40] J. Mahdavi, M. Tabandeh, and A. Shahriari. Comparison of conducted RFI emission from different unity power factor AC/DC converters. In *Power Electronics Specialists Conference, 1996. PESC '96 Record., 27th Annual IEEE*, volume 2, pages 1979–1985, Baveno, 1996.
- [41] S. Mandrek and P. J. Chrzan. Patent: Pośredni przemiennik częstotliwości z quasi-rezonansowym obwodem pośredniczącym. *Biuletyn Urzędu Patentowego ISSN - 0137 - 8015*, (P.372473, BTT/79/05), 2006.
- [42] S. Mandrek and P. J. Chrzan. Quasi resonant dc link inverter with reduced number of active components. : To be published in *IEEE Transactions on Industrial Electronics No 2*. 2007.
- [43] D. G. Manolakis, V. K. Ingle, and S. M. Kogan. *Statistical and adaptive signal processing: spectral estimation, signal modeling, adaptive filtering, and array processing*. Artech House, Inc, 2005.
- [44] C. Martin, J. L. Schanen, and R. Pasterczyk. Power integration: electrical analysis of new emerging package. *EPE'03*, June 2002.
- [45] W. Mi. *Extraction des paramètres et domaine de validité du modèle d'un composant de puissance*. PhD thesis, INSA de Lyon, 01 2004.
- [46] H. Morel, S. Gamal, and J. Chante. State variable modeling of the power pin diode using an explicit approximation of semiconductor device equations: a novel approach. *IEEE Transactions on Power Electronics*, 9(1):112–120, 1994.
- [47] P. Mugur, J. Roudet, and J. Crebier. Power electronic converter EMC analysis through state variable approach techniques. *IEEE Transactions on Electromagnetic Compatibility*, 43(2):229–238, 2001.
- [48] P. Musznicki, P. J. Chrzan, S. Mandrek, and J. Jamet. Modelling of PCB layout parasitic for resonant dc link inverter. In *V Summer Seminar on Nordic Network for Multi Disciplinary Optimised Electric Drives*, September 2005.

BIBLIOGRAPHY

- [49] P. Musznicki, J. L. Schanen, B. Allard, and P. J. Chrzan. Accurate modeling of layout parasitic to forecast EMI emitted from a DC-DC converter. In *Power Electronics Specialists Conference, 2004. PESC 04. 2004 IEEE 35th Annual*, volume 1, pages 278–283, 2004.
- [50] P. Musznicki, J. L. Schanen, and P. J. Chrzan. Design of high voltage busbar: trade off between electrical field and stray inductance. In *3rd International Workshop Compatibility in PowerElectronics CPE 2003*, 2003.
- [51] P. Musznicki, J. L. Schanen, P. Granjon, and P. J. Chrzan. Better understanding EMI generation of power converters. In *Power Electronics Specialists, 2005 IEEE 36th Conference on*, pages 1052–1056, June 2005.
- [52] P. Musznicki, J. L. Schanen, P. Granjon, and P. J. Chrzan. EMI estimation for dc/ac hard switching converter using wiener filter. In *12th International Power Electronics and Motion Control Conference - EPE-PEMC 2006*, Portoroz, Slovenia, 2006.
- [53] M. Nagrial and A. Hellany. EMI/EMC issues in switch mode power supplies (SMPS). In *Electromagnetic Compatibility, 1999. EMC York 99. International Conference and Exhibition on (Conf. Publ. No. 464)*, pages 180–185, 1999.
- [54] P. Okyere and L. Heinemann. Computer-aided analysis and reduction of conducted EMI in switched-mode power converter. In *Applied Power Electronics Conference and Exposition, 1998. APEC '98. Conference Proceedings 1998., Thirteenth Annual*, volume 2, pages 924–928, 1998.
- [55] C. R. Paul. *Introduction to Electromagnetic Compatibility*. Wiley-Intersciences, New York, 1992.
- [56] X. Pei, K. Zhang, Y. Kang, and J. Chen. Analytical estimation of common mode conducted EMI in PWM inverter. In *Industry Applications Conference, 2004. 39th IAS Annual Meeting. Conference Record of the 2004 IEEE*, volume 4, pages 2651–2656, Oct. 2004.
- [57] A. Petrie and C. Hymowitz. A SPICE model for IGBTs. In *Applied Power Electronics Conference and Exposition, 1995. APEC '95. Conference Proceedings 1995., Tenth Annual*, number 0, pages 147–152, /Mar. 1995.
- [58] L. Ran, S. Gokani, J. Clare, K. Bradley, and C. Christopoulos. Conducted electromagnetic emissions in induction motor drive systems part II : Frequency domain models. *IEEE Transactions on Power Electronics*, 13(6):1229–1229, Nov. 1998.
- [59] B. Revol. *Modélisation et optimisation des performances CEM d'une association variateur de vitesse - machine asynchrone*. PhD thesis, Université Joseph-Fourier - Grenoble I, 11 2003.
- [60] B. Revol, J. Roudet, J. Schanen, and P. Loizelet. EMI study of a three phase inverter-fed motor drives. In *Industry Applications Conference, 2004. 39th IAS Annual Meeting. Conference Record of the 2004 IEEE*, volume 4, pages 2657–2664, Oct. 2004.

-
- [61] B. Revol, J. Roudet, J. L. Schanen, and P. Loizelet. Fast EMI prediction method for three-phase inverter based on laplace transforms. In *Power Electronics Specialist Conference, 2003. PESC '03. 2003 IEEE 34th Annual*, volume 3, pages 1133–1138, 2003.
- [62] L. Rossetto, S. Buso, and G. Spiazzi. Conducted EMI issues in a 600-W single-phase boost PFC design. *IEEE Transactions on Industry Applications*, 36(2):578–585, 2000.
- [63] L. Rossetto, G. Spiazzi, and P. Tenti. Boost PFC with 100-hz switching frequency providing output voltage stabilization and compliance with EMC standards. *IEEE Transactions on Industry Applications*, 36(1):188–193, 2000.
- [64] L. Rossetto, P. Tenti, and A. Zuccato. Electromagnetic compatibility issues in industrial equipment. *IEEE Industry Applications Magazine*, 5(6):34–46, 1999.
- [65] L. Rossetto, P. Tenti, and A. Zuccato. Electromagnetic compatibility issues in industrial equipment. *IEEE Industry Applications Magazine*, 5(6):34–46, 1999.
- [66] S. Ruayariyasub, W. Thammasiriroj, W. Khan-ngern, and S. Nitta. An analysis of the conducted emi emission using the transient response model. In *EMC'04/Sendai*, pages 833–837, 2004.
- [67] A. E. Ruehli. Inductance calculations in a complex integrated circuit environment. *j-IBM-JRD*, 16(5):470–481, Sept. 1972.
- [68] J. Saiz, M. Mermet, D. Frey, P. Jeannin, J. L. Schanen, and P. Musznicki. Optimisation and integration of an active clamping circuit for IGBT series association. In *Industry Applications Conference, 2001. Thirty-Sixth IAS Annual Meeting. Conference Record of the 2001 IEEE*, volume 2, pages 1046–1051, 2001.
- [69] S. Salama and Y. Tadros. Quasi resonant 3-phase IGBT inverter. In *Power Electronics Specialists Conference, 1995. PESC '95 Record., 26th Annual IEEE*, volume 1, pages 28–33, June 1995.
- [70] M. Sayani. DC-DC converter using all surface-mount components and insulated-metal substrate. In *Applied Power Electronics Conference and Exposition, 1992. APEC '92. Conference Proceedings 1992., Seventh Annual*, pages 639–646, 1992.
- [71] J. L. Schanen, E. Clavel, and J. Roudet. Modeling of low inductive busbar connections. *IEEE Industry Applications Magazine*, 2(5):39–43, 1996.
- [72] J. L. Schanen, L. Jourdan, and J. Roudet. Layout optimization to reduce EMI of a switched mode power supply. In *Power Electronics Specialists Conference, 2002. pesc 02. 2002 IEEE 33rd Annual*, volume 4, pages 2021–2026, 2002.
- [73] J. L. Schanen, J. Roudet, and W. Teulings. Prediction of current distribution between paralleled capacitors in hard switching operation: application to decoupling capacitor. *IAS'97*, Oct. 1997.
- [74] C. Serporta, G. Tine, G. Vitale, and M. Di Piazza. Conducted EMI in power converters feeding AC motors: experimental investigation and modelling. In *Industrial*

BIBLIOGRAPHY

- Electronics, 2000. ISIE 2000. Proceedings of the 2000 IEEE International Symposium on*, volume 2, pages 359–364, 2000.
- [75] J. Shao, R. Lin, F. Lee, and D. Chen. Characterization of EMI performance for hard and soft-switched inverters. In *Applied Power Electronics Conference and Exposition, 2000. APEC 2000. Fifteenth Annual IEEE*, volume 2, pages 1009–1014, New Orleans, LA, Feb. 2000.
- [76] K. C. Siddabattula. Electromagnetic modeling of packaging layout in power electronic modules. Master's thesis, Virginia Polytechnic Institute, 12 1999.
- [77] Y. Tang, H. Zhu, B. Song, J. Lai, and C. Chen. EMI experimental comparison of PWM inverters between hard- and soft-switching techniques. In *Power Electronics in Transportation, 1998*, pages 71–77, Dearborn, MI, Oct. 1998.
- [78] W. Teulings, J. L. Schanen, and Roudet. Switching performances and *EMI* noise generation of a chopper on insulated metal substrate. *EPE'97*, pages 134–138, 8-9Sept. 1997.
- [79] S.-V. Vaseghi. *Advance digital signal processing and noise reduction*. John Wiley and Sons Ltd, 2000.
- [80] M. Vlach. Modeling and simulation with saber. In *ASIC Seminar and Exhibit, 1990. Proceedings., Third Annual IEEE*, Rochester, NY, 1990.
- [81] S.-P. Weber, E. Hoene, S. Guttowski, W. John, and H. Reichl. Modeling induction machines for EMC-analysis. In *Power Electronics Specialists Conference, 2004. PESC 04. 2004 IEEE 35th Annual*, volume 1, pages 94–98, 2004.
- [82] Y. Weens, N. Idir, J. J. Franchaud, and R. Bausiere. High-frequency modeling of an adjustable speed drive. In *12th International Power Electronics and Motion Control Conference - EPE-PEMC 2006*, Portoroz, Slovenia, 2006.
- [83] B. Widrow, J. Glover, J.R., J. McCool, J. Kaunitz, C. Williams, R. Hearn, J. Zeidler, J. Eugene Dong, and R. Goodlin. Adaptive noise cancelling: Principles and applications. *Proceedings of the IEEE*, 63(12):1692–1716, 1975.
- [84] N. Wiener. *Extrapolation, Interpolation, and Smoothing of Stationary Time Series*. New York: Wiley, 1949.
- [85] P. Willcock, J. Ferreira, and J. van Wyk. A probe for measuring the propagation of conducted EMI in power converters. In *Industry Applications Conference, 2000. Conference Record of the 2000 IEEE*, volume 5, pages 3091–3096, Rome, 2000.
- [86] W. Wladzinski, P. J. Chrzan, and P. Musznicki. Modeling of conducted emission of dc-dc switch-mode converter. In *3rd International Workshop Compatibility in PowerElectronics CPE 2003*, 2003.
- [87] L. Yang. *Modeling and Characterization of a PFC Converter in the Medium and High Frequency Ranges for Predicting the Conducted EMI*. PhD thesis, Virginia Polytechnic Institute, 08 2003.

- [88] Z. Ye. *Modeling and control of parallel three-phase PWM converters*. PhD thesis, Virginia Polytechnic Institute, 09 2000.
- [89] R. Zhang, X. Wu, and T. Wang. Analysis of common mode EMI for three-phase voltage source converters. In *Power Electronics Specialist Conference, 2003. PESC '03. 2003 IEEE 34th Annual*, volume 4, pages 1510–1515, June 2003.
- [90] W. Zhang. *Integrated EMI/Thermal Design for Switching Power Supplies*. PhD thesis, Virginia Polytechnic Institute, 02 1998.
- [91] H. Zhu, J.-S. Lai, J. Hefner, A.R., Y. Tang, and C. Chen. Analysis of conducted EMI emissions from PWM inverter based on empirical models and comparative experiments. In *Power Electronics Specialists Conference, 1999. PESC 99. 30th Annual IEEE*, volume 2, pages 861–867, 1999.
- [92] H. Zhu, J.-S. Lai, J. Hefner, A.R., Y. Tang, and C. Chen. Modeling-based examination of conducted EMI emissions from hard and soft-switching PWM inverters. In *Industry Applications Conference, 1999. Thirty-Fourth IAS Annual Meeting. Conference Record of the 1999 IEEE*, volume 3, pages 1879–1886, Phoenix, AZ, Oct. 1999.
- [93] H. Zhu, J.-S. Lai, J. Hefner, A.R., Y. Tang, and C. Chen. Modeling-based examination of conducted EMI emissions from hard and soft-switching PWM inverters. *IEEE Transactions on Industry Applications*, 37(5):1383–1393, 2001.

Appendix A

Appendix A

The validation of Wiener filtering method - *Matlab*® m-file

```
0001 function [pert,tfall,irall]=hard(vds1,vds2,vds3,vlism,t);
0002
0003 % HARD SWITCHING INVERTER ELECTROMAGNETIC EMISSIONS RECONSTRUCTION
0004 %
0005 % [pert,tfall,irall]=hard(vds1,vds2,vds3,vlism,t);
0006 %
0007 % Inputs :
0008 %   vds1, vds2, vds3 - voltages across the 3 upper switches (EMI source)
0009 %   vlism : measured electromagnetic perturbations
0010 %   t - time vector
0011 %
0012 % Outputs :
0013 %   pert : total EM perturbations reconstructed
0014 %   tfall - all transfer functions
0015 %   irall - all impulse response
0016 %
0017
0018 global c;
0019 global L;
0020 global tfall;
0021 global irall;
0022
0023 %line vectors
0024 vds1=vds1(:).';
0025 vds2=vds2(:).';
0026 vds3=vds3(:).';
0027 t=t(:).';
0028
0029
0030 % vectors length
0031 L=length(vds1);
0032
0033 % sampling frequency
0034 fe=1/(t(2)-t(1));
0035
0036 % subtraction of the mean average
0037 u1=vds1;u2=vds2;u3=vds3;
0038 vds1=vds1-mean(vds1);
0039 vds2=vds2-mean(vds2);
0040 vds3=vds3-mean(vds3);
0041 vlism=vlism-mean(vlism);
0042
0043 % oscillation filtering for state detection
0044 display('Apply oscillation filtering?')
0045   filtrind = input('Y/N : ', 's');
0046
0047   if (isequal (filtrind,'Y') | isequal (filtrind,'y'))
0048       % oscillation filtering
0049       vds1f=filtervs(vds1);
0050       vds2f=filtervs(vds2);
0051       vds3f=filtervs(vds3);
0052
```

```

0053     % time-derivation of vswitch = state indefication
0054     dvds1=[vds1f(2:L)-vds1f(1:L-1) 0];
0055     dvds2=[vds2f(2:L)-vds2f(1:L-1) 0];
0056     dvds3=[vds3f(2:L)-vds3f(1:L-1) 0];
0057
0058     else
0059         % time-derivation of vswitch = source of perturbations
0060         dvds1=[vds1(2:L)-vds1(1:L-1) 0];
0061         dvds2=[vds2(2:L)-vds2(1:L-1) 0];
0062         dvds3=[vds3(2:L)-vds3(1:L-1) 0];
0063     end
0064
0065 %threshold definition for vs and derivative of vs
0066
0067     figure;plot(dvds1);
0068     grid on;
0069     hold; plot(dvds2,'r');plot(dvds3,'g');
0070     title('switch waverform derivatives ');
0071     display('Derivative threshold definition')
0072     dthresholdplus = input('Threshold for turn off (0<=threshold<=max) ? : ');
0073     dthresholdminus = input('Threshold for turn on (min<=threshold<=0) ? : ');
0074     close
0075
0076
0077 % finding state change points
0078 tvds=zeros(1,L);
0079
0080 indices1o=find(dvds1>=dthresholdplus);
0081 tvds(indices1o-adv)=1.0;
0082
0083 indices1c=find(dvds1<=dthresholdminus);
0084 tvds(indices1c-adv)=2.0;
0085
0086 indices2o=find(dvds2>=dthresholdplus);
0087 tvds(indices2o-adv)=3.0;
0088
0089 indices2c=find(dvds2<=dthresholdminus);
0090 tvds(indices2c-adv)=4.0;
0091
0092 indices3o=find(dvds3>=dthresholdplus);
0093 tvds(indices3o-adv)=5;
0094
0095 indices3c=find(dvds3<=dthresholdminus);
0096 tvds(indices3c-adv)=6;
0097
0098 % determine switching samples
0099 dvds=tvds(2:L)-tvds(1:L-1);dvds=[dvds 0];
0100
0101 switching=[find(dvds>=1) L];
0102 nb=length(switching);
0103
0104 % bloc characterization (switch state, first and last samples, nbr of samples)
0105 svds1ao=0;svds1bo=0;svds1co=0;svds1do=0;
0106 svds1ac=0;svds1bc=0;svds1cc=0;svds1dc=0;
0107 svds2ao=0;svds2bo=0;svds2co=0;svds2do=0;
0108 svds2ac=0;svds2bc=0;svds2cc=0;svds2dc=0;
0109 svds3ao=0;svds3bo=0;svds3co=0;svds3do=0;
0110 svds3ac=0;svds3bc=0;svds3cc=0;svds3dc=0;
0111
0112 vds1aobloc.duration=0;vds1bobloc.duration=0;
0113 vds1cobloc.duration=0;vds1dobloc.duration=0;
0114
0115 vds1acbloc.duration=0;vds1bcbloc.duration=0;
0116 vds1ccbloc.duration=0;vds1dcbloc.duration=0;
0117
0118 vds2aobloc.duration=0;vds2bobloc.duration=0;
0119 vds2cobloc.duration=0;vds2dobloc.duration=0;

```

```

0120
0121 vds2acbloc.duration=0;vds2bcbloc.duration=0;
0122 vds2ccbloc.duration=0;vds2dcbloc.duration=0;
0123
0124 vds3aobloc.duration=0;vds3bobloc.duration=0;
0125 vds3cobloc.duration=0;vds3dobloc.duration=0;
0126 vds3acbloc.duration=0;vds3bcbloc.duration=0;
0127 vds3ccbloc.duration=0;vds3dcbloc.duration=0;
0128
0129 for ind=1:nb-1
0130     w=switching(ind);
0131     % open 1 state
0132     if (dvds(w)==1 & vds2(w)>=0 & vds3(w)>=0)
0133         svdslao=svdslao+1;
0134         vds1aobloc(svdslao).firstlastsample=[switching(ind)+1 switching(ind+1)];
0135         vds1aobloc(svdslao).duration=switching(ind+1)-switching(ind);
0136     elseif (dvds(w)==1 & vds2(w)>=0 & vds3(w)<=0)
0137         svdslbo=svdslbo+1;
0138         vds1bobloc(svdslbo).firstlastsample=[switching(ind)+1 switching(ind+1)];
0139         vds1bobloc(svdslbo).duration=switching(ind+1)-switching(ind);
0140     elseif (dvds(w)==1 & vds2(w)<=0 & vds3(w)>=0)
0141         svdslco=svdslco+1;
0142         vds1cobloc(svdslco).firstlastsample=[switching(ind)+1 switching(ind+1)];
0143         vds1cobloc(svdslco).duration=switching(ind+1)-switching(ind);
0144     elseif (dvds(w)==1 & vds2(w)<=0 & vds3(w)<=0)
0145         svdsldo=svdsldo+1;
0146         vds1dobloc(svdsldo).firstlastsample=[switching(ind)+1 switching(ind+1)];
0147         vds1dobloc(svdsldo).duration=switching(ind+1)-switching(ind);
0148
0149     % close 1 state
0150     elseif (dvds(w)==2 & vds2(w)>=0 & vds3(w)>=0)
0151         svdslac=svdslac+1;
0152         vds1acbloc(svdslac).firstlastsample=[switching(ind)+1 switching(ind+1)];
0153         vds1acbloc(svdslac).duration=switching(ind+1)-switching(ind);
0154     elseif (dvds(w)==2 & vds2(w)>=0 & vds3(w)<=0)
0155         svdslbc=svdslbc+1;
0156         vds1bcbloc(svdslbc).firstlastsample=[switching(ind)+1 switching(ind+1)];
0157         vds1bcbloc(svdslbc).duration=switching(ind+1)-switching(ind);
0158     elseif (dvds(w)==2 & vds2(w)<=0 & vds3(w)>=0)
0159         svdslcc=svdslcc+1;
0160         vds1ccbloc(svdslcc).firstlastsample=[switching(ind)+1 switching(ind+1)];
0161         vds1ccbloc(svdslcc).duration=switching(ind+1)-switching(ind);
0162     elseif (dvds(w)==2 & vds2(w)<=0 & vds3(w)<=0)
0163         svdsldc=svdsldc+1;
0164         vds1dcbloc(svdsldc).firstlastsample=[switching(ind)+1 switching(ind+1)];
0165         vds1dcbloc(svdsldc).duration=switching(ind+1)-switching(ind);
0166     % open 2 state
0167     elseif (dvds(w)==3 & vds1(w)>=0 & vds3(w)>=0)
0168         svds2ao=svds2ao+1;
0169         vds2aobloc(svds2ao).firstlastsample=[switching(ind)+1 switching(ind+1)];
0170         vds2aobloc(svds2ao).duration=switching(ind+1)-switching(ind);
0171     elseif (dvds(w)==3 & vds1(w)>=0 & vds3(w)<=0)
0172         svds2bo=svds2bo+1;
0173         vds2bobloc(svds2bo).firstlastsample=[switching(ind)+1 switching(ind+1)];
0174         vds2bobloc(svds2bo).duration=switching(ind+1)-switching(ind);
0175     elseif (dvds(w)==3 & vds1(w)<=0 & vds3(w)>=0)
0176         svds2co=svds2co+1;
0177         vds2cobloc(svds2co).firstlastsample=[switching(ind)+1 switching(ind+1)];
0178         vds2cobloc(svds2co).duration=switching(ind+1)-switching(ind);
0179     elseif (dvds(w)==3 & vds1(w)<=0 & vds3(w)<=0)
0180         svds2do=svds2do+1;
0181         vds2dobloc(svds2do).firstlastsample=[switching(ind)+1 switching(ind+1)];
0182         vds2dobloc(svds2do).duration=switching(ind+1)-switching(ind);
0183     % close 2 state
0184     elseif (dvds(w)==4 & vds1(w)>=0 & vds3(w)>=0)
0185         svds2ac=svds2ac+1;
0186         vds2acbloc(svds2ac).firstlastsample=[switching(ind)+1 switching(ind+1)];

```

```

0187     vds2acbloc(svds2ac).duration=switching(ind+1)-switching(ind);
0188     elseif (dvds(w)==4 & vds1(w)>=0 & vds3(w)<=0)
0189         svds2bc=svds2bc+1;
0190         vds2bcbloc(svds2bc).firstlastsample=[switching(ind)+1 switching(ind+1)];
0191         vds2bcbloc(svds2bc).duration=switching(ind+1)-switching(ind);
0192     elseif (dvds(w)==4 & vds1(w)<=0 & vds3(w)>=0)
0193         svds2cc=svds2cc+1;
0194         vds2ccbloc(svds2cc).firstlastsample=[switching(ind)+1 switching(ind+1)];
0195         vds2ccbloc(svds2cc).duration=switching(ind+1)-switching(ind);
0196     elseif (dvds(w)==4 & vds1(w)<=0 & vds3(w)<=0)
0197         svds2dc=svds2dc+1;
0198         vds2dcbloc(svds2dc).firstlastsample=[switching(ind)+1 switching(ind+1)];
0199         vds2dcbloc(svds2dc).duration=switching(ind+1)-switching(ind);
0200
0201     % open 3 state
0202     elseif (dvds(w)==5 & vds1(w)>=0 & vds2(w)>=0)
0203         svds3ao=svds3ao+1;
0204         vds3aobloc(svds3ao).firstlastsample=[switching(ind)+1 switching(ind+1)];
0205         vds3aobloc(svds3ao).duration=switching(ind+1)-switching(ind);
0206     elseif (dvds(w)==5 & vds1(w)>=0 & vds2(w)<=0)
0207         svds3bo=svds3bo+1;
0208         vds3bobloc(svds3bo).firstlastsample=[switching(ind)+1 switching(ind+1)];
0209         vds3bobloc(svds3bo).duration=switching(ind+1)-switching(ind);
0210     elseif (dvds(w)==5 & vds1(w)<=0 & vds2(w)>=0)
0211         svds3co=svds3co+1;
0212         vds3cobloc(svds3co).firstlastsample=[switching(ind)+1 switching(ind+1)];
0213         vds3cobloc(svds3co).duration=switching(ind+1)-switching(ind);
0214     elseif (dvds(w)==5 & vds1(w)<=0 & vds2(w)<=0)
0215         svds3do=svds3do+1;
0216         vds3dobloc(svds3do).firstlastsample=[switching(ind)+1 switching(ind+1)];
0217         vds3dobloc(svds3do).duration=switching(ind+1)-switching(ind);
0218     % close 3 state
0219     elseif (dvds(w)==6 & vds1(w)>=0 & vds2(w)>=0)
0220         svds3ac=svds3ac+1;
0221         vds3acbloc(svds3ac).firstlastsample=[switching(ind)+1 switching(ind+1)];
0222         vds3acbloc(svds3ac).duration=switching(ind+1)-switching(ind);
0223     elseif (dvds(w)==6 & vds1(w)>=0 & vds2(w)<=0)
0224         svds3bc=svds3bc+1;
0225         vds3bcbloc(svds3bc).firstlastsample=[switching(ind)+1 switching(ind+1)];
0226         vds3bcbloc(svds3bc).duration=switching(ind+1)-switching(ind);
0227     elseif (dvds(w)==6 & vds1(w)<=0 & vds2(w)>=0)
0228         svds3cc=svds3cc+1;
0229         vds3ccbloc(svds3cc).firstlastsample=[switching(ind)+1 switching(ind+1)];
0230         vds3ccbloc(svds3cc).duration=switching(ind+1)-switching(ind);
0231     elseif (dvds(w)==6 & vds1(w)<=0 & vds2(w)<=0)
0232         svds3dc=svds3dc+1;
0233         vds3dcbloc(svds3dc).firstlastsample=[switching(ind)+1 switching(ind+1)];
0234         vds3dcbloc(svds3dc).duration=switching(ind+1)-switching(ind);
0235
0236     end
0237 end
0238 clear nb ind;
0239
0240 % time-derivation of vswitch = source of perturbations
0241 if (isequal (filtrind,'Y') | isequal (filtrind,'y'))
0242     clear dvds1 dvds2 dvd3;
0243     dvds1=[vds1(2:L)-vds1(1:L-1) 0];
0244     dvds2=[vds2(2:L)-vds2(1:L-1) 0];
0245     dvds3=[vds3(2:L)-vds3(1:L-1) 0];
0246 end
0247
0248 % Wiener filtering calculation for 24 states- call function calpert
0249
0250 [pert1ao,vds1aoir,tflaoir]=calpert(vds1aobloc,svds1ao,dvds1,vlism,L,1);
0251 [pert1bo,vds1boir,tflboir]=calpert(vds1bobloc,svds1bo,dvds1,vlism,L,2);
0252 [pert1co,vds1coir,tflcoir]=calpert(vds1cobloc,svds1co,dvds1,vlism,L,3);
0253 [pert1do,vds1doir,tfldoir]=calpert(vds1dobloc,svds1do,dvds1,vlism,L,4);

```

```

0254
0255 pert1o=pert1ao+pert1bo+pert1co+pert1do;
0256
0257 pert1ac=calpert(vds1acbloc,svds1ac,dvds1,vlisn,L,5);
0258 pert1bc=calpert(vds1bcbloc,svds1bc,dvds1,vlisn,L,6);
0259 pert1cc=calpert(vds1ccbloc,svds1cc,dvds1,vlisn,L,7);
0260 pert1dc=calpert(vds1dcbloc,svds1dc,dvds1,vlisn,L,8);
0261
0262 pert1c=pert1ac+pert1bc+pert1cc+pert1dc;
0263
0264 pert2ao=calpert(vds2aobloc,svds2ao,dvds2,vlisn,L,9);
0265 pert2bo=calpert(vds2bobloc,svds2bo,dvds2,vlisn,L,10);
0266 pert2co=calpert(vds2cobloc,svds2co,dvds2,vlisn,L,11);
0267 pert2do=calpert(vds2dobloc,svds2do,dvds2,vlisn,L,12);
0268
0269 pert2o=pert2ao+pert2bo+pert2co+pert2do;
0270
0271 pert2ac=calpert(vds2acbloc,svds2ac,dvds2,vlisn,L,13);
0272 pert2bc=calpert(vds2bcbloc,svds2bc,dvds2,vlisn,L,14);
0273 pert2cc=calpert(vds2ccbloc,svds2cc,dvds2,vlisn,L,15);
0274 pert2dc=calpert(vds2dcbloc,svds2dc,dvds2,vlisn,L,16);
0275
0276 pert2c=pert2ac+pert2bc+pert2cc+pert2dc;
0277
0278 pert3ao=calpert(vds3aobloc,svds3ao,dvds3,vlisn,L,17);
0279 pert3bo=calpert(vds3bobloc,svds3bo,dvds3,vlisn,L,18);
0280 pert3co=calpert(vds3cobloc,svds3co,dvds3,vlisn,L,19);
0281 pert3do=calpert(vds3dobloc,svds3do,dvds3,vlisn,L,20);
0282
0283 pert3o=pert3ao+pert3bo+pert3co+pert3do;
0284
0285 pert3ac=calpert(vds3acbloc,svds3ac,dvds3,vlisn,L,21);
0286 pert3bc=calpert(vds3bcbloc,svds3bc,dvds3,vlisn,L,22);
0287 pert3cc=calpert(vds3ccbloc,svds3cc,dvds3,vlisn,L,23);
0288 pert3dc=calpert(vds3dcbloc,svds3dc,dvds3,vlisn,L,24);
0289
0290 pert3c=pert3ac+pert3bc+pert3cc+pert3dc;
0291
0292
0293 pert=pert1o+pert1c+pert2o+pert2c+pert3o+pert3c;
0294
0295 % Estimation of reconstruction normalized error
0296
0297 string=sprintf('Normalized estimation error : \%.1f
0298 \%\%',100*(std(vlisn-pert.)/std(vlisn))^2);
0298 disp(string);
0299
0300 end
0301
0302 % function callpert - Wiener filter calculation
0303
0304 function [partpert,vdsirf,tf]=calpert(vdsbloc,svds,dvds,vlisn,L,progres)
0305
0306
0307 % Leaveing if there no state
0308 if (svds<=0)
0309     partpert=0;
0310     vdsirf=0;
0311     tf=0;
0312 else
0313 %bloc length
0314 lengthvds=2^nextpow2(max([vdsbloc.duration]))*1;
0315
0316 % matrices of signals with zero-padding used for identification task
0317     vdsmatrixvswitch=zeros(lengthvds,svds);
0318     vdsmatrixvvlisn=zeros(lengthvds,svds);
0319

```

```

0320     for ind=1:svds
0321         vdsmatrixvswitch(1:vdsbloc(ind).duration,ind)=dvds(vdsbloc(ind).
.firstlastsample(1):vdsbloc(ind).firstlastsample(2)).';
0322         vdsmatrixvvlisn(1:vdsbloc(ind).duration,ind)=vvlisn(vdsbloc(ind).
.firstlastsample(1):vdsbloc(ind).firstlastsample(2)).';
0323     end
0324 end
0325
0326 % system estimation
0327 % power spectral densities (auto and cross)
0328     if svds==1
0329         TFR=fft(vdsmatrixvswitch(:,1));
0330         TFM=fft(vdsmatrixvvlisn(:,1));
0331     else
0332         TFR=fft(vdsmatrixvswitch(:,2:svds-1));
0333         TFM=fft(vdsmatrixvvlisn(:,2:svds-1));
0334     end
0335
0336     TFRR=sum((TFR.*conj(TFR)).');
0337     TFMR=sum((TFM.*conj(TFR)).');
0338 % state transfert function
0339     tf=TFMR./TFRR;
0340 % state impulse response
0341     vdsirf=real(ifft(tf));
0342
0343     clear crr cmr Mcrr Vcmr
0344
0345     % multiplication signals for reconstruction
0346     vdsmult=zeros(1,L);
0347     for ind=1:svds
0348         vdsmult(vdsbloc(ind).firstlastsample(1):vdsbloc(ind).firstlastsample(2))=1.0;
0349     end
0350
0351     \% input signals for reconstruction
0352     vdsinput=filter(vdsirf,1,dvds);
0353     vdspert=vdsinput.*vdsmult(1:L);
0354
0355     partpert=vdspert;
0356
0357 end
0358     tfall(1:length(tf),progres)=tf;
0359     irall(1:length(vdsirf),progres)=vdsirf;
0360 end
0361
0362 % signal filering
0363 function cy=filtervs(vsf)
0364     eY=fft(vsf);
0365     fY=fix(eY/10000)+10000;
0366     cy=real(ifft(fY));
0367
0368 end

```

